UNIVERSITY OF CALIFORNIA SAN DIEGO

SAN DIEGO STATE UNIVERSITY

Engineering novel selectivity into metalloantibodies and targeting PcrV

A dissertation submitted in partial satisfaction of the requirements for the degree

Doctor of Philosophy

in

Chemistry

by

Elinaz Farokhi

Committee in charge:

San Diego State University

Professor Tom Huxford, Chair

Professor Jing Gu

University of California San Diego

Professor Stacey Brydges

Professor Stephen Hedrick

Professor Navtej Toor

2020

The Dissertation of Elinaz Farokhi is approved, and it is acceptable in quality and form for publication on microfilm and electronically:

_____

_____

_____

_____

_____

Chair

University of California San Diego

San Diego State University

2020

Dedication

I dedicate this dissertation to my wonderful husband, my lovely parents and to my sister and brother for their unconditional love and support during these so many years.

Table of Contents

List of Abbreviations

Ab	Antibodies
ADC	Antibody drug conjugates
ACT	Antibody conjugated therapies
CER	Ceramide
CHO	Chinese hamster ovary
CD4	Cluster of differentiation 4
CDR	Complementarity determining region
CH	Constant heavy
CL	Constant light
dsDNA	Double stranded DNA
DAR	Drug-to-antibody ratio
ELISA	Enzyme-linked immunosorbent assay
EGFRvIII	Epidermal growth factor receptor
EDTA	Ethylenediaminetetraacetic acid

FAAS	Flame atomic absorbance spectroscopy
Fab	Fragment antigen binding
Fc	Fragment crystallizable
FDA	Food and drug administration
IgG	Immunoglobulin G
ITC	Isothermal Titration Calorimetry
LPA	Lysophosphatidic acid
MHC	Major histocompatibility complex molecules
MMPs	Matrix metalloproteinases
MADH	Methylamine dehydrogenase
MST	Microscale thermophoresis
mAbs	Monoclonal antibodies
NF-κB	Nuclear factor -κB
PcrV	*P. aeruginosa* V-antigen
PK	Pharmacokinetics

PAGE	Polyacrylamide gel electrophoresis
PEG	Polyethylene glycol
PCR	Polymerase chain reaction
ScFv	Single chain variable fragment
SEC	Size exclusion chromatography
SDS	Sodium dodecyl sulfate
SPH	Sphingosine
S1P	Sphingosine-1-phosphate
SLE	Systemic lupus erythematosus
TNF-α	Tumor necrosis factor alpha
T3SS	Type III secretion system
VH	Variable heavy
VL	Variable light
VEGF	Vascular endothelial growth factor

List of Figures

List of Tables

Acknowledgements

It was my honor to work and perform research in Dr. Tom Huxford's lab. I learned different techniques in his lab ranging from protein crystallization and protein expression to designing plasmid, etc. I found his work ethic and support truly exceptional. I will never forget all the good experiences that I have gained in these years.

It was my pleasure and honor for the educational system I am privileged to be a part of and by the people I came to know. The SDSU-UCSD Joint Doctoral Program granted me access to a full array of biochemical instruments available at SDSU while allowing me access to the resources of a large research institution of UCSD and their facilities that they provided me.

I would like to thank my committee members for all of their support and time that they spend on reading my dissertation. My committee members are as follows: Dr. Navtej Toor, Dr. Stephen Hedrick, Dr. Stacey Bridges and Dr. Jing Gu.

I would like to thank the Institute for Integrated Research in Materials, Environments and Society (IIRMES) at California State University, Long Beach for letting me use their ICP-MS instrument.

I would like to thank InhibRx LLC, for collaborating with us on the PcrV project and for one academic year of support.

I would like to thank California State University Program for Education and Research in Biotechnology (CSUPERB) and NSF/Chemistry: Chemistry of Life Processes for supporting my education and research.

I would like to thank my lab members whom without their support I couldn't have gone

so far. My lab mates are as follow: Sheri Wu, Samantha Cohen, Sally Luong and Citlayi Villaseñor, James Caldwell and other lab mates and friends that during these years helped me.

I would like to thank Dr. Jack Dixon lab and Dr. Sandra Wiley for supporting me during one year at UCSD and teaching me tissue culture techniques.

Lastly, I would like to thank my co-authors on the paper we are publishing Aaron D. Ward, M. Frank Erasmus, Jonathan Wojciak, and Jonathan K. Fleming. Chapter II is currently being prepared for submission for publication of the material. The dissertation author is the primary author of this chapter.

Vita

2008 Bachelor of Science, Azad University, Tehran, Iran

2011 Master of Science, Kharazmi University, Tehran, Iran

2014 Master of Science, University of Kansas

2020 Doctor of Philosophy, University of California San Diego

San Diego State University

Publications

Farokhi, E., Hollands, A., Huxford, T., (under preparation) X-ray crystal structure of antigen recognition by two single chain camelid antibody variable domains with PcrV.

Farokhi, E., Ward, E., Erasmus, M.F., Fleming, J.K., Wojciak, J., Huxford, T. Ion binding properties of a naturally occurring metalloantibody. Under review, *Antibodies*, 2020.

Alaofi, A., Farokhi, E., Prasasty, VD., Anbanandam, A., Kuczera, K., Siahaan, TJ., "Probing the interaction between cHAVc3 peptide and the EC1 domain of E-cadherin using NMR dynamics molecular simulations". *Journal of Biomolecular Structure and Dynamics*, 35 (1), 92-104, 2017.

Sheikhhosseini, E., Farokhi, E., Bigdeli, M.A. "Synthesis of novel tetrahydroquinoline from α,α'-bis(substituted-benzylidene)cycloalkanones." *Journal of Saudi Chemical Society,* 20, S227-S230, 2016.

Farokhi, E. Determination of Binding Sites of Cadherin Peptides on the EC1 domain using NMR Spectroscopy. M.S. thesis, submitted to the Faculty of Pharmaceutical Chemistry of University of Kansas May 1, 2014.

Bigdeli, M.A., Marjani, K., Farokhi, E., Sheikhhosseini, E., and Ghazanfari, D. "Synthesis of novel pyrano[2,3-b]pyridines from α,α'-bis(substituted-benzylidene)cycloalkanones". *Journal of Heterocyclic Chemistry,* 50, 3,625-629, 2013.

Habibi, A., Sheikhhosseini, E., Bigdeli, M.A., Balalaie, S., and Farokhi, E. "Solvent free of α,α'-bis(substituted- benzylidene)cycloalkanones using covalently anchored sulfonic acid on silica gel (SiO2-R-SO3H) as an efficient and reusable heterogeneous catalyst". *International Journal of*

Organic Chemistry, 1, 4, 143-147, 2011.

Farokhi, E. Derivatives of Chalcones. M.S. thesis, submitted to the Faculty of Chemistry of the Kharazmi University on February 1, 2011.

ABSTRACT OF THE DISSERTATION

Engineering novel selectivity into metalloantibodies and targeting PcrV

by

Elinaz Farokhi

Doctor of Philosophy in Chemistry

University of California San Diego, 2020

San Diego State University, 2020

Professor Tom Huxford, Chair

Antibodies are a class of proteins that are secreted from our immune system to neutralize pathogens. They are very specific to the target cells and stably folded therefore they have become engaging for many scientists for decades. We were interested to study a novel group of antibodies that interacts to metals. Our findings indicated that metals are effective on stabilizing the antigen: antibody interaction. Previously, we were able to crystallize LT1009 antibody which is a humanized version of murine LT1002 IgG antibody. The crystal structure indicated that LT1009 employs two bridging calcium ions in the binding site to antigen. The biologically active lipid

sphingosine-1-phosphate (S1P) was the antigen.

Flame atomic absorption spectroscopy (FAAS) confirmed that murine LT1002 also binds calcium in solution and inductively coupled plasma-mass spectrometry (ICP-MS) indicates that, although calcium is the preferred metal binding cofactor, LT1002 can also bind to magnesium and to a much lesser extent, barium. Isothermal titration calorimetry revealed that LT1002 binds two calcium ions endothermically with dissociation constants in the high μM range. Finally, an engineered, recombinantly expressed and purified antibody Fab fragment consisting of the murine germ-line encoded light and heavy chain genes from which LT1002 is likely derived and exhibits calcium binding profile as the mature antibody.

Furthermore, we were interested to apply other metal bindings to the precursor metalloantibody. Therefore, we designed a large scale expression method to express the precursor antibody in Sf9 cells. Then, we were interested to design a plasmid by using site directed mutagenesis to change the key residues that were involved with the binding sites of Ca^{2+} and antigen. After that we were able to express and purify mutant antibody but this time the new metalloantibody binds to Zn^{2+}. Engineered zinc antibodies can have the potential for site specific conjugation. Moreover, Zn^{2+} can protect cysteine from oxidation at the binding site. We propose that LT1002 is representative of a class of naturally occurring metalloantibodies that are evolutionarily conserved within the genomes of mammalian species.

Chapter I

Introduction

1. Properties of antibodies

Antibodies are the most useful and profitable biological resources in biotechnology and pharmaceuticals. Monoclonal antibodies are the leaders of biological therapeutics due to their epitope specificity (Espiritu, Collier, and Bingham 2014). Biologic therapeutics, like antibody drugs, target specific cancer cells and kill the unhealthy cells instead of chemotherapeutics that have an effect on all healthy cells. Nowadays, a few antibody drug conjugates have gotten the approval form FDA (Food and Drug Administration) and the rest of the drugs are under development (Bajorath 2015).

Antibodies are proteins secreted from B cells of our adaptive immune cells to neutralize pathogens, such as viruses and bacteria. They are critical for immunity against infectious diseases, and extensively used for prevention and treatment of infection caused by bacteria, virus, and other infectious agents to improve public health. Antibodies recognize a unique part of the pathogens called antigens with their fragment antigen binding (Fab) variable region and the part of the antigen that antibodies bind to is called epitope (Janeway and Travers 1994; Litman et al. 1993; Maverakis et al. 2015).

Emil von Behring was awarded the first Nobel Prize in Physiology or Medicine in 1901 for his discovery of serum therapy for diphtheria. This led to the term antitoxin and later named as “antikörper” translated to “antibody” by Paul Erlich in a 1891 paper (Graham and Ambrosino 2015).

The advantage of antibodies is their high effectiveness when compared to small molecule drugs. They usually react highly specific against one target, which results in less undesirable side

effects and low toxicity. A major barrier for the success of biologics, especially peptide and protein drugs, has been their lack of oral absorption. Recently, new delivery systems have been developed to overcome this disadvantage. Another barrier of biologics has been the transition of antibody candidates from academic to industrial research, which stems from difficulties in large scale production of biotechnological products. Compared to the production of small molecules, antibodies production is highly complex. For example, antibodies therapeutics are produced in living cells, so they require several post-translational modifications to enhance their specificity and complex purification processes to ensure their safety (Ecker, Jones, and Levine 2015).

1.1. Structures of antibodies

Antibodies (Ab), also known as immunoglobulins (Ig), are proteins secreted mainly by plasma B cells that is used by the immune system to neutralize pathogens, such as pathogenic bacteria and viruses (Jackson and Thomas 2013). Antibodies are built from four polypeptide chains. They consist of two identical heavy chains (H chains) and two identical light chains (L chains), which assemble into a structure that looks like the Y shape. An IgG molecule has a molecular weight of about 150 kDa, each heavy chain is approximately 50 kDa and each light chain is approximately 25 kDa. Each arm of the Y is made up of a complete light chain paired with the amino-terminal part of a heavy chain, covalently linked by a disulfide bond. The stem of the Y consists of the paired carboxy-terminal portions of the two heavy chains. The two heavy chains are also linked to each other by disulfide bonds.

Heavy and light chain each consists of a series of similar sequence motifs; a single motif is about 100–110 amino acids long and folds up into a compact and exceptionally stable protein

domain, called an immunoglobulin domain. The V region at the amino-terminal end of each heavy or light chain is composed of a single variable domain (V domain): A VH and a VL domain together form an antigen-binding site. The other domains have little or no sequence diversity and are called the constant domains (C domains), which make up the C regions. The constant region of a light chain is composed of a single CL domain, whereas the constant region of a heavy chain is composed of three or four CH domains, depending on the isotype. The γ heavy chains of IgG, IgD, and IgA have three domains—C_H1, C_H2, and C_H3. IgM and IgE also have a fourth C domain—C_H4. Four different IgG subclasses include: IgG1, IgG2, IgG3, and IgG4 (T. Sharma and Gupta 2019). They differ in the constant region of the heavy chain and in the hinge. Furthermore, two β sheets are held together by strong hydrophobic interactions between their constituent amino acid side chains (the filling). The structure is stabilized by a disulfide bond between the two β sheets. The three hypervariable loops are called complementarity-determining regions (CDR1, CDR2, and CDR3) because they provide a binding surface that is complementary to the antigen (Sutton et al. 2019).

There are three antibody chromosomal locations in human: the heavy-chain locus on chromosome 14, the κ light chain locus on chromosome 2, and the λ light-chain locus on chromosome 22. Different gene segments encode the leader peptide (L), the V region (V), and the constant region (C) of the heavy and light chains. The light chain variable domain consists of V and J (joining) gene segments and the constant domain includes C gene segments. The heavy chain variable domain contains V, D (diversity) and J, while the constant domains of the heavy chain includes C_H1, C_H2 and C_H3 gene segments. Diversity between V gene segments are in the sequences that encode CDR1 and CDR2 of the V domain. CDR3 is determined by the sequence

difference introduced at the junction between the V and J segments (Cook 2000).

1.2. Humanization of antibodies

Antibodies have emerged as effective tools in the treatment and diagnosis of different human diseases. Non-human antibodies have been demonstrated to induce human immune responses, which result in neutralization of administered antibody and limits the application of such antibodies in the treatment of human diseases. To overcome this problem, the technology of antibody humanization has been developed. Antibody humanization is an efficient approach to eliminate or reduce the immunogenicity of these antibodies (Adamkewicz, Kiialainen, and Paz-Priel 2019). The complementarity determining regions (CDRs) are responsible to bind to a specific antigen. CDR grafting is a humanization technique whereby humanized antibody sequences are generated by selecting the CDRs of the original antibody (usually murine, but increasingly other species are being humanized, including rabbits) and grafting them into a human framework (Buick 2016).

In our studies, we used LT1009 antibody, which is a humanized monoclonal antibody and we studied its crystal structure. LT1009 binds specifically to lipid sphingosine-1-phosphate (S1P). S1P has an effect in heart disease and cancer (J. M. Wojciak et al. 2009).

Another example of humanized monoclonal antibody that has shown promising results to treat Alzheimer by engineering of antibody using the CDR-grafting method has been published. Both humanized scFv (single chain variable fragment) and Fab fragments have great affinity in the range of low nanomolar for $Aß_{1–16}$ peptide. Aß peptide is generated from the proteolytic

cleavage of amyloid plaques, which causes Alzehmer (an effective target for therapy). Interestingly, *in vitro* humanized antibody fragments were able to inhibit amyloid fibril formation, oligomer mediated neurotoxicity, and disaggregating preformed amyloid fibrils (Robert et al. 2010).

Furthermore, omalizumab is a humanized recombinant monoclonal anti-IgE antibody treats allergic diseases and it has been effective on adult patients with moderate-to-severe allergic asthma. The anti-IgE antibody inhibits free IgE from blood serum to bind to cellular receptors. By reducing IgE levels and IgE receptor expression in blood serum, inflammatory cells in the context of allergic reduces. Omalizumab therapy is well tolerated and effectively improves symptoms, reducing asthma exacerbations and the need to use high dosage of inhaled corticosteroids to control diseases. In addition, omalizumab improves quality of life of patients with severe allergic asthma that is inadequately controlled by currently available asthma medications. In conclusion, omalizumab represents an approach to the treatment of asthma and may help an important need in patients with moderate-to-severe asthma (Gennaro et al. 2007).

1.3. B cells activation and affinity maturation

Circulating B cells that do not have antigens are known as naive B cells. They express both IgM and IgD on their surfaces, which are the only immunoglobulin isotypes that are expressed simultaneously by a B cell. Once the antigenic peptide is taken by the B cell through receptor mediated endocytosis, it must appear at the cell surface in order to bound to the antigen-specific T cell receptor. This is accomplished by binding the peptide to a membrane-associated protein inside the cell, then carries the antigen to the cell surface. The human glycoproteins that

binds and transports peptide antigens to cell surface are called MHC molecules (major histocompatibility complex molecules). Only when a peptide has been bound to MHC molecule, it can travel from inside the cell to the surface. Antigen-specific CD4+ T-cell receptor can recognize the peptide antigen and MHC molecule. Interaction of the B cell with a T helper cell is necessary to produce full activation of the B cell and antibody generation following antigen binding (Reth et al. 2004).

Interestingly, single-nucleotide substitutions (point mutations) happens when the B cell gets activated by the antigen. B cells bearing these mutant high-affinity immunoglobulin receptors compete most effectively for binding to antigen and are preferentially selected to mature into antibody-secreting plasma cells. The changes are concentrated at positions in the heavy-chain and light chain of the CDR loops that form the antigen-binding site and directly contact antigen. This process is called affinity maturation which is an evolution that variant immunoglobulins generated in a random manner are selected for the purpose of improving binding to the antigen. This capacity for extraordinarily rapid evolution in pathogen-binding immunoglobulins is helpful for human immune system to catch up with the generally faster-evolving pathogens (Shehata et al. 2019).

1.4. Monoclonal antibody

A single species of immunoglobulin molecules is produced by culturing a single clone of a hybridoma cell. MAbs recognize only one chemical structure, i.e., they are directed against a single epitope of the antigenic substance used to raise the antibody (Morrow and Felcone 2004). The first commercial development of therapeutic monoclonal antibodies is, Orthoclone OKT3,

was approved for prevention of kidney transplant rejection. Since the approval of OKT3, therapeutic monoclonal antibodies and antibody- related products, such as Fc-fusion proteins, antibody fragments, and antibody-drug conjugates (collectively referred to hereafter as monoclonal antibody products) have grown to become the dominant product class within the biopharmaceutical market (Patterson 2005).

1.4.1 Applications of monoclonal antibodies

Monoclonal antibody are approved for the treatment of a variety of diseases, ranging from those that treat patient populations of a few thousand or less for such orphan indications as paroxysmal nocturnal hemoglobinuria or the cryopyrin associated periodic syndromes to those treating hundreds of thousands of patients for some cancers and multiple sclerosis or even millions of patients for diseases such as asthma and rheumatoid arthritis (Ecker, Jones, and Levine 2015).

1.4.2 Therapeutic properties

Antibody-mediated therapy utilizes antibodies that have the ability to bind specifically to certain cells or proteins with high affinity. The advantages of antibodies as therapeutics are: it is stably folded; it is specific to the target site; and it can clear by the body's natural immunological processes when the antibody has bound to its target. One of the advantages to develop antibody-conjugated therapies (ACTs) is to use mAbs to deliver potent therapeutic agents directly into tumor cells expressing cancer-specific antigens. This can cause less exposure of normal tissues and reduce toxicity compared to chemotherapy (Parakh et al. 2016). A monoclonal antibody (Avastin) is able to directly stop certain tumor growth by binding to VEGF (vascular endothelial

growth factor). VEGF can go through mutations; therefore, Avastin can be ineffective at removing VEGF (Motzer and Bukowski 2006).

1.5. Antibody engineering

In 1997, the first engineered antibody was approved by the US Food and Drug Administration (FDA). It was a murine monoclonal antibody that binds to tumor-specific antigens and could differentiate cancer cells from healthy cells. After that, more than 300 programs for the development of therapeutic antibodies have been described in industrial and academic laboratories. The development of antibodies is now very critical to cure several notable pathogenic diseases. They can defend against transmissible diseases or completely eliminate an infection. Polyclonal antibodies contain varying concentrations of different antibodies, and as such are not commonly used clinically. Conversely, monoclonal antibodies are highly specific, permitting more enhanced clinical diagnostics (Filpula 2007). In my research, I have engineered monoclonal antibody to enhance the binding of the antibody to different antigens followed by greater affinity binding. Nowadays, human antibodies are generated *in vitro* by antibody engineering technologies, such as phage display, construction of antibody fragments, immunomodulatory antibodies, and cell-free systems (Edwards and He 2012).

1.5.1 Single Chain Variable Fragment (ScFv)

Single chain variable fragment has great affinity, solubility, and binding specificity to antigen and has been used for antibody engineering, biotechnology, cancer research, and biomedical applications. ScFv is constructed by a peptide linker that binds the heavy chain to light chain of immunoglobulins. Engineered ScFv enhances the effective functions of full-length

antibodies. It can also carry toxins to kill cells, or cytokines to activate the immune system. Moreover, multiple target sites can bind to bispecific antibodies (AlDeghaither, Smaglo, and Weiner 2015). Recombinant antibody expression and engineering has eased the expression of antibody fragments in bacteria (*E. coli*), as well as mammalian (Chinese hamster ovary (CHO), or myeloma cell lines e.g., Sp2/0), yeast (*Pichia pastoris*), plant (*Arabidopsis*), and insect cells (*Drosophila melanogaster*) (Frenzel, Hust, and Schirrmann 2013). The benefits of smaller fragments over full length antibodies are better tumor and tissue penetration, blood clearance, short retention times. In addition, they have better fusion in bacteria, and display on filamentous phage (Saeed et al. 2017).

1.5.2 Engineered Immunomodulatory Antibodies

Immunomodulatory techniques are adjustment of the immune system in order to increase the clinical efficacy of therapeutic antibodies. Overexpressed or mutated cell surface antigens are target for modulated antibody based drugs. This technology developed on engineering the antigen or receptor of the immune system, changing the Fc function and T cell activation and antibody drug conjugates (ADC) targeting a specific antigen. Immunomodulatory antibodies have been successful in clinical studies (Scott, Wolchok, and Old 2012).

Development of antibody drug conjugates (ADCs) has been effective to treat infectious diseases and target cancer cells. ADCs are being processed by antibody generation and contains a selection of highly cytotoxic molecules, and stable linkers that connects the payloads to the antibody (Vincent and Zurini 2012).

Site-specific conjugation strategy has been used for antibody-drug conjugates and employing metal binding motif is important for site specific conjugation. There are several site-selective conjugation strategies to selectively label highly cytotoxic payloads onto antibodies, including enzymatic conjugation. The use of site-specific conjugation has significant advantages over conventional chemistry conjugations and is used for antibody-drug conjugates (ADCs). To enhance drug-to-antibody ratio (DAR) in order to have a better pharmacokinetics, (PK), disposition, and efficacy of the ADC, site-specific payload placement will control it. Furthermore, linker composition has also effect on an ADC properties. Drake et al. (2014) reported a novel site-specific conjugate to engineer aldehyde tags on antibody's backbone. This chemistry provides stable C-C bond between the cytotoxin payload and the antibody which is more stable than the other linker chemistries used to generate ADCs. The flexibility and versatility of the aldehyde tag has impact on the conjugation site as well as the linker composition on ADC properties. In this paper, IgG was tagged with aldehyde on different locations on the IgG1 backbone and the characterization of product is being described. The site of the conjugation has efficacy and pharmacokinetic behavior in rodents. This benefit causes improved safety profile in rats as compared to conventional lysine conjugate (Drake et al. 2014).

1.5.3. Nonconventional antibodies

Single chain antibodies or nanobodies are a novel class of therapeutic proteins based on immunoglobulin single variable domains. Like a full length antibody, it can bind to antigen specifically. It has a molecular weight about 12-15 kDa. The immunoglobulin single variable domains may be derived from the variable domains of heavy chain-only antibodies that naturally occur in camelids. Compared to conventional antibodies, nanobodies are missing C_H1 domain of

their heavy chain (Muyldermans 2013). The single heavy chain domain antibody were engineered from heavy chain domain found in camelids and it is called V_HH fragments (Harmsen and De Haard 2007). Furthermore, single variable heavy chain has also found in shark and Cartilaginous fishes, which are the oldest living organisms, and it is called immunoglobulin new antigen receptor V_{NAR} fragment. Moreover, the Cartilaginous fishes and sharks have 4 and 5 constant heavy domain in their Fc region respectively (Feige et al. 2014; Möller et al. 2010).

The advantages of using nanobodies over full length antibodies are that nanobodies can penetrate into tissues for instance, crossing the blood brain barrier compared to conventional antibodies. They have uniques binding capacity to small cavities and have high affinity and specificity to antigens. Moreover, they are highly soluble with great rapid clearance *in vivo*. In contrast to conventional antibodies, nanobodies have high stability in different abnormal temperature and pH (Širochmanová et al. 2018; Morrison 2019; Rissiek, Koch-Nolte, and Magnus 2014). Although most of nanobodies are form heavy chain single variable domain, there are also reports on nanobodies derived from light chain single domain that can bind to antigen specifically (Ghannam et al. 2015).

1.5.3.1 Bispecific nanobodies

Bispecific antibodies have great therapeutic and diagnostic applications. They can recognize two different epitopes either from the same antigen or different antigens. Single domain antibodies, such as V_HH and V_{NAR} and nanobodies can be used to generate bispecific molecules. Combination of two or more single domain antibodies can make divalent, trivalent and multivalent molecules, which they can bind to specific epitopes (Brinkmann and Kontermann 2017). In a study, bivalent camel VHH domains have been fused with a linker that

has stability in serum and flexibility (Els Conrath et al. 2001). They used a linker which was derived from llama IgG2a upper hinge. Moreover, tetravalent bispecific VHH molecules were generated by liking four VHH, two directed against TcdA and two against TcdB.

Antibiotic-associated diarrhea can be caused by *Clostridium difficile* and the causing agent is pseudomembranous colitis which is associated with inflammation of the colon. Two large exotoxins, TcdA and TcdB are the primary reasons for *C. difficile* infection (CDI). This bispecific nanobodies have shown neutralizing effect *in vivo* and *in vitro (Yang et al. 2014)*.

Moreover, nanobodies that neutralizes *Pseudomonas aeruginosa* has been discovered. Large and random formatting library of bivalent and biparatopic (combinations of two different) nanobodies to study the blockage of *Pseudomonas aeruginosa* has been explored. PcrV is an important part of the type III secretion system (T3SS). Its oligomeric nature provides several bindings and blocking options. Screening the library showed several promising biparatopic options for nanobody building block. Best potencies were certified with further characterization in two different *P. aeruginosa* T3SS-mediated cytotoxicity assays. Three biparatopic nanobodies confirmed 100% survival with using prophylactic and reducing lung *P. aeruginosa* burden of lethal mouse by up to 2 logs. At a very low doses it protected mice from infection related changes in lung. At last the process of screening such libraries for potency improving is useful for other target and therapeutic platforms (Tavernier et al. 2016).

We have crystallized PcrV with two monovalent VHH nanobodies and solved the structure for the first time. In Chapter III we will further discuss T3SS secretion system, PcrV, and the methods used to crystallize the complex.

2. Metals in biology

One-third of all proteins are expected to be metalloproteins (Waldron and Robinson 2009). Therefore, they have different applications in cell, for example storage and transport of proteins, enzymes and signal transduction proteins, or infectious diseases (Marmion 2014). It can also get involved in electron transfer reactions (cytochromes), may act as storage (e.g., ferritin for iron) or transport proteins (e.g., transferrin for iron). In the latter groups of proteins, the metal storage is reversible and the metal is a temporary component (Sigel and Pyle 2007).

The relative amount of metalloproteins could be inherent to the amino acid sequence of the proteins. However, the use of metals by antibodies to recognize and bind to antigens is still somewhat of a novelty.

2.1. Metalloproteins

One of the most common metalloproteins is zinc finger, which is a small protein motif that is recognized by the coordination of one or more zinc ions (Zn^{2+}) in order to stabilize the fold (Klug and Rhodes 1987). The crystal structures of zinc finger-DNA complexes solved in 1991 and 1993 indicated the canonical pattern of interactions of zinc fingers with DNA. The binding of DNA to protein is different from what was expected and is not through the 2-fold symmetry of the double helix, instead zinc fingers are linked linearly in tandem to bind nucleic acid sequences of varying lengths (Pavletich and Pabo 1991). Zinc finger proteins (ZNFs) have a wide range of applications. It can interact with DNA, RNA and other proteins. Therefore, ZNFs are involved in transcriptional regulation, ubiquitin- mediated protein degradation, signal transduction, actin targeting, DNA repair, cell migration, and numerous other processes

(Cassandri et al. 2017).

Moreover, specific metal binding properties of monoclonal antibody to metal-EDTA complexes has been studied by Blake et al. (1996). This monoclonal antibody that recognizes cadmium-EDTA complexes covalently coupled to a carrier protein. The quality of the antibody to recognize 16 different metal-EDTA complexes was evaluated using KinExATM immunoassay instrument. The dissociation constant of the antibody to cadmium and mercury-EDTA complexes was 21 and 26 nM, respectively. Other metal-EDTA complexes tested includes, Mn(II), In(III), Ni(II), Zn(II), Co(II), Cu(II), Ag(I), Fe(III), Pb(II), Au(III), Tb(III), Ga(III), Mg(II), and Al(III) bound and their affinities were from 20- to 40,000-fold less than determined for the cadmium-EDTA complex. The binding of divalent metal-chelate complexes correlates to the size of the metal ion, mercury and magnesium are exceptions here. The amino acid variable regions of the heavy and light chains were deduced from polymerase chain reaction amplification and subsequently used to construct models for the antigen binding regions. The key residue for the cadmium binding appeared to be His96 in the heavy chain (Blake et al. 1996).

Furthermore, a monoclonal antibody that can detect uranium (VI) has been reported recently. The groundwater contamination with uranium has been the subject of concern these days. Uranium toxicity can cause lots of health problems such as renal failure, genotoxicity and cancer. The usual methods for detecting uranium were time-consuming, expensive non-portable equipment and the detection were not observed in-filed unless the water samples were analyzed. Moreover, the other methods available do not have quantitative analysis and the detection limit is not low enough to be in the range of recommendations for drinking water (30 ppb or 126 nM of

uranium). For the first time in this research sensitive paper-based biosensor strip has been introduced by Quesada-González et al. (2018) which includes U(VI) selective gold nanoparticle-based lateral flow strips. This method is portable, fast, cheap and the detection limit is 36 nM which is lower than the action level (126 nM) established by the World Health Organization and the U.S. Environmental Protection Agency for drinking water. The antibody gold nanoparticles enhance high sensitivity and are biocompatible to antibody. Antibody can recognize soluble U complexes with DCP (2,9-dicarboxyl-1,10-phenanthroline) chelator. This assay has a limit of detection of 36.38 nM, which is because of the small size of the U(VI)-DCP complex. This research can perform *in situ* and the results only takes 20 minutes. The strips can do both qualitative and quantitative analysis by using a mobile phone application (Quesada-González et al. 2018).

The metal binding ion motif site-specific conjugation strategy has been reported by Chung, Lee, and Park (2016). Cysteine containing motifs as single repeat or tandem repeat were investigated. The tandem repeat of cysteine-glycine-histidine (CGH) metal binding motif has demonstrated binding to Co (II) ions suggesting that conformational transition of peptide was affected by the sequential metal ion binding. The free thiol reduction after reduced by reducing reagents illustrated strong retardation of cysteine oxidation in the order of Zn (II)>Ni (II)>Co (II). The metal binding motif CGH was cloned to the C-terminus of the antibody heavy chain and the ion-dependent oxidation characteristics were investigated. CGH-motif-introduced antibody showed strong dependence to the metal binding protect against oxidation. The cysteine reactivity for 22 hours with saturating O_2 condition retained when the Zn (II) saturated antibody with tandem repeat of CGH motifs presented. Fluorophore labeling indicated that metal binding motif

can be used as an efficient tool for site-specific conjugation. Whereas, Trastuzumab without the tandem repeat of CGH motif showed non-specific dye conjugation. Zn (II) ion binding with the CGH motif showed fluorophores were site-specifically conjugated to the heavy chain of the antibody. The future goal of this research is to propose a method for strong metal ion dependence on oxidation protection and highly site-selective and specific conjugation for proteins that have multiple intrinsic cysteine like antibodies (Chung, Lee, and Park 2016).

2.2. Metalloenzymes

Metalloenzymes are protein enzymes that contain metal ions (metal cofactors), which are either directly bound to the protein or to the enzyme-bound nonprotein components (prosthetic groups). About one-third of all enzymes known so far are metalloenzymes. Also ribozymes, i.e., RNA molecules with enzyme function may contain structurally and/or functionally important metal ions (mostly divalent metal ions such as Mg^{2+}) (Sigel and Pyle 2007).

Recent publication on metalloprotease by Jennings et al. (2018) concluded that GtgA, GogA and PipA zinc metalloprotease effector proteins from type III secretion system are translocated into the host cell during *Salmonella* infection. They can cleave subunits of NF-κB (κ-light-chain-enhancer of activated B cells), therefore, suppressing host immune system. GtgA, GogA and PipA cleave p65, RelB and cRel subunits of NF-κB, whereas effector protein NleC of enteropathogenic and enterohemorrhagic *Escherichia coli* cleaved all five NF-κB subunits. Mutation results indicated that a single nonconserved residue in NF-κB1 and NF-κB2 that relates to Arg41 in p65 prevents cleavage of these subunits. This demonstrates the specificity of this enzyme cleavage. Crystal structure of apo-form of GtgA with p65 N-terminal domain valued the

importance of Arg41 residue. Furthermore, by mimicking the shape and negative charge of the DNA phosphate backbone GtgA can recognize NF-κB subunits. Moreover, structural based mutations explained the importance of GtgA key residues with p65 subunit which blocks NF-κB activation. This research provides detailed mechanism of substrate recognition by this family of proteins which is important for bacterial virulence (Jennings et al. 2018).

Matrix metalloproteinases (MMPs) which includes collagenases, stromelysins, gelatinases, and membrane-anchored disintegrin metalloproteinases (ADAMs), and meprins are also structurally related zinc-dependent proteases family. These family initially was known to degrade extracellular matrix (ECM) but now it is known that has a wide range of biological and immune processes such as cellular development, adhesion, infiltration, activation and effector function, ligand–receptor interactions, cytokine, chemokine and growth factor activation, regulation of clotting factors, tissue damage, remodeling, and repair. Wide variety of cells secrete these metalloproteases which includes fibroblasts, myofibroblasts smooth muscle cells, epithelial cells, endothelial cells, neutrophils, macrophages, and lymphocytes. One of their major roles is to regulate the activation of cytokines like TNFα, chemokines, adhesion molecules, OX-40, and Fas and others. Cytokines, growth factors, pathogen-associated molecular patterns (PAMPS), and damage-associated molecular patterns (DAMPS) can stimulate the activity of MMP. Dysregulation of MMP has so many effects such as inflammatory diseases; RA, MS, inflammatory bowel disease (IBD), asthma, pemphigus vulgaris (PV), atherosclerosis, ischemic stroke, and other neuroinflammatory diseases. Whereas, increased level of cytokines and other inflammatory pathways can cause excess of MMP release, uncontrolled degradation of the ECM, and tissue injury. As shown by Dübel and Reichert (2014), Key factor in causing colonic damage

could be because of expressed MMP-9 (gelatinase B) and MMP-2, in the gastrointestinal (GI) tract during IBD and being absent from the colonic epithelial in normal colonic tissue. Transgenic overexpression of MMP-9 in mice has shown increased epithelial cell proliferation and apoptosis. Furthermore, MMP-2 was shown to protect against tissue damage, whereas MMP-9 mediates tissue injury. However, significant side effects and lack of specific inhibitor in cancer clinical trial has urged the use of other precise gelatinase inhibitors that blocks both MMP-9 and MMP-2. Therefore, an anti-MMP-9 mAb could enhance this specificity and the optimal balance between efficacy and safety. Recently phase I of GS-5745 from Gilead Sciences Inc. a human IgG mAb, specific for MMP-9 for a solid tumor is ongoing (Dübel and Reichert 2014).

3. Metalloantibodies in nature

Sphingosine-1-phosphate (S1P) is a signaling bioactive lipid that contributes in many signaling pathways. It has an important role in physiological processes, such as cell growth, differentiation, survival, and pathophysiological processes, such as cancer, cardiovascular disease, multiple sclerosis, neuropathic pain, involve S1P signaling (Gardell, Dubin, and Chun 2006; Murph and Mills 2007; Skoura et al. 2007); (Tsai and Han 2016; Kawabata et al. 2018). In the sphingolipid signaling pathway, S1P has a key role and is produced from ceramide (CER) and sphingosine (SPH) with the kinase activity of sphingosine (SPHK) (Milstien and Spiegel 2006).

In recent years, antibodies that target biologically active lipids have been studied as promising therapeutic agents. Previously, expression and purification of murine LT1002 and LT1009 the humanized version of LT1002 antibody was done. It has shown that both antibodies

bind to sphingosine-1-phosphate with high affinity and specificity and do not cross react with other structurally similar lipids (O'Brien, Jones, et al. 2009).

Furthermore, Inductively-coupled plasma-mass spectrometry (ICP-MS) indicates that LT1002 binds to calcium, magnesium and, to a much lesser extent, barium (M. F. Erasmus 2012) (O'Brien, Jones, et al. 2009). Previously in our lab, a 1.9 Å X-ray crystal structure of humanized LT1009 Fab antibody version of the murine LT1002 anti-S1P antibody was determined. The X-ray crystal data indicates the novel finding that it employs two bridging calcium ions in binding to its lipid antigen. Inductively coupled plasma-mass spectrometry (ICP-MS) indicates that LT1009 binds to calcium. The two calcium interact with aspartic acid residues from the CDR-L1 and -L3 loops of the antibody variable light chain (VL) (Figure I.1) (J. M. Wojciak et al. 2009). Furthermore, the amino acids involved in metal coordination are encoded in the germ-line sequences of immunoglobulin kappa light chain genes within the genomes of diverse mammalian species and are included in several antibodies that have been previously analyzed.

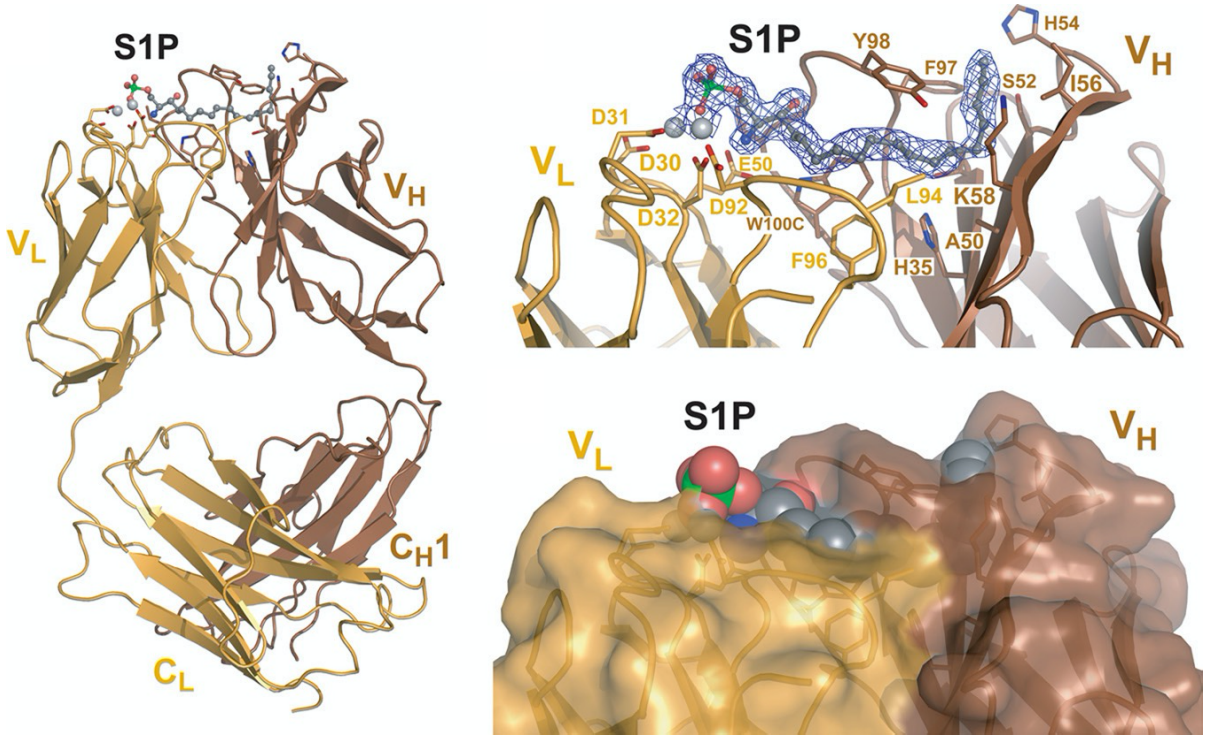

Figure I.1 X-ray crystal structure of the LT1009 Fab: S1P complex. The light chains are colored gold and the heavy chains are colored light brown. Bridging Ca^{2+} ions are grey spheres and S1P antigen is depicted as a ball and stick model (J. M. Wojciak et al. 2009).

Interestingly, in another study X-ray crystal structure of variable domain antibody fragment (Fv) with mutant epidermal growth factor receptor (EGFRvIII) was solved. This antibody is called MR1 and binds specifically to EGFRvIII and not EGFR. Epidermal growth factor receptor is a membrane glycoprotein and is involved in protein tyrosine kinase activity. Many cancer cells such as breast and ovarian cancers, non-small cell lung carcinomas and prostate cancers have expressed receptor mutant, EGFRvIII. 1.8 Å X-ray crystal structure of MR1 disulfide stabilized Fv (dsFv) in complex with peptide antigen of the tumor cells was solved. It was the first time that the structure of MR1dsFv with synthetic peptide was characterized (Figure I.2). Furthermore, the CDR loops sequence of the light chain of the

antibody is similar to the CDRL1-L3 sequence of the metalloantibody that we studied. However, MR1 crystal structure is not indicating any metal in cooperation with the peptide. Moreover, the peptide binding site to the antibody is different from our metalloantibody binding site (Landry et al. 2001).

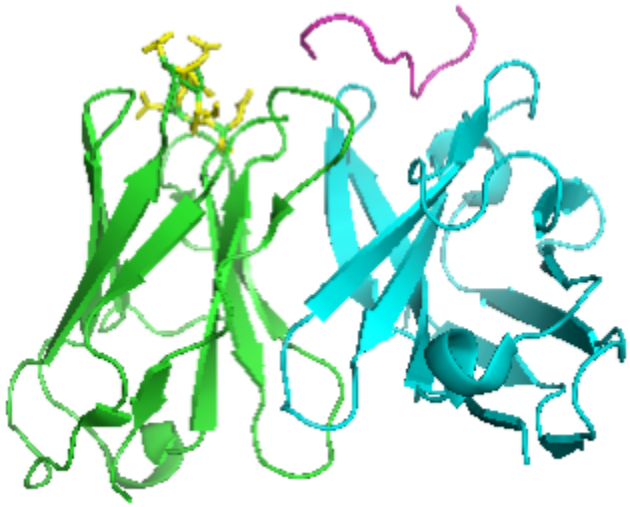

Figure I.2 X-ray crystal structure of the MR1dsFv: synthetic peptide complex. MR1dsFv antibody domains are colored in green and cyan. Synthetic peptide is colored in purple. The CDR loops of the light chain sequence that are similar to our metalloantibody is represented as stick model and has yellow color (Landry et al. 2001).

Previously, X-ray crystal structure of Q425 monoclonal antibody that protects against HIV has been discovered. CD4 is a glycoprotein found on the surface of immune cells such as T helper cells. CD4 with T helper cells are necessary for the human immune system. If CD4 knocks out against untreated HIV infection or other immunosuppressive, the body will be resistless to a wide range of infection. CD4:Q425 can block viral entry but it does not interrupt the CD4: HIV-1 gp120 envelope glycoprotein binding. In this study, surface-plasma resonance

has shown that Q425 requires Ca^{2+} for recognition of CD4. Interestingly, calcium increases the affinity of Q425 to CD4 55,000-fold. X-ray crystal analysis data suggested that Q425 binds to CD4 in the presence of Ca^{2+} and Ba^{2+}. This data suggests that Q425 held calcium has binding energy approximately 1.5 kcal/mol which is greater than usual protein atom. Indicating that metal ligation has significant role in antigen recognition (T. Zhou et al. 2005). Interestingly, the CDRL1-L3 sequences of Q425 is similar to our metalloantibody. However, the crystal structure indicates the presence of only one metal ion and the binding site of the CD4 to Q425 antibody is different from our metalloantibody (Figure I.3).

Figure I.3 X-ray crystal structure of the Q425. Q425 antibody Fab domains are colored in green and cyan. DIDDD sequence is shown as sticks on the CDR loop1 and 3 of the light chain in yellow color. The orange sphere is indicating Ca^{2+} ion (T. Zhou et al. 2005).

In the presence of Ca^{2+}, we have crystallized Fab fragment of humanized LT1009 anti-sphingosine-1-phosphate antibody. The crystal structure shows that LT1009 binds to Ca^{2+} in the absence of antigen. The difference is the space between two Ca^{2+} ions are shorter in the presence of S1P and it is because of the electrostatic interaction of the oxygen ions on the phosphate group of sphingosine-1-phosphate. I will further discuss the crystal structure of humanized LT1009 with Ca^{2+} and other homolog antibodies of LT1002 in different species in Chapter II.

Moreover, other studies have shown the competition binding between carrier proteins and monoclonal anti-S1P and anti-LPA antibodies to sphingosine-1-phosphate (S1P) and Lysophosphatidic acid (LPA) lipids, respectively, where their dissociation constants (K_D) values have been calculated. The competition binding analysis suggested the affinity of monoclonal anti-S1P is 102-103 times greater than the affinity of the carrier protein for individual LPA species (Jonathan K. Fleming et al. 2016). However, anti-LPA antibody (LT3015) shows no metal binding and the crystal structure confirms binding to Lysophosphatidic acid (LPA) independent of metals (J. K. Fleming et al. 2011).

In order to study the chemical properties of this novel metalloantibody, we first must develop methods for recombinant expression and purification. We will then alter the residues observed to coordinate the Ca^{2+} ions and test their ability to bind more biochemically active metals. It is expected that these novels, engineered metalloantibody scaffolds might serve as substrates for further development as a class of engineered metalloantibodies with the ability to be used as a site specific metalloantibody to conjugate to other drugs. This research is designed to identify other naturally occurring functional metalloantibodies and to test the hypothesis that

the use of metal coordination chemistry by antibodies to recognize their antigens is evolutionarily conserved in the mammalian immune system.

Chapter II

Ion binding properties of a naturally occurring metalloantibody

1.Introduction

At least one-third, and perhaps as many as one-half, of all functioning proteins are predicted to be metalloproteins (Thomson and Gray 1998)(Waldron and Robinson 2009)(Hu et al. 2014). Included among these metal-dependent biological factors are the vast collection of diverse metalloenzymes, which includes many oxidoreductases, proteases, and all protein kinases, as well as metal-dependent extracellular receptors, signaling proteins, transcription factors, and charge transport complexes (Kretsinger, Uversky, and Permyakov 2013).

However, the involvement of metals in antigen presentation and recognition by proteins of the adaptive immune system remains somewhat of a novelty. In 2009, as part of an effort aimed at developing novel anti-inflammatory and potential anti-cancer antibody-based therapies that function by selectively binding to signaling lipids, we determined the X-ray crystal structure of the Fab fragment of a humanized mouse monoclonal antibody bound to its antigen sphingosine-1-phosphate (S1P) (O'Brien et al. 2009; Wojciak et al. 2009). The complex crystal structure revealed that the humanized anti-S1P antibody, known as LT1009 and derived from the murine anti-S1P antibody LT1002, employs two bridging Ca^{2+} ions that are required for antigen recognition and binding. The two Ca^{2+} are partially coordinated within close proximity (<4 Å) of one another by three aspartic acid residues (Asp30-Asp31-Asp32) from light chain complementarity-determining region loop 1 (CDR-L1) and a fourth aspartic acid (Asp92) from CDR-L3. This arrangement allows for one oxygen atom from the phosphate head group of S1P to complete a μ bridging bond to both bound Ca^{2+}. Subsequent *in vitro* analysis confirmed that the bound ions are indeed Ca^{2+} and characterization of the antibody:antigen complex by surface plasmon resonance (SPR) spectroscopy revealed the binding to be extremely favorable with a

dissociation equilibrium constant (K_D) in the low n*M* range. Removal of Ca^{2+}, by addition of chelators such as EDTA or EGTA, as well as mutation of Ca^{2+}-coordinating amino acid residues completely disrupted the complex to the same or even greater extent than did mutation of residues that contact the antigen directly.

This direct observation of an antibody that was raised by immunization in mice employing interfacial bridging metal ions as a required component of its antigen recognition site called to mind several questions concerning the chemical nature of the anti-S1P antibody:Ca^{2+} interactions. For example, can the antibody bind Ca^{2+} independently of antigen or is prior interaction with S1P a requirement for Ca^{2+} binding? Does the antibody bind to metal ions other than Ca^{2+}? And, with what affinity is the Ca^{2+} bound? It also raised questions about the biology underlying the anti-S1P antibody such as, did the metalloantibody develop its ability to bind to Ca^{2+} during the processes of somatic recombination and/or affinity maturation or is the potential to coordinate Ca^{2+} evolutionarily conserved within germline antibody gene sequences? And, are there other examples of antibodies that employ Ca^{2+} or other metal ions in this fashion to recognize different antigens?

In this study, we report results from a series of structural, *in vitro* biochemical, and protein engineering experiments that were performed in order to characterize the metal ion binding properties of the anti-S1P antibody and in order to test the hypothesis that Ca^{2+}-mediated antigen binding is an evolutionarily conserved component of a complete and robust antibody repertoire. Our results suggest that the anti-S1P antibody does not require antigen in order to bind Ca^{2+} and that the default Ca^{2+} binding mode is similar to that observed in the LT1009:Ca^{2+}:S1P complex X-ray crystal structure. We observe that the antibody binds Ca^{2+}

selectively, with an appreciable, but significantly lower capacity for binding Mg^{2+} and even lower affinity toward Ba^{2+}. We measure the Ca^{2+} binding affinity and find that its dissociation constant (K_D) is an order of magnitude lower than the typical concentration of Ca^{2+} in plasma, suggesting that the anti-S1P antibody is preloaded with Ca^{2+} *in vivo*. We identify the Ca^{2+} binding sequence in previously characterized antibodies, some, but not all, of which also require Ca^{2+} for binding to their respective antigens. Finally, we observe that the amino acid sequence signature for Ca^{2+} binding is encoded for within the germline sequences of select antibody kappa light chain gene variable regions across diverse species and that an antibody Fab fragment expressing the mouse germline-encoded sequences from which the anti-S1P antibody is likely derived also binds to Ca^{2+} in solution. These results strongly suggest that the Ca^{2+}-dependent antigen binding observed in the anti-S1P antibody is an evolutionarily conserved and diversely applied component of a functional adaptive immune system.

2. Materials and Methods

2.1 DNA, oligos, plasmids

Plasmids encoding murine (LT1002) and humanized (LT1009) anti-S1P antibodies have been described previously (O'Brien et al. 2009). For construction of a shuttle plasmid containing both chains of the naïve germline-encoded Fab, we followed the previously reported protocols of Furuta, et al. (Furuta et al. 2010). cDNA encoding the murine Ighv1-78 variable heavy chain in frame with Ighd1-1, Ighj2, and IgG1 constant heavy domain 1 with an N-terminal Gp64 signal peptide a C-terminal TEV protease-cleavable C-terminal hexa-histidine tag was synthesized with codons optimized for insect cell expression and containing 5'-EcoRI and 3'-HindIII sites and

introduced between EcoRV sites in a pUC57 plasmid (Genscript). An analogous second pUC57 plasmid was prepared containing a codon-optimized murine light chain gene fragment consisting of Igkv17-121 in frame with Igkj4 and the kappa gene constant light domain with N-terminal Gp64 signal sequence between 5'-NheI and 3'-SphI restriction sites. Heavy and light chain cDNA were then prepared from the plasmids by double digestion with appropriate restriction enzymes and purified fragments were ligated into the corresponding restriction sites in the pFastBacDual plasmid (Thermo Fisher). This arrangement places the heavy chain Fab under transcriptional control of the P10 promoter and expression of the light chain under the Polyhedrin promoter.

2.2 Antibodies and Fab fragment generation

Full length murine (LT1002) and humanized (LT1009) anti-S1P antibodies were produced in stable CD-CHO cell lines as previously described (O'Brien et al. 2009). Briefly, antibodies were purified by affinity chromatography on ProSep-vA-Ultra resin (Millipore). Fab production from whole IgG has been described previously (Wojciak et al. 2009). Briefly, full length LT1009 IgG was digested at a 100:1 ratio with activated papain (Worthington); the reaction was quenched with iodoacetamide, dialyzed, and purified by anion exchange chromatography. Fab-containing fractions were passed through a ProSep-vA-Ultra protein-A column, concentrated to 12 mg/mL, and stored at 4°C. For preparation of recombinant naïve germline-encoded antibody Fab, we followed protocols for bacmid production, transfection of Sf9 insect cell monolayers, and recombinant baculovirus titer optimization that have been established in this laboratory and reported previously (Shaul, Farina, and Huxford 2008). 0.5 L

of media was prepared by centrifugation at 500 x g for 5 min. and vacuum filtration through 0.2 μm nitrocellulose membrane (Millipore) and passed by gravity through 1 mL of Ni Sepharose Fast Flow resin (GE Healthcare) at 4°C. The column was washed with 25 mM TRIS-HCl pH 8.0, 150 mM NaCl, 25 mM imidazole and protein was eluted with wash buffer containing 150 mM imidazole. The eluted protein was treated with 0.1 M EDTA pH 8.0, filtered through 0.2 μm syringe tip filter (Millipore), and purified on a SuperDex75 16/60 size exclusion chromatography column (GE Healthcare) in 25 mM TRIS-HCl pH 8.0, 150 mM NaCl. Peak fractions were combined and concentrated to 5 mg/mL in 10 kDa molecular weight cutoff (MWCO) centrifugal concentrator (Millipore), flash frozen in liquid nitrogen, and stored at -80°C.

2.3 LT1009 Fab:Ca^{2+} complex formation and co-crystallization

Crystals were grown by the hanging drop-vapor diffusion method at room temperature. Initial screening of for conditions that promote crystallization of antigen-free LT1009 Fab were identified by testing Crystal Screen I (Hampton Research) reagents supplemented with 10 mM $CaCl_2$. For optimal crystal growth, 1 μL of 12 mg/mL LT1009 Fab was mixed with 1 μL reservoir solution comprised of 0.1 M 4-(2-hydroxyethyl)-1-piperazineethanesulfonic acid (HEPES) pH 7.5, 1.5 M Li_2SO_4, and 10 mM $CaCl_2$ on a siliconized coverslip and sealed with high vacuum grease over 1 mL of reservoir solution. Plate-like crystals of dimensions 0.3 × 0.3 × 0.02 mm grew in 63 days at room temperature. Crystals were harvested with nylon loops and immersed into 0.1 M TRIS-HCl pH 8.5, 0.2 M Li_2SO_4, 30% w/v polyethylene glycol 4000, 10

mM $CaCl_2$, and 10% glycerol for approximately ten seconds prior to flash cooling in liquid nitrogen.

2.4 X-ray crystallography

Synchrotron data were collected at 100K on a NOIR-1 CCD detector at the Advanced Light Source Beamline 4.2.2, Lawrence Berkeley National Laboratory. Diffraction data indexing and scaling of intensities were carried out with HKL2000 (Otwinowski and Minor 1997). Data collection statistics are presented in Table II.1. Molecular replacement was performed via Phaser-MR in PHENIX using LT1009 Fab (PDB ID 3I9G) as a probe with ions, antigen, and solvent molecules removed and variable and constant domains separated, as described previously (King et al. 2017; McCoy et al. 2007). Rigid-body and initial restrained maximum-likelihood refinements with all working data to 3 Å resolution and difference Fourier electron density map calculation to identify potential Ca^{2+} binding sites were carried out using REFMAC5 and FFT, respectively, in CCP4 (Murshudov, Vagin, and Dodson 1997). Model building was completed in COOT (Emsley et al. 2010). All further refinements were made in PHENIX (Adams et al. 2010). Final assessment of the refined model was carried out using MolProbity (Chen et al. 2010). Refinement statistics are presented in Table II.1. Final atomic coordinates and structure factors were submitted to the Protein Data Bank (PDB ID: 6VRT). Figures were prepared using PyMOL (DeLano et al. 2002).

2.5 Equilibrium dialysis

Prior to testing, proteins were treated with 0.1 M EDTA pH 8.0 and purified either by dialysis (LT1002/LT3015 FAAS and ICP-MS experiments) or by size exclusion chromatography

(naïve germline-encoded Fab antibody ICP-MS). 200 µL of 100 mM stock solution of $CaCl_2 \cdot 2H_2O$ (EMD® #401800) prepared in 20 mM Na-HEPES pH 7.2., 20 mM NaCl was added to 1.8 mL of 1 mg/mL LT1002, 1 mg/mL LT3015, 1 mg/mL naïve Fab, or Na-HEPES buffer. The resulting solutions at 10 mM $CaCl_2$ were applied to 3.5 kDa MWCO dialysis units (Slide-A-Lyzer™ MINI Dialysis Unit #88403). In order to monitor the rate of equilibration, samples were dialyzed against 0.5 L of 20 mM Na-HEPES pH 7.2, 20 mM NaCl and analyzed at time points 0, 1.5, 3.5, 7.5, and 22.5 hours. In subsequent studies samples were dialyzed against Na-HEPES buffer for 24 hours with four changes of buffer. Addition metals were tested by substituting with 100 mM stock solutions of $MgCl_2 \cdot 6H_2O$ (VWR® #VW1483-01), $SrCl_2 \cdot 6H_2O$ (MP Biomedicals #9631K), $BaCl_2 \cdot 2H_2O$ (EMScience #43129930), $Zn(C_2H_3O_2)_2 \cdot 2H_2O$ (Fisher Scientific® #053087), $CdCl_2$ (MD Biomedical #8107K), $MnCl_2 \cdot 4H_2O$ (Fisher Scientific #041398), $CoCl_2 \cdot 6H_2O$ (Fisher Scientific® #040819), $NiSO_4 \cdot 6H_2O$ (EMDTM 35044548), $CuSO_4 \cdot 5H_2O$ (CAS 7758-99-8), $YbCl_3 \cdot 6H_2O$ (CAS 10035-01-05), $GdCl_3$ (CAS 10138-52-0), and $EuCl_3 \cdot 6H_2O$ (CAS# 13758-92-7) in 20 mM Na-HEPES pH 7.2, 20 mM NaCl.

2.6 Flame atomic absorption spectroscopy (FAAS)

20 µL of sample solution was removed from the dialysis unit, treated nitric acid (5% final concentration), and heated at 98°C for 30 min. and centrifuged at 14,000 x g for 5 min. Analysis was carried out on a 240 AA instrument (Agilent), which was calibrated by a 6-point dilution of 1.0 ppm $CaCO_3$ standard. Instrument settings: lamp current, 70% of 10 mA; compressed air, 9.0 psi; burner height, 15 mm; burner position, 90°C; fuel flow, 1.1 L/min.; Ca^{2+} absorbance, 422.7

nm; slit width, 0.5 nm. Between samples, the injection port was washed with 5.0% (v/v) HNO_3 solution.

2.7 Inductively coupled plasma-mass spectrometry (ICP-MS)

Samples were prepared as for FAAS and analyzed on an Agilent 4500 Series Inductively Coupled Plasma Mass Spectrometer (ICP-MS) through the Institute for Integrated Research Materials, Environments and Society at California State University, Long Beach.

2.8 Isothermal titration calorimetry (ITC)

A 20 mM $CaCl_2$ solution was titrated at 2.0 μL increments into solutions of 300 μM LT1002, 300 μM LT3015, or no antibody in 50 mM Na-HEPES pH 7.2 and the bindings were measured on a MicroCal™ iTC200 instrument (Malvern) available through Protein Production and Analysis at the Sanford Burnham Prebys Medical Discovery Institute. Data were analyzed by Origin™ software.

2.9 Antibody sequence analysis

Heavy and light chain variable domain light chain sequences were analyzed on the IgBlast server (http://www.ncbi.nlm.nih.gov/igblast) to identify naïve V, D, and J genes from which the LT1002 anti-S1P antibody is most likely derived (Ye et al. 2013). In order to identity antibodies with four Asp residues in CDR-L1 and -L3, a python function was applied to search for three neighboring Asp residues ([D][D][D]) in the abYsis database (Swindells et al. 2017). Output was analyzed by hand to identify whether the three Asp appeared in CDR-L1 and whether a fourth Asp was present in CDR-L3. Identification of conserved kappa light chain gene

sequences in species other than mouse was performed by Blast (http://blast.ncbi.nlm.nih.gov) search with murine Igkv17-121 gene sequence (Madden, Tatusov, and Zhang 1996).

3. Results

3.1. X-ray crystal structure of a Ca^{2+}-bound to Fab fragment in the absence of antigen

We first analyzed whether the anti-S1P antibody is capable of binding Ca^{2+} in the absence of S1P or, alternatively, if their interaction is dependent upon the presence of antigen (Figure II.1). We also wished to determine by what mode the antibody might bind Ca^{2+} in the absence of antigen. This second question arose from our analysis of the results from a previous study in which X-ray crystallography was employed to determine the site of Ca^{2+} binding by the murine Q425 antibody. Q425 selectively binds to the extracellular portion of the human CD4 co-receptor in a Ca^{2+}-dependent manner that inhibits steps subsequent to virus binding and protects against HIV infection of $CD4^+$ T cells (Healey et al. 1990). By crystallizing and determining the X-ray crystal structure of the Q425 Fab fragment separately in the presence of 10 m*M* Ba^{2+}, 10 m*M* Ca^{2+}, and 10 m*M* EDTA, researchers concluded that one Ca^{2+} binds to a site at the interface between the light and heavy chains employing amino acid side chains from CDR-H3 and CDR-L2 and -L3 (Zhou et al. 2005). This site, which was also able to accommodate binding of the significantly larger Ba^{2+} ion, is completely different than what we observed in the LT1009:Ca^{2+}:S1P complex structure, where two Ca^{2+} are coordinated by four Asp residues from light chain CDR-L1 and -L3 and the phosphate group on the S1P antigen (Wojciak et al. 2009).

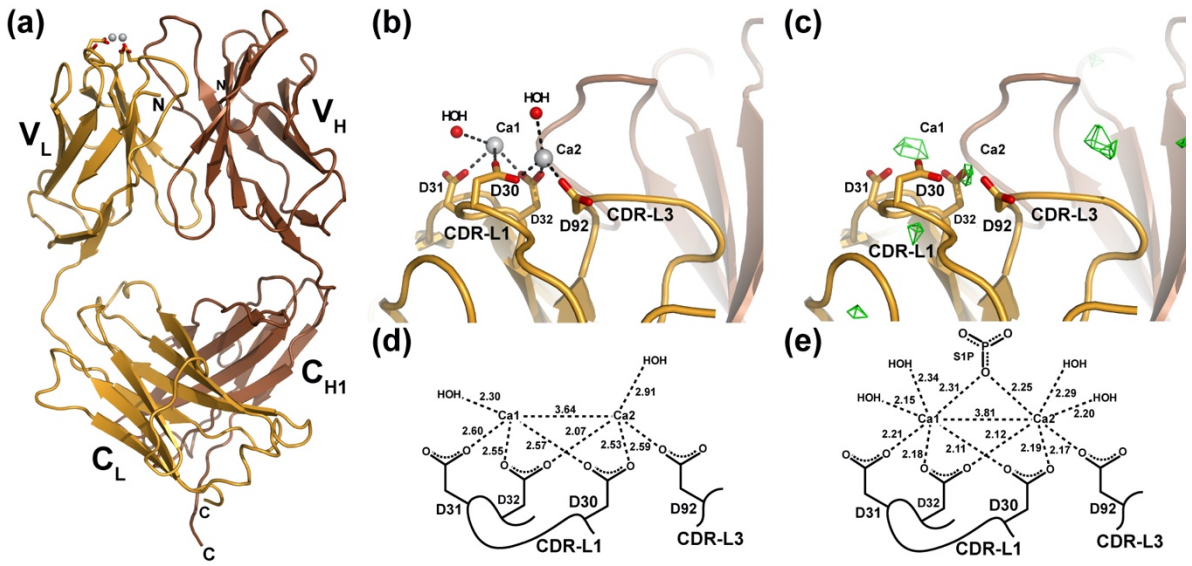

Figure II.1 X-ray crystal structure of the LT1009 anti-sphingosine-1-phosphate antibody Fab fragment in complex with Ca^{2+}. (**a**) The complete LT1009 Fab fragment is depicted in ribbon diagram representation with the light chain in gold and the heavy chain in brown. Two Ca^{2+} ions are represented as light grey spheres with the side chains that partially coordinate them shown as sticks. Individual immunoglobulin domains are labeled as are the N- and C-termini of the heavy and light chains. (**b**) A close-up view of the Ca^{2+} binding in LT1009. Side chains from CDR-L1 and CDR-L3 that coordinate Ca^{2+} are depicted as sticks and labeled and two water molecules that are within generous hydrogen bonding distance of the Ca^{2+} ions are depicted as red spheres. (**c**) An F_O-F_C difference electron density omit map built with phases from the apo LT1009 molecular replacement probe after rigid-body refinement and contoured at 3.5 sigma (see text) is shown in green and reveals two strong peaks at sites of the bound Ca^{2+} ions. (**d**) A schematic diagram of Ca^{2+} ion coordination by LT1009 with bond lengths in Å and light chain amino acids labeled. (**e**) For comparison, a similar schematic diagram of Ca^{2+} coordination taken from the LT1009:S1P complex X-ray crystal structure is shown.

Following closely the approach employed in the Q425 structural study, we prepared crystals of the LT1009 humanized anti-S1P antibody Fab fragment in 10 m*M* Ca^{2+} and collected a complete set of X-ray diffraction data. Experimental estimates of phase were provided by molecular replacement with a search model consisting of atomic coordinates for LT1009 from the Fab:Ca^{2+}:S1P complex crystal structure (PDB ID 3I9G) with S1P antigen and all nonbonded atoms (water, ions) removed. After rigid-body and restrained refinement of the model against diffraction data to 3.0 Å resolution, F_O-F_C difference Fourier maps were calculated and analyzed for the presence of unaccounted for peaks of electron density. Two spheres of positive electron

density were visible at the CDR-L1/CDR-L3 binding sites at contour level of 4.0 σ (Figure II.1c). These corresponded in position almost exactly to the sites of the two Ca^{2+} observed in the antigen bound LT1009 Fab complex X-ray crystal structure. Importantly, no significant peak was observed at the interface between LT1009 Fab heavy and light chain variable domains, strongly suggesting that, at 10 m*M* concentration, Ca^{2+} is found at the same sites as was observed in the antigen-bound anti-S1P complex crystal structure and not in the site proposed by crystallographic analysis of antibody Q425. The significance of this observation is that the light chains of Q425 and LT1009 are highly similar with CDR loop sequences that differ at only four positions and preservation of all four Ca^{2+}-coordinating Asp residues.

Table II.1 X-ray crystallography data collection and refinement statistics.

	LT1009 Fab:Ca^{2+} complex
Data collection	
X-ray source	ALS 4.2.2
Wavelength (Å)	1.0000
Space Group	I222
Unit cell (Å)	
a	87.80
b	114.41
c	133.70
Molecules/asymm. unit	1
Resolution Range (Å)[1]	50.0-2.55 (2.59-2.55)
R_{sym} (%)	8.7 (77.0)
Observations	161,860
Unique reflections	22,135
Completeness (%)	100.0 (100.0)
Redundancy	7.3 (5.8)
$\langle I/\sigma \rangle$	23.6 (2.3)
Refinement	
Number of reflections	22,124
R_{work} (%)	20.9 (35.3)
R_{free}[2]	26.0 (46.4)
Protein Atoms	3,365
$Ca^{2+}/H_2O/SO_4^{2-}$ atoms	42
Geometry (R.m.s.d.)	
Bond lengths (Å)	0.012
Bond angles (°)	1.142
Ramachandran plot[3]	
Favored	93.6
Allowed	6.2
Disallowed	0.2
MolProbity score[4]	1.81
PDB accession code	6VRT

[1]Data in parentheses are for highest resolution shell.
[2]Calculated against a cross-validation set of 5.1% of data selected at random prior to refinement.
[3]Calculated by MolProbity (Chen et al., 2010).
[4]Combines clashscore, rotamer, and Ramachandran evaluations to a single score, normalized to the same scale as X-ray resolution (Chen et al., 2010).

We continued with model building and refinement against all data to a resolution limit of 2.56 Å, ultimately yielding a model for LT1009 Fab in complex with Ca^{2+} with working *R*-factor

(R_{work}) of 20.9% and R_{free} of 26.0% and with very good stereochemistry (Table II.1). The crystallographic model, which consists of heavy chain amino acids 1-217, light chain amino acids 1-214, two Ca^{2+}, 28 waters, and one sulfate ion, reveals the familiar and expected Fab fragment immunoglobulin domain organization (Figure II.1a). The antigen-free and -bound Fab models are practically identical with a root-mean squared deviation (rmsd) of 0.630 Å for C_α positions upon superposition. The elbow angles**,** a measure for relative displacement of the variable and constant domains upon antigen binding, are also in close agreement with the elbow angle for the Fab:Ca^{2+}:S1P complex structure at 167.5° and that of the antigen-free Fab:Ca^{2+} complex measuring 170.1° (Stanfield et al. 2006). Where the two crystallographic models differ is with respect to the average distance in the bonds to the two Ca^{2+} ions. The interionic distance of 3.64 Å in the antigen-free model compares well with that of the antigen-bound complex, where the refined distance between the bound Ca^{2+} ions is 3.81 Å (Figure II.1d,e). This suggests that the cationic charges are effectively shielded from one another upon antibody binding. However, each of the six bonds between Asp side chain oxygen atoms and Ca^{2+} as well as to two ordered water molecules are longer than the corresponding bonds in the antigen-bound complex. Although the magnitude of these differences is less than the estimated coordinate error as calculated by maximum-likelihood methods, which for the antigen-free model is 0.51 Å, the resulting longer bond distances agree well with established Ca—O bond distances while the significantly shorter Ca—O bonds observed in the 1.9 Å resolution antigen-bound complex approach the limits for what has been observed (Gagné and Hawthorne 2016). Therefore, our crystallographic analyses suggest that at 10 m*M* Ca^{2+} concentration and in the absence of S1P antigen, two Ca^{2+} bind to the anti-S1P antibody through association with the four Asp side chains

from CDR-L1 and -L3 and that binding of the phosphate head group of S1P is accompanied by Ca—O bond shortening that likely correlates with significant increased Ca^{2+} binding affinity.

3.2. Detection of Ca^{2+} binding by LT1002 in solution

Having established by X-ray crystallography that the anti-S1P antibody binds two Ca^{2+} at the same sites as was previously observed in the LT1009 Fab:Ca^{2+}:S1P complex crystal structure, we next wished to establish methods for assessing Ca^{2+} binding in solution. To this end, we employed equilibrium dialysis of whole murine LT1002 anti-S1P IgG1 antibody and detection by flame atomic absorption spectroscopy (FAAS). By this approach, buffered solutions of LT1002 anti-S1P antibody that had been rendered metal ion-free by pretreatment with EDTA were incubated in solution containing Ca^{2+} and dialyzed against excess amounts of Ca^{2+}-free buffer. In order to monitor the rate of dialysis under the conditions tested, we first carried out an experiment in which the amount of Ca^{2+} retained within the dialysate fraction was monitored over time relative to similarly prepared and buffered whole LT3015, an antibody specific for lysophosphatidic acid (LPA) that we had previously demonstrated does not involve Ca^{2+} in binding to its lipid antigen (Fleming et al. 2011). By this approach, LT1002 anti-S1P antibody-dependent retention of Ca^{2+} could be detected relative to LT3015 anti-LPA antibody by FAAS after 24 hours and the amount of Ca^{2+} remaining within the dialyzed antibody samples did not change significantly during the final 15 hours of dialysis (Figure II.2).

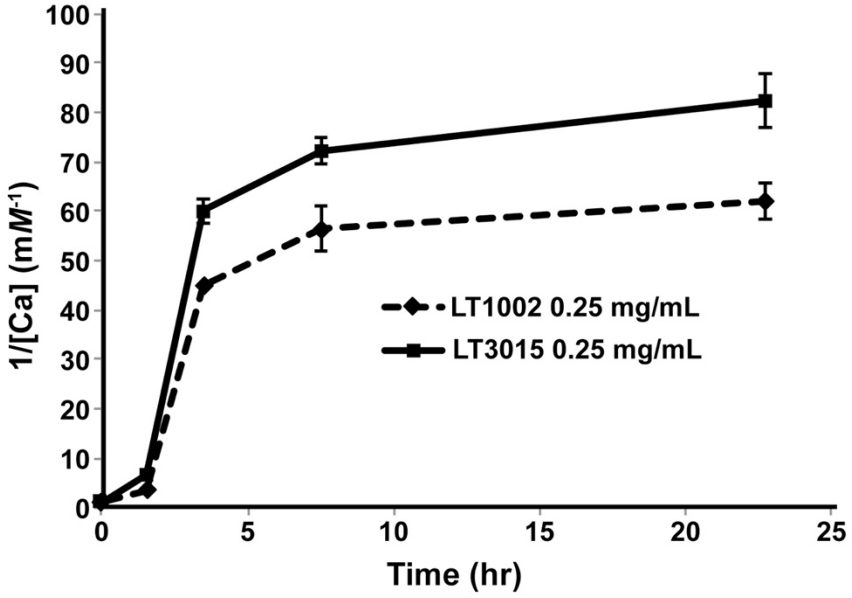

Figure II.2 The rate of decrease in Ca^{2+} concentration versus time by as monitored by FAAS after equilibrium dialysis. The Ca^{2+} concentrations (reported in reciprocal units to aid in visualization) remaining in solutions of 10 m*M* $CaCl_2$ and either 0.25 mg/mL LT1002 anti-S1P antibody (dashed line) or control LT3105 anti-LPA antibody (solid line) were measured via FAAS at 0, 1.5, 3.5, 7.5, and 22.5 hours of dialysis against excess buffer.

We next performed an experiment in which the concentration of Ca^{2+} remaining after dialysis was measured by FAAS and comparison was made between samples containing 10 m*M* $CaCl_2$ in 20 m*M* Na-HEPES pH 7.2 buffer without antibody, 10 m*M* $CaCl_2$ in buffer with 0.9 mg/mL LT3015, 0.9 mg/mL LT1002 in buffer without Ca^{2+}, and 10 m*M* $CaCl_2$ in buffer with 0.9 mg/mL LT1002 (Figure II.3). After 24 hours, the samples containing LT1002 and 10 m*M* $CaCl_2$ were observed to contain significantly higher amounts of calcium on average. These experiments strongly suggest that the anti-S1P antibody is capable of binding Ca^{2+} in solution independent of its antigen.

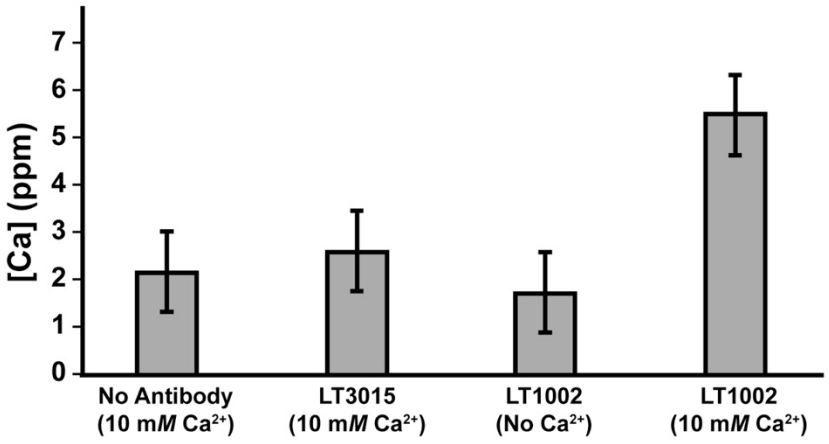

Figure II.3 Comparison of Ca^{2+} concentration measured by FAAS after 24 hours dialysis of 10 m*M* Ca^{2+} in the absence of antibody, in the presence of 0.9 mg/mL LT3015 anti-LPA antibody, and in the presence of 0.9 mg/mL LT1002 anti-S1P antibody.

3.3. Metal ion binding specificity of LT1002

We next wished to determine whether metal ions other than Ca^{2+} are bound efficiently by LT1002 in solution. For this experiment, we again employed replicate measurements of metal ions in solution after equilibrium dialysis in the presence of buffer alone, with LT1002 anti-S1P antibody, or in the presence of control LT3015 anti-LPA antibody. In order to both improve the sensitivity and accuracy of our metal ion detection as well as expand the repertoire of metals we could test, we employed inductively coupled plasma-mass spectrometry (ICP-MS) detection. As observed previously in the FAAS experiments, LT1002 retains Ca^{2+} to a significantly greater degree than the control LT3015 antibody (Figure II.4). Interestingly, we also observe by this approach that LT1002 can bind to Mg^{2+}, though to a significantly lower extent than it binds to Ca^{2+}. It bears mentioning that the original LT1009 anti-S1P antibody Fab:Ca^{2+}:S1P complex crystal was grown in 100 m*M* $MgSO_4$ and that it was initially assumed that the bridging metals in the X-ray crystal structure must be Mg^{2+} before crystallographic model refinement suggested

otherwise. The presence of Ca^{2+} in the complexes was then confirmed by ICP spectroscopy (Wojciak et al. 2009). Taken together these observations suggest that the anti-S1P antibody binds appreciably to Mg^{2+} in solution though it displays a preference for Ca^{2+} when binding to its S1P antigen. This is likely a consequence of the difference in ionic radius of Mg^{2+} and Ca^{2+} and the constraints of coordinating carboxylate groups of three vicinal aspartic acid residues in CDR-L1.

Interestingly, we observe a slight, but significant, increased binding of Ba^{2+} by LT1002 relative to LT3015 control antibody. As mentioned previously, the Ca^{2+}-dependent anti-CD4 antibody Q425 was observed by X-ray crystallography to bind Ba^{2+} at a distinct site at the interface between its variable heavy and light domains. This same site was also observed to house one Ca^{2+} when the Q425 Fab fragment was crystallized in 10 m*M* $CaCl_2$, though the coordination geometry, bond lengths, and ligand atoms are nonideal (Zhou et al. 2005). It is possible that Ba^{2+} could bind in a similar manner in LT1002.

We did not observe significant binding to Sr^{2+}. Similarly, we do not observe binding by LT1002 anti-S1P antibody to any of the transition metal ions tested including Zn^{2+}, Cd^{2+}, Mn^{2+}, Co^{2+}, and Ni^{2+}. Several of these ions require rather specific ligand atom types and bonding geometries, whereas Ca^{2+} has been shown to be capable of adapting to a much broader range of coordination spheres (Katz et al. 1996). Finally, in single experiments we failed to observe any evidence of LT1002 binding with lanthanide metal ions Yb^{3+}, Gd^{3+}, or Eu^{3+} (data not shown).

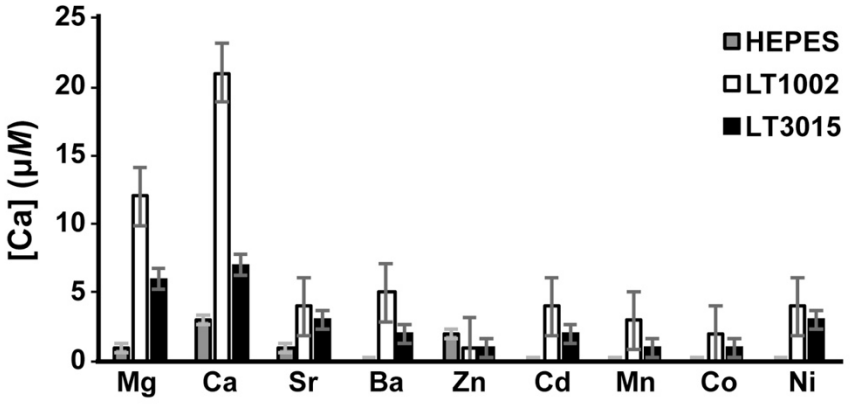

Figure II.4 Average metal ion concentrations after 24 hours of dialysis in the presence of Na-HEPES buffer alone (grey), LT1002 anti-S1P antibody (white), or control LT3015 anti-LPA antibody. Triplicate samples were analyzed by ICP-MS.

3.4. Isothermal titration calorimetry of Ca^{2+} binding to LT1002

In order to thermodynamically characterize the interaction of Ca^{2+} and the anti-S1P antibody in solution, we next carried out isothermal titration calorimetry (ITC). By this approach, controlled amounts of Ca^{2+} were introduced to a HEPES buffered solution of LT1002 antibody and the change in electrical current required to maintain a steady solution temperature is carefully measured. This allows for direct determination of the enthalpy associated with binding. Analysis of the titration endpoint can be fit to determine binding association constants, though which enthalpic components of the binding free energy can be deduced. Through this method, full thermodynamic profiles of metals for proteins, including binding affinities, have been determined (Grossoehme, Spuches, and Wilcox 2010; Wilcox 2008).

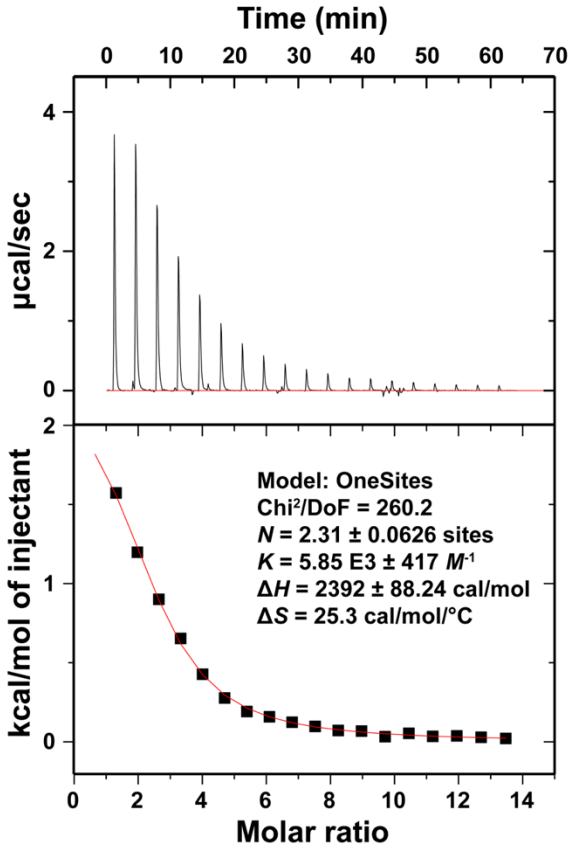

Figure II.5 Isothermal titration calorimetry (ITC) analysis of Ca^{2+} binding by the LT1002 anti-S1P antibody. Binding isotherms were measured as $CaCl_2$ was titrated into a Na-HEPES buffered solution containing LT1002. The data fit to a model in which slightly more than 2 ions bind per site with an equilibrium dissociation constant (K_D) of 177 µ*M*.

ITC measurements on the LT1002 antibody interaction with Ca^{2+} immediately revealed that binding of the metal is an endothermic (heat requiring) process (Figure II.5). This is interesting as it implies that the driving force behind assembly of the observed antibody:metal complex is an increase in entropy (disorder) in the complex relative to the free protein and ions in solution. The increased disorder that accompanies complex formation is almost certainly a consequence of freeing waters from the hydration sphere of Ca^{2+} upon binding to LT1002. Indeed, a similar dependence upon increased entropy is observed when Ca^{2+} is bound by EDTA

in Na-HEPES buffered solution, though the binding affinity is several orders of magnitude tighter for EDTA:Ca^{2+} than we measured for LT1002:Ca^{2+} complex formation (Ràfols et al. 2016).

The titration data were fit starting from a model of two ions per binding event and refined to roughly 2.3 ions binding with an average equilibrium binding affinity of 171 μ*M* (K_D). This represents a relatively low affinity interaction. However, when one considers the energy associated with shielding the charges on the two Ca^{2+} as they bind within close proximity of one another as well as the fact that only three coordination sites on each of the two bound ions are filled by the carboxylate oxygens of the critical four Asp residues, it seems reasonable that the binding affinity would not be too strong. The measured value is certainly consistent with our observation that at 10 m*M* $CaCl_2$, there appears to be full occupancy of Ca^{2+} bound throughout the crystal. From the perspective of physiological relevance, 171 μ*M* is roughly an order of magnitude lower than the typical plasma concentration of Ca^{2+}. This suggests that under physiological conditions, the anti-S1P antibody exists in it predominantly Ca^{2+}-bound state. As indicated from our previous antigen binding and X-ray crystallographic studies, subsequent binding to S1P antigen significantly increases the Ca^{2+} binding affinity. Titration of Ca^{2+} into buffered LT3015 anti-LPA antibody or HEPES buffer alone revealed no interaction between Ca^{2+} and HEPES or the control antibody. Finally, measurement LT1002:Ca^{2+} binding was performed three times with similar results.

3.5. Sequence conservation of LT1002 Ca^{2+}-coordinating residues in other antibodies

Upon confirming that LT1002 binds Ca^{2+} in solution and having previously identified the specific amino acid residues responsible for Ca^{2+} binding, we next sought to determine what

previously characterized antibodies might also contain these residues. To this end, we performed a search through the abYsis database for antibodies with three neighboring Asp residues (corresponding to Asp30-Asp31-Asp32) in CDR-L1 a fourth Asp residue equivalent to Asp92 in CDR-L3 (Swindells et al. 2017). Among the antibodies that fit this profile is the murine Q425 anti-CD4 antibody that has been described previously (Table II.2). Q425 was shown by surface plasmon resonance (SPR) spectroscopy to bind to its CD4 antigen with 85 μ*M* affinity (K_D) in the absence of Ca^{2+} and 1.6 n*M* affinity in the presence of 25 m*M* Ca^{2+}, clearly identifying it as a *bona fide* metalloantibody (Zhou et al. 2005). It is worth noting that when the researchers employed SPR to assess the affinity of Ca^{2+} for Q425 indirectly, they arrived at a value of 187 μ*M*, which agrees surprisingly well with what we measured by ITC for Ca^{2+} binding to LT1002. This is despite the fact that X-ray crystallography of the Q425 Fab fragment in 10 m*M* $CaCl_2$ suggests that only one Ca^{2+} binds to Q425 at a site that differs completely from what is observed in the anti-S1P antibody crystal structures (Zhou et al. 2005).

Table II.2 Conservation of LT1002 metal-contacting residues (bold) in CDR-L1 and -L3

Antibody	**CDR-L1**	**CDR-L2**	**CDR-L3**	**Organism**	**Antigen**	**Metal**
LT1002	ITTTDI**DDD**MN	EGNILRP	LQS**D**NLPFT	Mouse	S1P	Ca^{2+}
Q425	ITSTDI**DDD**MN	EGNTLRP	LQS**D**TLPLT	Mouse	CD4	Ca^{2+}/Ba^{2+}
2C10	ITNTDI**DDD**MN	EGNTLRP	LQS**D**NMPLT	Mouse	dsDNA	
EGFRvIII	ITSTDI**DDD**MN	EGNTLRP	LQS**D**NLPLF	Mouse	EGFR	
Gene	**CDR-L1**	**CDR-L2**	**CDR-L3**	**Organism**		
Igkv17-121	ITSTDI**DDD**MN	EGNTLRP	LQS**D**NLP..	Mouse		
Igkv17-127	ITSTDI**DDD**MN	EGNTLRP	LQS**D**NMP..	Mouse		
Igkv17-134[1]	THNTDI**DDE**MH	EGNTLHP	LQS**G**NMP..	Mouse		
Igkv5-2	KASQDI**DDD**MN	EATTLVP	LQH**D**NFP..	Human		
Igkv17S1	KTSTDI**DDD**MN	EGNTLRP	QQS**D**NVP..	Rat		
Vk5.4	RAGQDI**DDD**MN	DATTLVS	LQH**D**NFP..	Macaque		

[1]Igkv17-134 is a pseudogene

A second antibody identified by virtue of its close homology to LT1002 that includes each of the four Ca^{2+}-coordinating Asp residues is murine 2C10, which was originally identified as an anti-double-stranded DNA (anti-dsDNA) antibody expressed in an MRL/1 mouse model of the autoimmune disease systemic lupus erythematosus (SLE) (Kubota, Akatsuka, and Kanai 1986). Subsequent studies on 2C10 have identified its preference for DNA containing dA:dT base pairs over dC:dG and enhancement of DNA oxidative cleavage (Kubota et al. 1996). Recently, it was shown that 2C10:dsDNA complexes can enter live monocytes in culture and promote the expression of cytokines associated with SLE (Inoue, Ishizawa, and Kubota 2020). No direct evidence for the involvement of divalent metal cations has ever been reported for 2C10, though the potential for metal-mediated coordination to phosphodiesters of the DNA backbone is an intriguing possibility.

A third antibody that shares all of the LT1002 Ca^{2+}-coordinating amino acid residues is the MR1 antibody that binds to a polypeptide epitope near N-terminus of a mutant epidermal growth factor receptor (EGFRvIII). X-ray crystallography of the complex between an MR1 single chain variable domain (scFv) and a 13-mer antigen peptide reveal that none of the CDR-L1 amino acids are involved in antigen binding and that no metal ions are observed or suspected in the complex (Landry et al. 2001). The CDR-L1 loop of the MR1 scFv adopts a conformation that is extremely similar to that observed in the anti-S1P and Q425 X-ray crystal structures and neither it nor CDR-L3 contact antigen directly. Therefore, it is possible that metal binding by the MR1 light chain might serve to enhance the interaction with an even larger epitope. However, a simpler alternative explanation is that antibodies bearing amino acids with Ca^{2+}-binding potential do not necessarily require metals for antigen recognition and binding.

3.6. LT1002 Ca^{2+}-coordinating residues are encoded in diverse light chain germline sequences

One of the fundamental questions that arose in response to our observation of the critical role played by Ca^{2+} in antigen binding by LT1002 regards the manner by which the anti-S1P antibody developed its ability to bind Ca^{2}. Individual antibodies arise in developing B lymphocytes through a series of well characterized yet complicated molecular biological reactions that include somatic hypermutation and recombination of naïve germline-encoded starting sequences throughout the processes of B cell receptor (BCR) gene assembly and antibody affinity maturation (Li et al. 2004). We wished to determine whether the potential for Ca^{2+} binding developed during these processes or if it can be found encoded within the germline DNA sequences of antibody light chain genes. Lacking access to the cells in which the anti-S1P antibody originally developed, we relied upon analysis by the IgBlast server to identify the likely murine variable and joining genes from which LT1002 is derived (Ye et al. 2013). This returned the variable kappa light chain gene Igkv17-121 as an 96.8 % likely source for the LT1002 light chain variable domain (Martinez-Jean, Folch, and Lefranc 2001). Analysis of Igkv17-121 reveals that only nine base mutations differ between what is encoded by the gene and the LT1002 light chain. Of these, five missense mutations alter the identities of amino acids: Ser26 encoded for by the germline sequence changes to Thr in LT1002, Tyr36 becomes Phe, Lys45 is altered to Asn, Thr53 changes to Ile, and Val72 becomes Leu. Notably, the four critical Ca^{2+}-coordinating residues, Asp30, Asp31, Asp32, and Asp92, are present in the naïve germline variable gene sequence (Table II.2). IgBlast identifies Igkj4 as the source for the light chain joining (J) gene.

The heavy chain was identified as derived from in frame junction of Ighv1-78 (V), Ighd1-1 (D), and Ighj2 (J).

Even more intriguingly, the mouse immunoglobulin kappa gene cluster contains a second, highly conserved variable domain sequence, Igkv17-127, that also encodes for the four Ca^{2+}-coordinating Asp residues of LT1002 (Brekke and Garrard 2004). Additionally, the unexpressed variable light chain pseudogene Igkv17-134 bears close homology to the consensus Ca^{2+}-binding motifs (Table II.2). The observation that the Ca^{2+}-coordinating Asp residues are encoded within the germline sequences of two murine variable light chain genes inspired us to seek out similar patterns within other mammalian genomes. Database searches revealed individual genes in each of rat (Igkv17S1), macaque (Vk5.4), and human (Igkv5-2) genomes that bear each of the four Asp residues in positions that correspond to murine LT1002 (Table II.2). Tellingly, the translated amino acid sequences flanking the four Asp residues as well as in CDR-L2 are also highly conserved indicating that these residues play important roles and strongly suggesting that this germline sequence encoding for antibody CDR loops that we have observed to involve bridging metal ions in antibody binding is evolutionarily conserved across diverse mammalian genomes.

3.7. The germline-encoded "precursor" to LT1002 binds Ca^{2+}

In order to test the hypothesis that binding to Ca^{2+} is preserved within germline sequences of antibody light chain genes across diverse mammalian species, we expressed and purified recombinant Fab fragments of the naïve germline-encoded light and heavy chain gene precursors to the murine LT1002 anti-S1P antibody (Figure II.6). Using the approach developed by Furuta,

et al., we engineered recombinant baculovirus containing the germline-encoded naïve sequences for LT1002 light and heavy chains with N-terminal Gp64 signal peptides on each chain and a C-terminal hexa-histidine tag on the heavy chain (Furuta et al. 2010). Our version of the Igkv17-121 light chain gene contained an in frame Igkj4 and constant light chain. Expression of the antibody in Sf9 insect cell suspensions and Western blot detection with an anti-His antibody revealed that significant amounts of the heavy chain were secreted into media and that the size of the heavy chain band correlated to intact, covalently Cys-linked Fab under nonreducing conditions. After optimizing virus titer for optimal expression yield, antibody Fab fragments were purified to homogeneity via nickel affinity and size exclusion chromatography (Figure II.6).

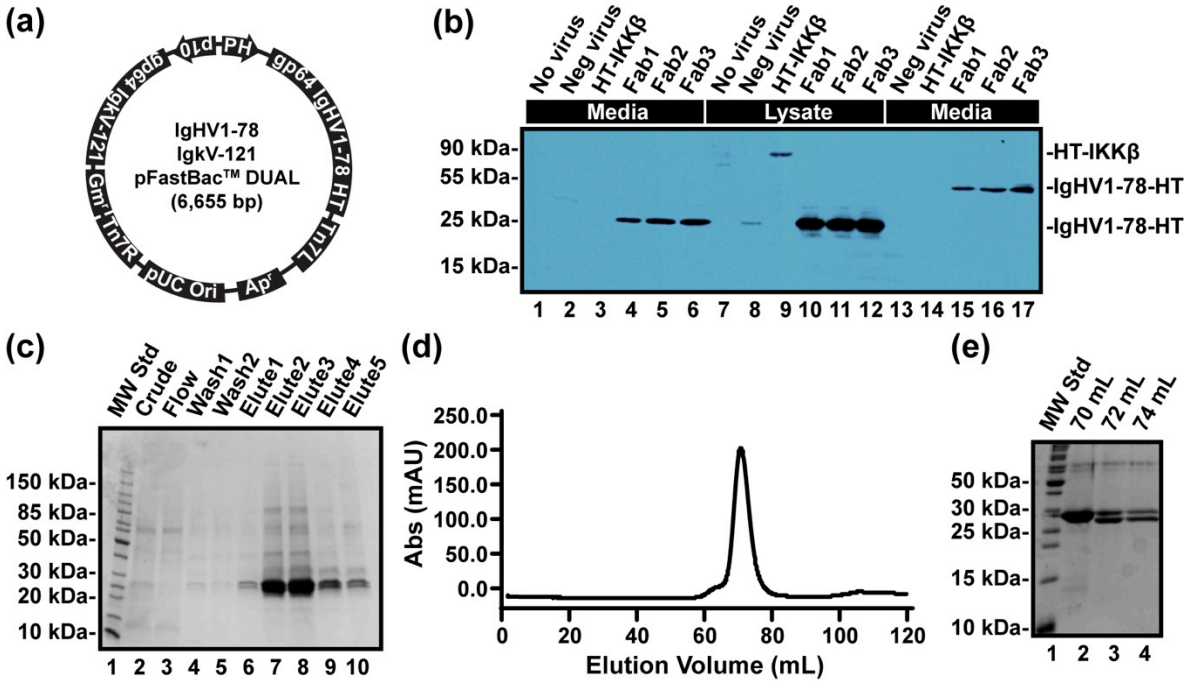

Figure II.6 Expression and purification of LT1002 germline-encoded precursor Fab fragment from Sf9 insect cell suspension cultures. (a) pFastBac Dual plasmid with both heavy and light chain inserted and polyhedrin promoter for the heavy chain and p10 promoter for the light chain was designed. Signal peptide gp64 was used to secret the antibody. (b) Anti-His Western blot detection of secreted metalloantibody precursor Fab fragment from P1 baculovirus-infected Sf9 cells. 1,2, and 3 secreted Fab antibodies, 4. negative control (cells with no virus), 5. negative control (intact virus), 6. IKK (Intracellular protein control), 7, 8, and 9 intracellular Fab antibodies, 10, 11, and 12 negative control, 13,14, and 15 secreted non-reduced Fab antibodies. (c) Coomassie-stained 15% SDS PAGE gel for samples from Ni column purification. The size of Fab antibody is 24kD, and the E2-E4 elutes contain most of the proteins were combined. The double bands show heavy and light chain of the antibody. (d) Size exclusion chromatography using Superdex 75 16/60 of the His-tagged Fab antibody. (e) Coomassie-stained 15% SDS PAGE gel indicating the fractions from SEC column purification.

The purified naïve germline antibody Fab was tested for its ability to bind Ca^{2+} by equilibrium dialysis and ICP-MS. For this experiment, solutions of Na-HEPES buffer at pH 7.2 with and without the addition of 10 m*M* $CaCl_2$ were used as controls to establish the detection range of the ICP-MS instrument (Figure II.7). After extensive dialysis of the buffered 10 m*M* $CaCl_2$ solution, there was almost no Ca^{2+} detected. Incubation of 10 m*M* $CaCl_2$ in the presence of the germline-encoded Fab fragment, however, resulted in retention of a significantly increased

amount of Ca^{2+}. Measurably significant levels of Ca^{2+} were detected after dialysis in the presence of control LT3015 anti-LPA antibody, but these were only slightly higher than for the buffer control. We conclude that the CDR amino acid sequences encoded for by the light chain of murine kappa light chain gene Igkv17-121 and conserved across genomes of diverse mammals harbor inherent Ca^{2+} binding potential.

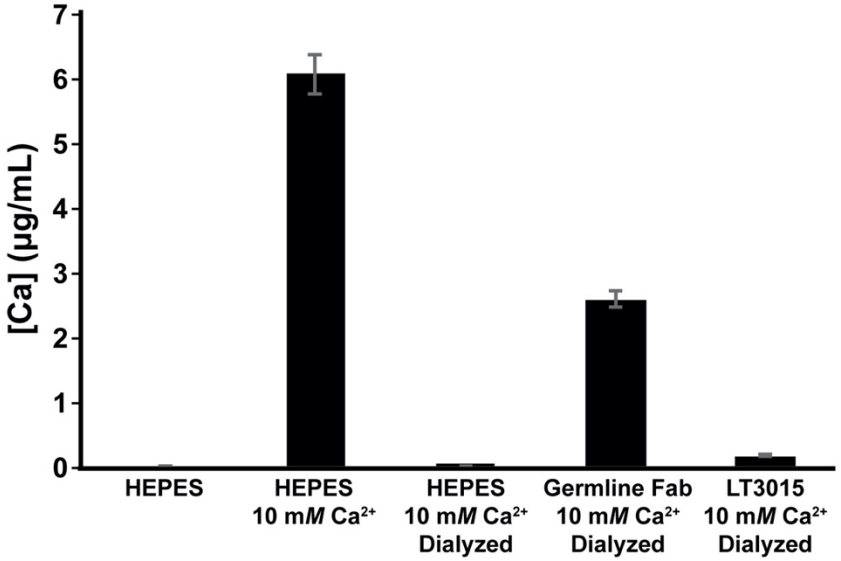

Figure II.7 ICP-MS detection of Ca^{2+} from aqueous samples. "HEPES" and "HEPES 10 m*M* Ca^{2+}" are samples that were not subjected to dialysis and represent the low and high levels of Ca2+, respectively, used in the solutions during this experiment. Samples labeled "Dialyzed" are measured after dialysis against excess Na-HEPES pH 7.2 buffer.

4. Discussion

The incorporation of metals as interfacial bridging factors greatly expands the potential of proteins for folding stability, catalysis, and selective binding to molecular targets. Although numerous metalloproteins have been identified and characterized, the involvement of interfacial metals in antigen recognition by proteins of the adaptive immune system has remained somewhat dubious. Where there is clear evidence for the involvement of metals in antigen binding, as in

the case of CD4 binding by the murine Q425 antibody, it is unclear exactly how Ca^{2+} binding promotes the observed significant enhancement of antigen binding and resultant disruption of HIV infection (Zhou et al. 2005). Another instance of suspected involvement of bridging metal ions in immunocomplex formation involves the human T Cell Receptor (TCR) ANi2.3 that is associated with Ni^{2+}-contact hypersensitivity (Vollmer et al. 1997; Lu et al. 2003). Previous structural and biochemical characterization of a complex between TCR ANi2.3 and MHCII protein DR52c bearing a peptide that was identified by *in vitro* selection to bind with high affinity and activate the ANi2.3 T cell reveals that the ε-amino group from a particular Lys residue on the peptide antigen interacts with TCR residues that likely provide a binding site for a bridging Ni^{2+} (Yin et al. 2012). However, direct observation of the bound Ni^{2+} has not been reported. Our structural and biochemical analyses of the murine LT1002 anti-S1P antibody and its humanized form, LT1009, provide a definitive case for the involvement of Ca^{2+} as a bridging factor to aid in selective binding to a target antigen.

Our X-ray crystallographic data strongly suggest that at 10 m*M* Ca^{2+} concentration and in the absence of S1P antigen, two Ca^{2+} bind at the same site as was observed in the antigen-bound complex. The two Ca^{2+} directly contact Asp30, Asp31, and Asp32 from CDR-L1 as well as Asp92 from CDR-L3 through coordinate bonds that are within the expected range for Ca—O (Gagne and Hawthorne 2016). This arrangement leaves three sites available (assuming octahedral coordination) for each bound Ca^{2+} that can be used to bind antigens. It bears mentioning that this portion of the anti-S1P antibody is exposed to solvent within the crystal and that no atoms from neighboring complexes are involved in stabilizing the two bound Ca^{2+}. We conclude that this is the preferred mode for Ca^{2+} binding to the anti-S1P antibody and that the

presence of antigen, while stabilizing the interaction and shortening the distances between bonded atoms, does not significantly alter the Ca^{2+} binding site. This is an important conclusion as comparison with the antigen-free Q425:Ca^{2+} complex X-ray crystal structure reveals an alternative Ca^{2+} binding site (Zhou et al. 2005). This is despite the fact that the Q425 and LT1002 antibody display 94.7% sequence identity through within their variable domains including sharing all of the LT1002 Ca^{2+}-coordinating residues. In the absence of more detailed study, it is impossible to know for certain how Q425 employs Ca^{2+} to bind to its CD4 antigen. Nonetheless, at present it appears that antibody kappa light chains derived from the murine Igkv-17 might be capable of employing multiple modes of metal binding in order to recognize and bind to diverse antigens.

Our characterization of ion binding by LT1002 in solution reveals that Ca^{2+} is preferred, though Mg^{2+} can also associate with the anti-S1P antibody. Ca^{2+} and Mg^{2+} bind to similar sites on proteins although, due primarily to the greater ionic radius of Ca^{2+} and consequent exclusive requirement for monodentate ligand binding, with differing consequences. In several notable cases, Ca^{2+} binding impedes catalysis by metalloenzymes where the smaller Mg^{2+} co-factor favors it (Mordasini, Curioni, and Andreoni 2003; Peeraer et al. 2004). ITC revealed a relatively low Ca^{2+} binding affinity for LT1002 with a measured dissociate constant (K_D) for binding to two Ca^{2+} at 171 μ*M*. This is significant on several counts. First, this is roughly ten times lower than the typical concentration of Ca^{2+} in blood plasma, which suggests that LT1002 is generally preloaded with Ca^{2+} as it circulates in the blood stream. We had previously speculated that the antibody might bind to Ca^{2+} and S1P simultaneously through a concerted binding mechanism or that initial antigen binding might induce subsequent affinity for Ca^{2+}. In light of the present

study, we are confident that circulating anti-S1P antibodies associate with Ca^{2+} independent of antigen. Secondly, the low affinity correlates with the significant increase in bond distances to the two Ca^{2+} ions observed in the antigen-free X-ray crystal structure relative to its S1P antigen-bound structure. This suggests that the Ca^{2+} are bound with significantly higher affinity upon antigen binding and explains why Ca^{2+} remained bound even at 100 m*M* Mg^{2+} concentration used for crystallization of the S1P antigen-bound complex (Wojciak et al. 2009). Finally, our measured value for Ca^{2+} binding agrees remarkably well with that deduced in an elegant SPR study on the closely related anti-CD4 Q425 antibody (Zhou et al. 2005).

Identification of the interfacial Ca^{2+}-coordination signature (three neighboring Asp residues at positions 30-32 in CDR-L1, Asp at position 92 in CDR-L3) in other antibodies immediately raises the question of whether implementation of bridging Ca^{2+} ions is a common mechanism employed by antibodies? Other than Q425, neither of the other two antibodies identified as containing the Ca^{2+}-coordination signature, the 2C10 anti-dsDNA antibody and the MR1 anti-EGFRvIII antibody, are known or suspected to rely upon bridging metal ions to bind their respective antigens. By expressing the murine Igkv17-121 germline sequence as part of a naïve antibody Fab fragment and confirming its ability to bind Ca^{2+} in solution, we have proven that Ca^{2+} binding potential is inherent to these sequences and preserved within the mouse germline repertoire. Our observation of antibody light chain genes that contain the Ca^{2+}-coordinating residues within germline sequences of diverse mammals makes a strong case for interfacial Ca^{2+}-dependent antigen recognition as an evolutionarily conserved component of the mammalian antibody repertoire.

Acknowledgment

Lastly, I would like to thank my co-authors on the paper we are publishing Aaron D. Ward, M. Frank Erasmus, Jonathan Wojciak, and Jonathan K. Fleming. Chapter II is currently being prepared for submission for publication of the material. The dissertation author is the primary author of this chapter.

Chapter III

X-ray crystallography of two camelid VHH antibodies with PcrV antigen

1.Introduction

Pseudomonas aeruginosa is a gram negative bacteria that its infections can cause disease and death among people with weakened immune responses, such as individuals suffering from HIV, acute pneumonia, cancer patients, or burn victims. People with cystic fibrosis also suffer from *Pseudomonas* (Kobayashi, Kobayashi, and Kawai 2009; Trautmann, Lepper, and Haller 2005). An important virulence factor of this bacteria shared with other gram negative bacteria is the type III secretion system (T3SS). T3SS is molecular needle machinery that transfers effector proteins directly from the bacterium cytosol into the host cell. This complex macromolecular machine can manipulate into the host cell in many different ways and works regulated (Galle, Carpentier, and Beyaert 2012). Recently, cryo-electron microscopy studies have investigated to find out the structure of T3SS. The virulence factors of T3SS has been a target site for many vaccines and therapeutics. T3SS uses a needle-like shape to transfer the effector protein into the host cell. T3SS assembly has different components including: a cytosolic ATPase complex, a cytoplasmic ring (C-ring), an inner membrane export apparatus, a basal body (which is in the bacterial inner and outer membranes, and encircles an inner rod and a needle), and a translocation pore in the host cell membrane (Figure III.1). The tip of the complex is responsible for sensing the environment around the host cell, regulation of secretion, and physically bridging the needle into the host membrane and facilitate the translocon pore in host cell membrane (Deng et al. 2017).

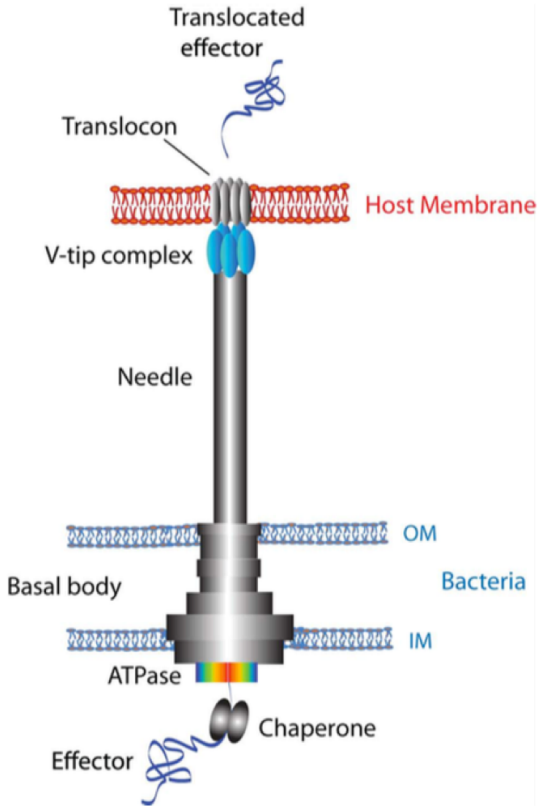

Figure III.1 Simple model that overviews the key structural elements for T3SS. The inner membrane and bacterial cytoplasm include ATPase complex, C-ring, Chaperone and Effector protein. The periplasm includes the basal body and the outer membrane includes the needle shape which connects to the V-tip complex and translocon pore in the host cell membrane (Sato and Frank 2011).

One of the unique mechanisms in T3SS is that the secreted protein does not have a conserved cleavable signal. Type III secreted proteins have a secreted signal and are enriched with serine, threonine, isoleucine and proline but have limited peptide sequence that is conserved. This explains why type III secretion signal can handle multiple mutations (Anderson 1997).

Moreover, studies have shown that an unknown signal triggers the conformational change of the translocator and follows with host cell contact. This leads to the interaction between the translocator and the tip protein known as PcrV (Armentrout and Rietsch 2016). PcrV is an essential part of *Pseudomonas* T3SS secretion system that has the ability to infect and kill the host cell. By knocking down the PcrV gene, the exotoxins leak to the bacterial growth medium results in stopping the cytotoxicity *in vivo* and *in vitro*. Therefore, PcrV is an attractive target for blocking *Pseudomonas* infection in patients (Audia et al. 2013; Lee et al. 2010).

Furthermore, recent studies have focused on nanobodies, which are the novel class of therapeutics. Nanobodies are based on immunoglobulin single variable domain. It could be derived from variable heavy chain only. These antibodies naturally derive from camelids. The benefits of using single chain heavy variable domain over the conventional antibodies is: (i) superior solubility, (ii) biophysically stability and (iii) easy amenability of connecting monovalent nanobodies with a linker sequence to form multivalent polypeptide chain (Coppieters et al. 2006; Jahnichen et al. 2010).

InhibRx, LLC is a San Diego-based pharmaceutical company that has raised antibodies that specifically bind to PcrV. The antibodies bind to the foreign pathogen and stabilize it for removal by blood cells. The InhibRx scientists chose camels for their source of anti-PcrV antibodies. We collaborated with InhibRx to use their camelid antibodies and prepare stable complexes with PcrV and crystalize and determine the complex structures. Unfortunately, PcrV is very flexible to crystallize on its own; therefore, we suspect that this is due to the inherent

flexibility in PcrV. Moreover, LcrV (Protein Data Bank entry 1R6F) is PcrV homologe that has been crystallized before. Figure III.2 is showing PcrV homologous and their similarity.

		No. of residues	Global alignment[a] with PcrV identity (similarity)	GenBank accession no.
V-tip protein (Ysc family)				
PcrV	*Pseudomonas aeruginosa*	294	Strain PA103, ours	
LcrV	*Yersinia* spp.	326	36.4% (64.4%)	P23994
AcrV	*Aeromonas* spp.	361	34.2% (59.8%)	YP_001144289
Vp1659	*Vibrio para-haemolyti-cus*	607	35.3%[b] (55.7%[b])	NP_798038

Figure III.2 Homologous of PcrV. It is showing V-tip protein Ysc family: PcrV, LcrV, AcrV and Vp 1659. There is 36.4% identity between PcrV and LcrV and 64.4% similarity (Sato and Frank 2011).

Figure III.3 is showing models of V-tip protein family. Using LcrV as a template, the other models were made by using Discovery Studio 3.0 software. The model is showing a conserved coiled-coil structure of two α-helices by globular domains at each end (Sato and Frank 2011).

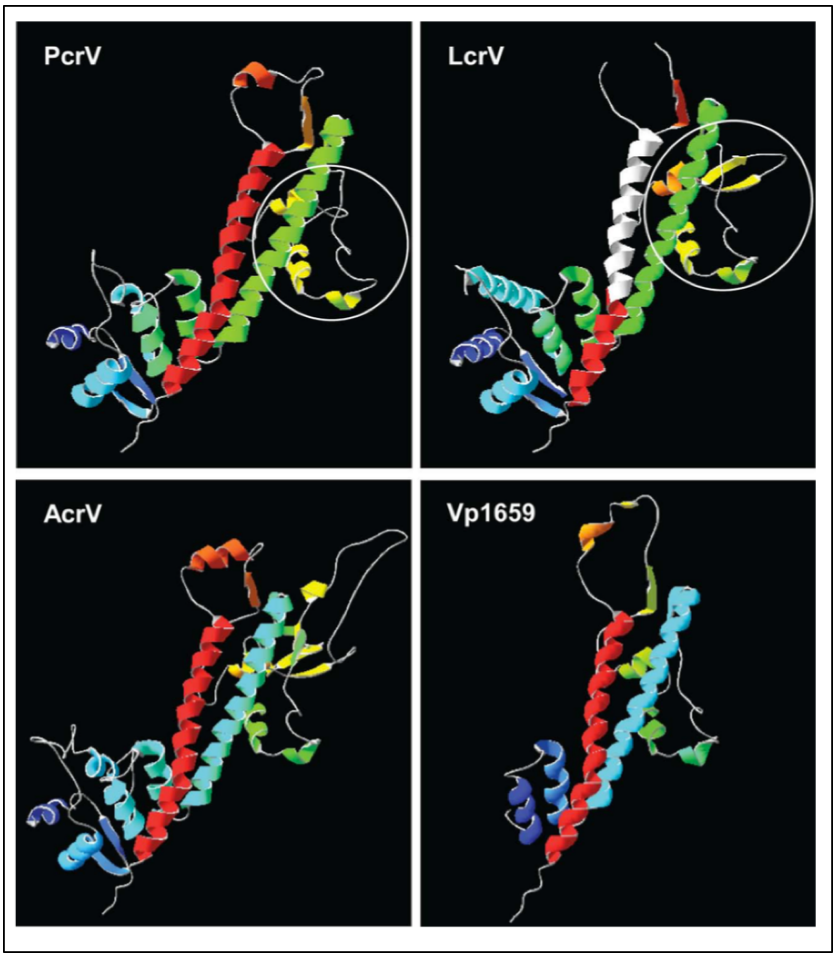

Figure III.3 Structural models of V-tip protein family. In all models coiled core α-helices structure is conserved. The white circle on the globular domain on PcrV and LcrV is indicating the epitope protecting (Sato and Frank 2011).

By looking at LcrV sequence, we found out that the first 24 amino acid residues of PcrV causes its flexibility and this is the reason it did not crystallize (Derewenda et al. 2004). Therefore, we removed 24 amino acid at the beginning of PcrV sequence and prepared the antibody:PcrV complex: PcrV:VHH15, PcrV:VHH18, PcrV:VHH15:VHH18, and PcrV:VHH18:VHH20. We were able to crystalize and solve the crystal structure at high (near atomic) resolution by X-ray crystallography. This is the first time that high resolution

crystallographic models of PcrV has been solved and it can help in the development of the next generation of therapies that target *Pseudomonas aeruginosa* infection.

In order to find out that bispecific VHH antibodies can bind to PcrV and neutralize the pathogen, we crystallized and solved PcrV with two covalently linked camelid antibodies structure.

2.Materials and Methods

2.1 PcrV and VHH plasmid

InhibRx, LLC has produced and supplies VHH15, VHH18 and VHH20 nanobodies with PcrV. The plasmid used for expression of PcrV-His tagged was pET15b and the plasmid used for PcrV with the nanobodies was pET21-PcrV (15,18,20)-VHH. Table III.1 describes the vector, plasmid name, number of amino acids, molecular weight, extinction coefficient and isoelectric point for PcrV and VHH nanobodies.

Table III.1 PcrV:VHH complex plasmid and vector.

Name	**Vector**	**Plasmid name**	**AA**	**MW**	**pI**	**Ext. coeff.**
PcrV-His	pET15b	pET15b-PcrV	314	34446.8	5.75	0.868
PcrV15-VHH-His	pET21	pET21-PcrV15-VHH	133	14662.4	8.64	1.642
PcrV20-VHH-His	pET21	pET21-PcrV20-VHH	133	14659.5	9.49	1.572
PcrV18-VHH-His	pET21	pET21-PcrV18-VHH	132	14574.24	9.03	1.754

2.2 PcrV:VHH complex preparation

We prepared PcrV:VHH15, PcrV:VHH18, PcrV:VHH15:VHH18, and PcrV:VHH18:VHH20 complexes using the 1:2 ratio. We were expecting that PcrV has two binding sites. After preparing the complexes, I ran it on superdex 75 16/60 size exclusion column that was connected to ÄKTA (GE Healthcare), it has been equilibrated with SEC buffer pH 7.5 (25 mM Tris-HCl pH 8.0, 150 mM NaCl). Fraction collector at 2 mL per fraction collected purified protein, and peak fractions has been combined and concentrated with 50 kDa-cutoff membrane concentrator (Millipore) to 10 mg/mL. Protein was flash frozen in liquid nitrogen and stored at -80°C. Protein concentration was determined by BioRad Protein Assay (BioRad). After collecting the samples from size exclusion column, I ran them on 15% SDS-PAGE gel to confirm the right molecular weight for the antibody: antigen complex and the nanobodies.

2.3 Removing His-tagged PcrV using Thrombin

In order to further stabilize PcrV and be able to crystalize it, I removed His-tagged from PcrV using Biotinylated Thrombin. PcrV has a cleavable specific Thrombin cut site sequence, which is LeuValProArg↓GlySer that cuts between Arg and Gly. I used the Novagen Biotinylated Thrombin kit and I incubated PcrV with different amounts of enzyme by making a serial dilution of Thrombin in Thrombin storage/dilution buffer, the dilutions were from 1:25, 1:50, 1:100 and 1:200 ratio. This dilution will contain approximately 0.04, 0.02, 0.01, and 0.005 U enzyme per µL. Also, I used different reaction (incubation) time at room temperature by taking 10 µL aliquots into 10 µL 2X SDS sample buffer after 2, 4, 8 and 16 h. Finally, I used different concentrations of PcrV in order to reach the optimum pure PcrV without His-tag.

2.4 PcrV: VHH15:VHH18 complex formation and co-crystallization

One of the methods used for crystallization of protein samples is sitting drop vapor diffusion method. I used Crystal Nanoliter Protein Crystallization Robot (mosquito®) to set up the crystal trays in Swissci 96-well 2-drop MRC Crystallization Plates. Different conditions of crystal screen were used, such as: PEG/Ion, HR2-126, PEG/Ion 2, HR2-098, Index HR2-144, Crystal Screen HT, and HR2-110 are from Hampton Research. Also, I used MCSG-1, MCSG-2, MCSG-3, and MCSG-4 Crystal Screen from Microlytic for extensive screening. In order to grow better crystals, I have optimized the crystal screening solutions by using different range of pH (4.0-10.5), different concentrations of PEG, different concentrations of Tris buffer and etc. Furthermore, I have used the micro seeding technique to grow larger crystals by using micro crystal of PcrV complex with the antibody and mixing it with optimized reservoir solution. In order to monitor crystal trays, I used automated Formulatrix Rock Imager.

Another method to grow crystals is hanging drop vapor diffusion method. For this method, I used 24-well plates at room temperature. Hampton research crystal screen HR2-110 was diluted with water by 1:2 ratio. 1 µL of protein was combined with an equal amount of reservoir solution on the surface of a siliconized glass cover slip. The slip was sealed with high vacuum grease over 1 mL of reservoir solution to allow for slow equilibration.

2.5 X-ray crystallography and structure solution and refinement

Synchrotron data were collected on a ALS 5.0.2 detector at the Advanced Light Source Beamline from Berkeley National Laboratory. Indexing and scaling was carried out with HKL2000 (Otwinowski and Minor 1997) and subsequently converted using ScalepacktoMTZ

within CCP4; data collection statistics are presented in Table 2. Molecular replacement was performed via Phaser-MR (McCoy et al. 2007) in PHENIX using LcrV (PDB ID 1R6F) as a probe with ions, antigen, and solvent molecules removed. Model building was carried out in COOT (Emsley and Cowtan 2004). All further refinements were made in PHENIX. Analysis was provided by MolProbity (Davis et al. 2007).

3.Results

We were able to crystalize PcrV: VHH15:VHH20 complex and solve the crystal structure with 2.67 Å resolution. This was the first time that crystal structure of PcrV with two covalently link VHH nanobodies was solved. In order to crystalize the complex, 24 amino acids were removed from the N-terminus of PcrV (PcrVΔ24).

3.1 Removing His-tag from PcrV using Thrombin

By using Biotinylated Thrombin, I removed the His-tag from PcrV. Figure III.4 is showing 15% SDS-PAGE gel where His-tag of PcrVΔ24 was removed. Based on incubating different Thrombin dilutions and with different incubation time, I used 4 hrs incubation with 1:200 ratio of diluted Thrombin in the dilution buffer.

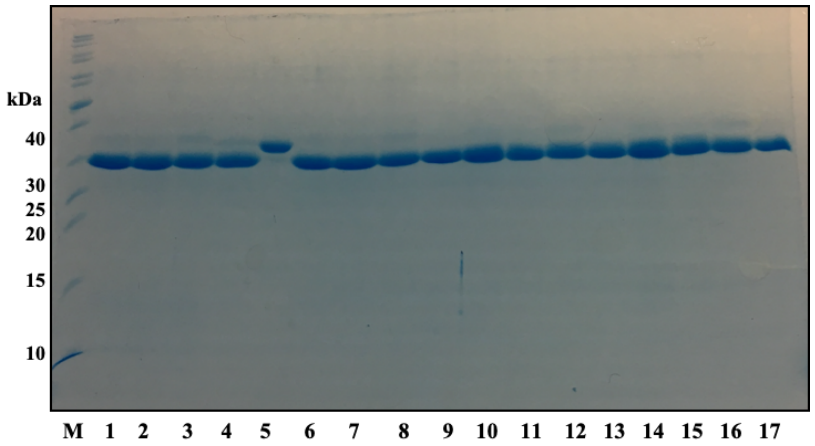

Figure III.4 Using Thrombin to remove His-tag from PcrV shown with 15% SDS-PAGE gel. First lane is the molecular marker, Lane 1is Thrombin dilution 1:25 ratio, Lane 2 is 1:50 ratio, Lane 3 is 1:100 ratio and Lane 4 is 1:200 ratio after 2 hrs. Lane 5 is the negative control. Lane 6 is Thrombin dilution 1:25 ratio, Lane 7 is 1:50 ratio, Lane 8 is 1:100 ratio and Lane 9 is 1:200 ratio after 4 hrs. Lane 10 is Thrombin dilution 1:25 ratio, Lane 11 is 1:50 ratio, Lane 12 is 1:100 ratio and Lane 13 is 1:200 ratio after 8 hrs. Lane 14 is Thrombin dilution 1:25 ratio, Lane 15 is 1:50 ratio, Lane 16 is 1:100 ratio and Lane 17 is 1:200 ratio after 16 hrs.

3.2 PcrV: VHH15:VHH18 complex formation and purification

Figure III.5 is indicating the complex formation of PcrV: VHH15:VHH18 using superdex 75 16/60 size exclusion column that was connected to ÄKTA. The top figure is the overlay chromatograms of PcrV: VHH15, PcrV: VHH18, PcrV: VHH15:VHH18, and PcrV: VHH18:VHH20 complexes. The peak that was eluted at 50 mL is the complex and the peaks that elute at 80-90 mL are the excess VHH antibody. Among all complexes, we were able to crystalize PcrV: VHH15:VHH18 complex. The bottom figure shows the complexes prepared from ÄKTA on 15% SDS-PAGE gel. The molecular weight of VHH and the PcrV are approximately 15 kDa and 30 kDa, respectively.

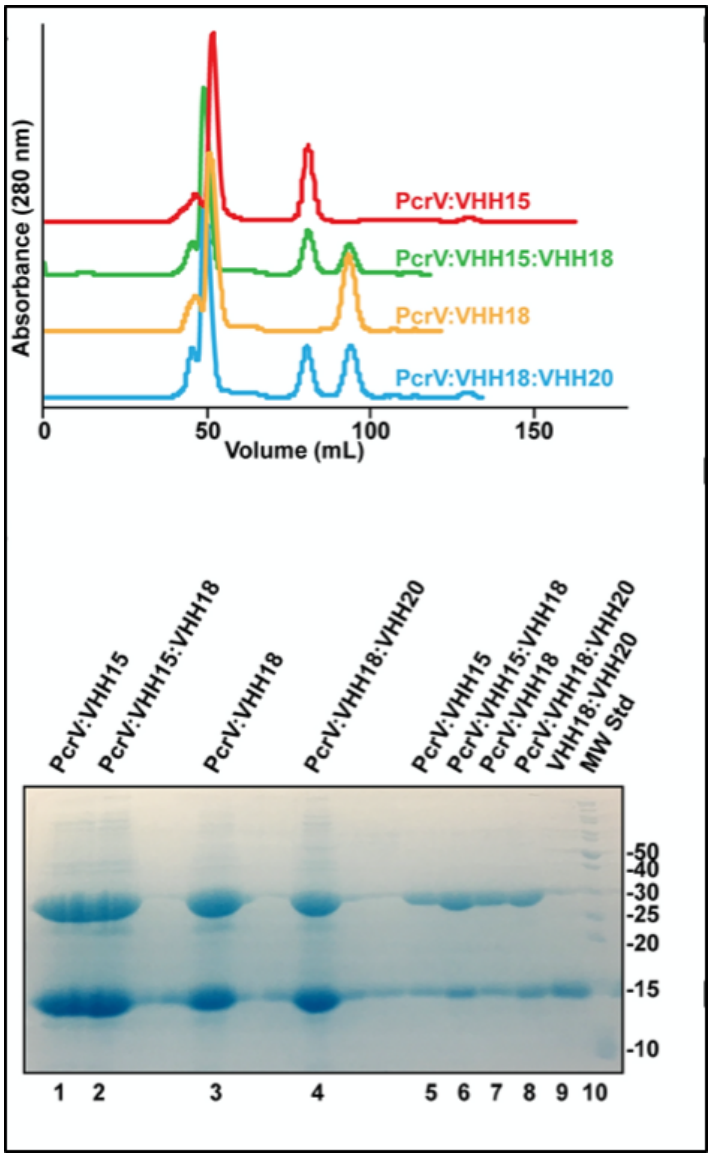

Figure III.5 PcrV:VHH15:VHH18 complex formation and purification. Top part is chromatograms monitoring the absorbance of protein complexes as they elute from a size exclusion column. The major peaks in each of the four runs are the PcrV: Antibody complexes indicated. Excess antibody peaks elute between 80-90 mL. The bottom part is coomassie-stained 15% SDS-PAGE gel showing the PcrV: Antibody complexes before (lanes 1- 4) and after (lanes 5-8) size exclusion chromatography. Lane 9 shows excess VHH18 and VHH20 antibodies, and lane 10 is a molecular weight standard.

3.3 Crystal screening of PcrV: VHH15:VHH18 complex

In order to grow crystals, I used different crystal screening solutions. By using sitting

drop diffusion method with mosquito robot, we first got microcrystals by using 2.0M sodium formate, 0.1M Bis-Tris propane pH 7.0; 0.1M Na_2HPO_4/KH_2PO_4 pH 6.2; 25 % (v/v) 1,2-propanediol, 10 % (v/v) glycerol screen solution. Also, we got needle cluster by using 10% PEG 8K; 10% EG; 0.1M HEPES screen solution. Then, we got hexagonal plate by using 1.5M ammonium chloride; 0.1M Bis-Tris propane pH 7.0; 0.1M imidazole: HCl, pH 8; 1M ammonium phosphate dibasic screen solution (Figure III.6A). Figure III.6B is showing larger crystals that grow over time by crystallization by hand using hanging drop diffusion method.

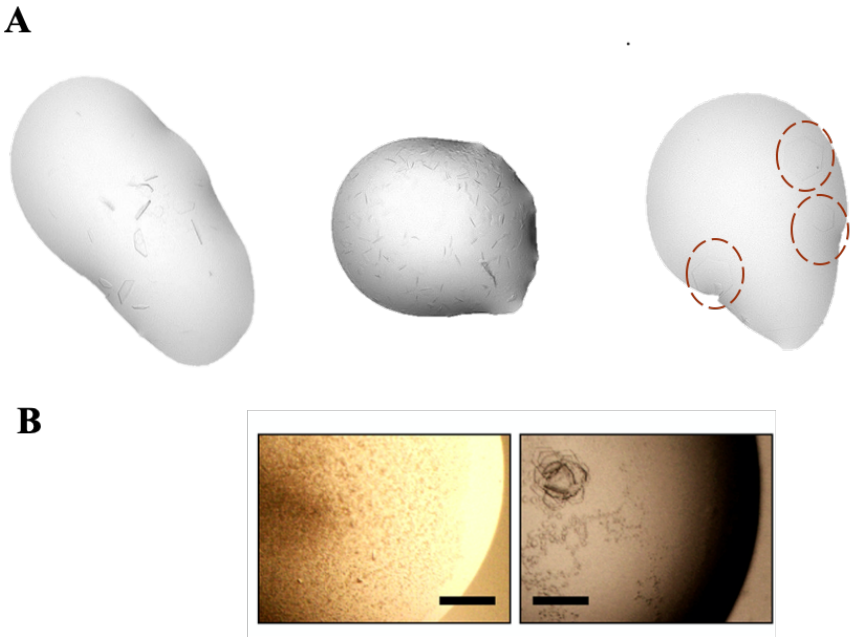

Figure III.6 Crystal figures for PcrV: VHH15:VHH18 complex (A) Photographs of microcrystals, needle clusters and hexagonal plates setting up by robot. The dotted red circles are showing the hexagonal plates. (B) Photographs of initial crystals of PcrV: VHH18:VHH20 (left) and PcrV: VHH18:VHH20 (right) complexes. The black bar is 100 μm.

3.4 Collection of the X-ray Diffraction

After crystallization of the complex, we have stored the crystals in optimum cryo solutions to avoid icing on the crystals. The crystals were shipped to Berkeley National

Laboratory. Synchrotron data were collected on ALS 5.0.2 detector at the Advanced Light Source Beamline. The crystal was mounted in front of the X-ray beam and the diffraction pattern of crystal was collected at different angles (Figure III.7). Complete X-ray diffraction data were collected at 2.67 Å resolution.

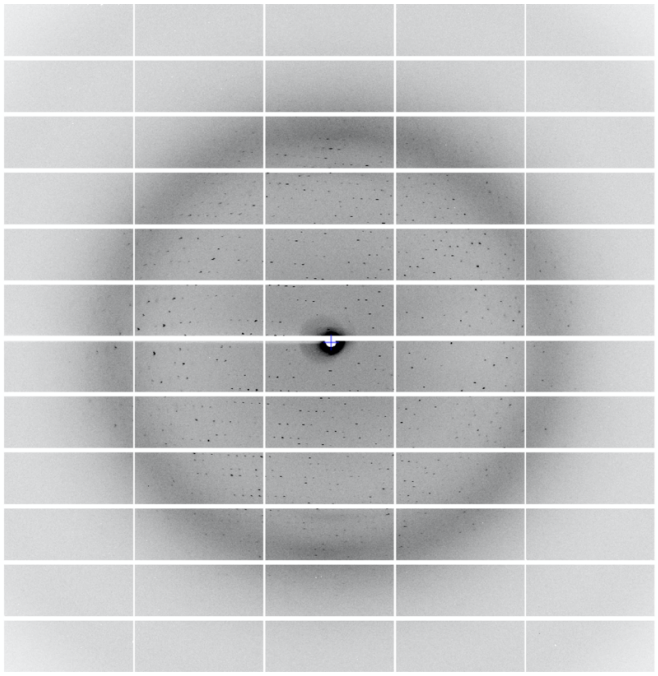

Figure III.7 Diffraction of protein crystal PcrV:VHH15:VHH18 in front of X-ray beam.

3.5 Table and refinement statistics

After collecting the diffraction pattern we used molecular replacement that was performed via Phaser-MR (McCoy et al. 2007) in PHENIX using LcrV (PDB ID 1R6F) as a probe with ions, antigen, and solvent molecules removed. Model building was carried out in COOT (Emsley and Cowtan 2004). All further refinements were made in PHENIX. Analysis was provided by MolProbity (Davis et al. 2007). The crystal was determined to be

made up of cubic unit cells with the space group P32. The dimension of the unit cell is a=106.56Å, b=106.56Å, c=126.45Å, and α=90°, β=90°, γ=120°.

Table III.2 X-ray crystallography data collection and refinement statistics.

Title 1	**Title 2Title 3**
	PcrV:VHH15:VHH18
Data collection	
X-ray source	ALS 5.0.2
Wavelength (Å)	1.0000
Space Group	*P32*
Unit cell (Å)	
a, b, c (Å)	106.56, 106.56, 126.45
α, β, γ (°)	90, 90, 120
Resolution Range (Å)[1]	126.44-2.67 (2.80-2.67)
R_{sym} (%)	14.9 (76.9)
Observations	229,021
Unique reflections	24,086
Completeness (%)	100.0 (100.0)
Redundancy	9.5 (9.6)
Average intensity (<*I*/σ>)	8.0 (1.8)
Refinement	
Number of reflections	22,799
R_{cryst} (%)	19.3 (31.5)
R_{free}[2]	26.8 (44.0)
Protein Atoms	4,055
Water Atoms	107
R.m.s.d.	
Bond lengths (Å)	0.014
Bond angles (°)	1.673
Mean B (Å^2)	86.57
Ramachandran plot[3]	
Favored	92.0
Allowed	6.2
Disallowed	1.8
MolProbity score[4]	2.39
PDB accession code	N/A

3.6 X-ray crystal structure of PcrV: VHH15:VHH18 complex

X-ray crystal structure of PcrV: VHH15:VHH18 complex indicates that the complex by itself is monomer but in the unit cell forms a trimer. Each VHH antibody at both ends of PcrV is

twisting with a 3- fold rotational symmetry. Figure III.8 shows the X-ray crystal structure of PcrV with VHH15 and VHH18.

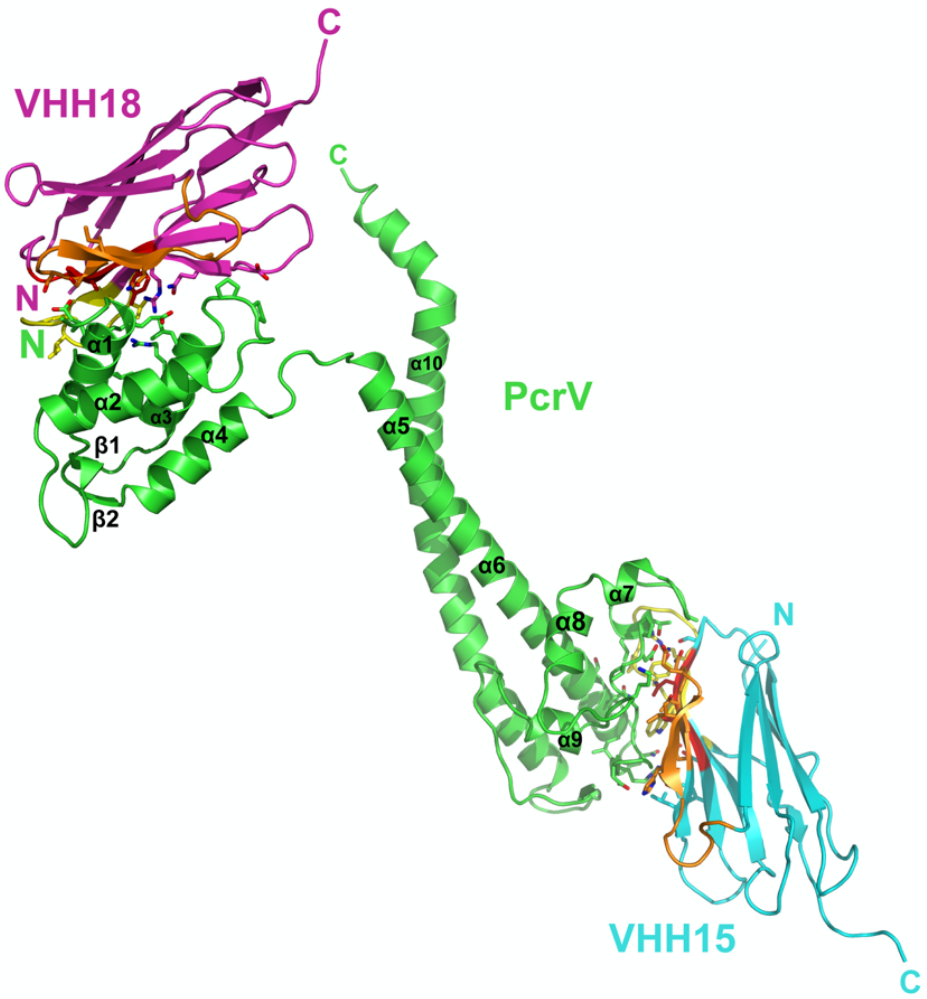

Figure III.8 X-ray crystal structure of PcrV:VHH15:VHH18 complex depicted in ribbon diagram. PcrV is illustrated with green color VHH15 and VHH18 are illustrated in cyan and purple color respectively. PcrV is represented as coiled core α-helices structure and VHH15 and VHH18 nanobodies have, immunoglobulin domains. Individual immunoglobulin domains VHH15 and VHH18 are presented at N- and C-termini of PcrV.

4.Conclusion and future direction

We were able to successfully get the crystal structure of PcrV with two covalently linked camelid nanobodies VHH15 and VHH18 for the first time. PcrV has always been an interesting

target for drugs. PcrV is the protein tip at the T3SS secretion system found in many gram-negative bacteria. PcrV has an essential role, which is the interaction of the needle-shape protein secretion system of T3SS to the host membrane cell. Disrupting PcrV can lead to the effector protein leakage and T3SS not working effectively. Many scientists have tried to crystallize PcrV with antibodies but because PcrV is very unstable, they were not able to crystalize it. As we searched further in the literature, we found out that the homolog of PcrV, LcrV has been crystallized before. By looking at its sequence, we found out the reason that PcrV is not crystalizing is due to the first 24 amino acid of the protein, which makes it floppy. By removing the amino acids and the His-tag from PcrV, we were able to get microcrystals, but with optimizing the crystal screening solutions we got crystals that were about 100 μm big. Also, the diffraction data confirmed that our results were good.

The crystal structure indicates that both VHH15 and VHH18 binds simultaneously to opposite ends of PcrV protein. Furthermore, in the crystal, PcrV forms an intertwined trimer (see the monomer illustration of the structure in Figure III.8). Moreover, the placement of VHH15 and VHH18 of neighboring PcrV proteins correlates with the length of the linker in the most potent bivalent antibody-based antibiotic.

For future research, I would like to suggest *in vivo* studies to test the efficiency and pharmacokinetics of camelid antibodies on *Pseudomonas aeruginosa* infection. Also, by looking at the literature, I found out that PcrV models are assembled as oligomers, possibly forming pentameric rings on top of *P. aeruginosa* T3SS needle. This model suggests multiple binding sites for PcrV. The potent nanobodies used for this therapy could be bivalent (combinations of two identical) and biparatopic (combinations of two different) nanobodies instead of monovalent

antibodies. By looking at our data, we found out that our crystal forms trimer in a unit cell, which could be consistent with the model suggesting oligomeric compound. In order to find out multiple binding sites on PcrV, screening biparatopic nanobodies library is necessary and we can test this with binding ELISA signals of nanobodies. By mutations of the binding sites, we can measure different antibody binding to PcrV.

Chapter IV

Engineering novel selectivity into metalloantibodies

1.Introduction

Metalloproteins have been identified either as catalytic enzymes or metals as cofactors for proteins, such as hemoglobin or cytochrome-c. Among many metalloproteins, Zn^{2+}, Cu^{2+} and Fe^{2+} are the most active metals used in metalloprotein structure. Our metalloantibodies binds to Ca^{2+} and much less extent to Mg^{2+}; therefore, we were interested in changing the metal binding to some interesting metals like zinc.

Engineering selectivity of metalloantibodies and antibodies generation can occur with site directed mutagenesis and phage display method. Nowadays, human antibodies are generated *in vitro* by antibody engineering technologies, such as phage display, construction of antibody fragments, immunomodulatory antibodies, and cell-free systems (Edwards and He 2012).

We were interested in using site directed mutagenesis to change the amino acid sequence on the CDRL1-L3 loops of the antibody. X-ray crystallography has showed us the binding coordinate sites of the antibody to metals. Aspartic acid 30-32 and aspartic acid 92 were the involved residues in the metal coordination site, therefore, we were interested to structurally change the amino acids that were involved in the metal coordination site (Figure IV.1). Moreover, by changing the residues we were expecting to change the specificity of the antibody to different metals. I have changed aspartic acids (D30,31,32) to cysteine (C30), histidine (H31) and cysteine (C32) and aspartic acid (D92) to histidine (H92). I also generated two other construct D3192H and D30D32C in order to change the metal binding coordination of the antibody from Ca^{2+} to Zn^{2+}, Ni^{2+} and Co^{2+}.

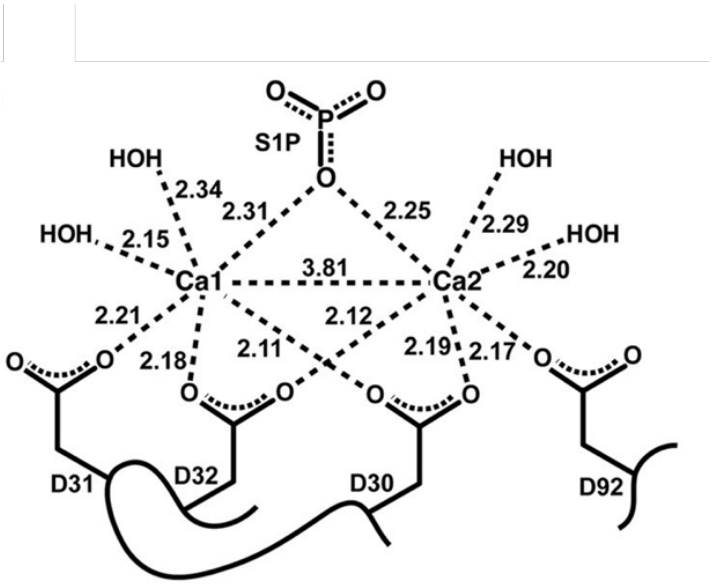

Figure IV.1 Schematic diagram of CDR loops of the light chain in coordination with Ca^{2+} and S1P. The bond lengths are shown in Å and the amino acid involved in the interaction are labeled (J. M. Wojciak et al. 2009).

With these sites directed mutagenesis, we wanted to test whether D3192H interacts with Cu^{2+} or D3032C interacts with Fe^{2+} or Cu^{2+}. As we searched in the literature, we found the protein copper complexes have the metal coordination by two histidine and a cysteine residue and the metal is used as a cofactor for protein. One example of that protein is amicyanin, which is a type I copper protein and is involved in electron transfer. In bacteria like *Paracoccus denitrificans*, amicyanin is part of the three membrane redox complex with methylamine dehydrogenase (MADH) and cytochrome c (Holm, Kennepohl, and Solomon 1996).

However, metal-to-donor atom coordination and distances and angles in proteins are also important in the metal protein binding. In small molecule crystal structure, the target distance between metal and the donor atom is usually within a + 0.75 Å distance (Harding 2002).

Moreover, looking at zinc finger motifs, one will find out that Cys_2His_2 like fold group is characterized as a zinc finger motif, which is common in mammalian transcription factor (Pabo,

Peisach, and Grant 2001). Engineered zinc finger motifs are applied in zinc finger transcription factors and zinc finger nucleases. There are other applications to zinc finger motifs that have been discovered (Jamieson, Miller, and Pabo 2003). In this case the metalloprotein is a catalytic enzyme.

Using site directed mutagenesis, we were able to express metalloantibody that binds to zinc with the D3032C/D3192H construct. We have confirmed its metal binding using Inductively Coupled Plasma-Mass Spectrometry **(**ICP-MS) and Microscale Thermophoresis (MST). In this chapter, I introduce the method that I used for mutating key residues as well as protein expression and purification of the mutant antibodies with the results from ICP-MS and MST techniques that I used.

2.Materials and Methods

2.1 Cloning heavy and light chain genes into pFastBac Dual plasmid

The mouse IgG has been found from database searches of Ig germline genes, and it is closest to murine LT1002. The pFastBac Dual plasmid was generated by miniprep IgKV17-21 and IgHV178 from pUC57 (GenScript) into XL1-Blue cell line and measured the concentration of DNA plasmid using Nanodrop. The signal peptide gp64 that working for both antibody and Sf9 cells were inserted in the beginning of the heavy chain for the antibody to be secreted out from the insect cell.

Double digestion of the pFastBac Dual plasmid with NEB enzymes were done with EcoRI-HF and NheI-HF enzymes in cut smart buffer. I ran the plasmid on 1% agarose gel after the restriction enzymes digestion and cut the appropriate band; then, I used gel extraction kit to

extract the DNA. I did the same process for pUC57 plasmid by double digestion of pUC57 plasmid light and heavy chain, then ran it on 1% agarose gel, cut the bands and used gel extraction kit. I did the ligation of the heavy chain with pFastBac Dual plasmid by using double digestion enzyme EcoRI and HindIII. For the ligation, I first used vector (1µL), inserted (0, 2, 5, 10 µL), 10 x buffer (2 µL), ligation enzyme (1µL) and water to adjust the volume to 16µL total. After leaving the reaction at room temperature for 3:45 hr, I transferred the ligation mixture into XL1-Blue cells and did miniprep. To check if the ligation worked, I did EcoRV-HF and PstI digestion at 37°C for 2 hr. After cloning both heavy and light chains into pFastBac Dual plasmid, I transformed 1.2 µL of the plasmid into DH10Bac cells and on ice for 30 min, 45 second in water bath 42°C and 2 min on ice again. I added 250 µL of SOC buffer to the same tube and let it shake in the incubator 37°C for about 6 hrs. I prepared and used fresh x-gal plates which contains Kanamycin, Gentamicin, and Tetracycline antibiotics. I covered the x-gal plates with aluminum foil and left it at the incubator for 48 hrs. I picked 5 white colonies and 2 blue colonies for the negative control. After doing the miniprep, I kept the cells in ethanol and stored them at -20°C.

2.2 Sf9 Transfection

Sf9 cells were grown in suspension culture with at least 95% viability and then seeded into 6-well tissue culture plates at 1 x 10^6 cells in 2 mL of ESF-921 insect cell culture medium (Expression Systems) per well. 1 µL bacmid DNA (when the miniprep was done on the same day) was mixed with 100 µL ESF-921 media, and 8 µL of CellFECTINâ II Reagent (Thermo Scientific) diluted in 100 µL of ESF-921 media. Here is the procedure that I followed: Mix the two solutions together to form complex for 45-60 minutes, and then add 209 µL of the complex

into the well. Incubate cells for 6 hours in a 27°C incubator, and aspirate the transfection mixture then add 2mL ESF-921 media with 10% heat inactive and filtered FBS (HyClone) in each well to incubate plates for 72 hours at 27°C. Harvest first generation (P1) of baculovirus. P1 baculovirus was purified from cells and debris by centrifugation at 500xG for 5 minutes and stored at 4°C.

2.3 Antibody fab expression optimization in Sf9 cells

2 x 10^6 cells in 2 mL ESF media per well were seeded as monolayer in a 6-well plate and allowed for attachment for approximately 30 minutes. In order to check for expression of recombinant proteins, 100 μL of P1 virus were then added to each well in the plate and mixed by rocking. After cells were infected for 72 hours at 27°C, due to the secretion signaling peptides, protein was secreted to the media. I pipetted media to wash cell off from the plate and collected the supernatant by centrifuge at 500xG for 5 minutes, then saved the cell pellets for intracellular expression check. For the cell pellets, I dissolved the pellets with 300 μL lysis buffer, and chilled on ice for 15 minutes. Then, centrifuged at 12,000 rpm for 20 minutes at room temperature, to separate the soluble and insoluble portion. Next, I collected the soluble protein for protein expression check on Western blot. For both the supernatant and the soluble protein portion from cell lysate, I checked the protein concentration by using BioRad Protein Assay (BioRad). I prepared both secreted protein samples and intracellular protein sample with equal amount of protein to load to the 15% SDS-PAGE gel. Protein was then treated with α-pentaHis antibody (Qiagen Cat#34660) then detected on Western blot anti 6x-histidine chemiluminescence Western blotting. The first generation of baculovirus (P1) was used to infect Sf9 cells to produce the

second generation of baculovirus (P2). The volumes of P1 virus (10 µL and 100 µL) and time (72 hours and 96 hours) as two variables has been used to make P2 virus in four 100 mm Tissue Culture Plates (BD-Falcon) that seeded with 7.5mL x 10^6 cells in total volume of 15 mL. The first two plates that induced with 10 µL and 100 µL P1 virus were harvested after 72 hours, and another two plates also induced with same volume of P1 virus was collected after 96 hours. These P2 viruses were used to infect 2 x 10^6 cells in 2mL ESF-921 per well of 6-well plates, and each well added 5 µL, 10 µL, 40 µL and 70 µL of each P2 virus. After 72 hours infection, Western blot with α-pentaHis antibody (Qiagen Cat#34660) were used for protein expression check. The lowest volume of virus that produces the highest relative amount of protein is designated as the best viral titer and was used as different amounts of the best tittered P2 virus to generate higher viral titer (P3) in order for large scale protein expression in Sf9 cells suspension culture. The third generation of virus was produced in 150 mm x 15 mm FisherBrandÒ Petri Dish (Fisher Scientific) that seeded with 15 x 10^6 cells in 30 mL ESF and 10% heat inactivated HyCloneÒ Fetal Bovine Serum Collected In Central America (Thermo Scientific) at volumes of 1 µL, 2 µL and 3 µL of the P2 virus (the one found the best titer) for 72 hours and 96 hours. Again, I infected 2 x 10^6 cells in 2 mL media per well in 6-well plates by added 1 µL, 5 µL, 10 µL and 20 µL of each P3 virus. Incubating for 72 hours, then checked protein expression assayed on α-histidine immunoblot. The best titer has been selected (P3.10.3 72 hours with 10 mL per well, 5 µL per 1 x 10^6 cells), however, this titer was generated from 6-well plates of adherent cells. Only half of this volume of virus is needed to infect suspension cells. The viral titer for suspension cells now is 1.25 µL per 1 x 10^6 cells, and it is ready for large-scale protein expression.

2.4 Protein purification of antibodies in Sf9 insect cells

The best titer that selected from P3 virus (P3.10.1 72 hours 1.25 µL per 1 x 10^6 cells) was used to infect 2 x 10^6/mL cells in 1L flask of 500 mL Sf9 suspension cells. I incubated the cells in a shaker at a speed of 105 rpm for 72 hours infection, collected the media to centrifuge at 500 x G for 5 minutes to harvest the secreted protein from the supernatant, and then purified with Ni affinity chromatography at 4°C. Preparing the gravity column of ratio of 1mL Ni Sepharose 6 Fast Flow (GE Healthcare) slurry per 500 mL suspension cell culture, allows the resin to settle then I washed it with 10 column volumes of water, and lastly equilibrated with 10 column volumes of 1X lysis buffer (25 mM Tris-HCl pH 8.0, 150 mM NaCl, 5 mM imidazole). After that, I let all supernatant go through the column (flow through), then washed with wash buffer (lysis buffer with additional 12.5 mM imidazole) as same volume as lysis buffer (wash trough). Next, I eluted protein in fractions from the column with Elute buffer (lysis buffer with additional 122.5 mM imidazole); combined the eluted fractions that contain Fab Antibody, and then went through the MILLEXÒ-GV 0.22 mm Filter Unit (Millipore) before loading it to size exclusion column. Superdex 75 16/60 size exclusion column was connected to ÄKTA (GE Healthcare), it has been equilibrated with SEC buffer pH 7.5 (25 mM Tris-HCl pH 8.0, 150 mM NaCl). Fraction collector at 2 mL per fraction collected purified protein, and peak fractions has been combined and concentrated with 15 kDa-cutoff membrane concentrator (Millipore) to 5 mg/mL. Protein was flash frozen in liquid nitrogen and stored at -80°C. Protein concentration was determined by BioRad Protein Assay (BioRad).

2.5 Site directed mutagenesis

In order to increase the selectivity of the metalloantibody to different metals other than calcium, I used site directed mutagenesis. Then, I designed primers with the mutations inserted to prepare D3032C, D3192H and D3032C/D3192H construct. To design the oligonucleotides, I looked at Stratagene quikchange manual, then I used the length between 40-45 bases and for the melting temperature (T_m) I used melting temperature greater or equal to 78°C. The primers had a minimum GC content of 40%. The formula used to estimate the melting temperature is as follows:

$$T = 81.5 + 0.41(\%GC) - 675/ N - \% \text{ mismatch}$$

Where N is the length of the primers.

The forward and reverse primer sequences with the mutagenesis inserts used in the pFastBac Dual plasmid is shown in Table IV.1.

Table IV.1 Primers sequence, GC content and melting temperature.

Primer	Sequence From 5'to 3'	GC Content	T_m
D30C-D32C-R	CTGCTGGTACCAGTTCATGCAGTCGCAGATGT CAGTGGAGGTGATGC	55.3%	70.3°C
D30C-D32C-F	GCATCACCTCCACTGACATCTGCGACTGCATG AACTGGTACCAGCAG	55.3%	70.3°C
D31H-WT-R	GCTGGTACCAGTTCATGTCGTGGTCGATGTCA GTGGAGGTG	56.1%	68.8°C
D31H-WT-F	CACCTCCACTGACATCGACCACGACATGAACT GGTACCAGC	56.1%	68.8°C
D92H-R	GAACAGAGGCAGGTTGTGGGACTGCAGGCAG TAGTA	56.8%	67.9°C
D92H-F	CTACTACTGCCTGCAGTCCCACAACCTGCCTCT GTTC	56.8%	67.9°C
D31H-CC-F	CACCTCCACTGACATCTGCCACTGCATGAACT GGTACCAGC	56.1%	69.3°C
D31H-CC-R	GCTGGTACCAGTTCATGCAGTGGCAGATGTCA GTGGAGGTG	56.1%	69.3°C

Synthesized complementary oligonucleotides that has the desired mutation were ordered at Integrated DNA Technology (IDT). In order to set up the reaction for polymerase chain reaction (PCR), a cocktail that contains: 5µL of 10x reaction buffer, 5µL of 2mM dNTP mix, 1µL PfuTurbo DNA polymerase, (5, 10, 20, and 50 ng) DNA template, 1µL primers both forward and reverse each 100 ng/µL, and double distilled water ddH_2O was prepared. For the negative control, same cocktail was prepared but this time without PfuTurbo DNA polymerase. The PCR was done at BioRad iCycler the denaturing temperature was 95°C for 30 seconds,

annealing and elongation steps were done at 95°C for 30 second, 55°C for 1 minute and 68°C for 2min/kb of plasmid length which for the pFastbac Dual plasmid was about 13 mins with 16 number of cycles.

After the PCR reaction, 1µL DpnI enzyme was added to the PCR tubes and incubated at 37°C for 30 min. To deactivate the enzyme, the PCR tubes were incubated at 80°C for 20 min and the PCR reaction was stored at 4°C. DpnI digests the PCR products of the parental supercoiled dsDNA.

The mutated plasmid was transformed into DH5α cells. 1.2 µL of the plasmid was pipetted into the DH5α cell and left on ice for 30 min, 45 second in water bath 42°C and 2 min on ice again. I added 250 µL of SOC buffer to the same tube and let it shake in the incubator 37°C for about one hour. After an hour, the cells were plated on LB-Amp plates and left inside the incubator 37°C for 12 hrs. Next day, about 10 colonies on the plates were selected and 5mL LB media under sterile conditions were added to the falcon tube with the 5 µl ampicillin 100 mg/mL and one single colony. The cells were shaking in the incubator for 12 hours. Next day I did miniprep to purify the plasmid and sent it for sequencing. The electropherograms are presented in the results section of this chapter.

2.6 Preparing samples for inductively coupled plasma-mass spectrometry (ICP-MS)

Aliquots of 2.6 mg/mL of LT3015 (LPath, Inc.) and Fab antibody were prepared. 5 samples (LT3015, Fab antibody, HEPES buffer without $CaCl_2$, HEPES buffer with 10 mM $CaCl_2$ dialyzed, and HEPES buffer with 10 mM $CaCl_2$ without dialyzing) were prepared and sent for ICP-MS. Aliquots of samples are transferred to 3.5K MWCO dialysis units (Slide-A-Lyzer™

MINI Dialysis Unit #88403). 0.1M EDTA solution was prepared and added to the samples and dialyzed against 20mM HEPES buffer, 0.22µm filtered, pH 7.2 buffer at 20°C to remove basal levels of metals from solution. EDTA is removed by dialysis against 20mM HEPES buffer, 0.22µm, pH 7.2 for >24 hours with 4 exchanges. Sample concentration is monitored at A_{280} using the Nanodrop 2000 (Thermo Scientific) spectrophotometer. The concentration of antibodies samples was about 1.45 mg/mL. 100mM stock solutions of $CaCl_2.2H_2O$ (EMD® #401800), are prepared in 20mM NaHEPES, pH 7.2. 200 µL of 100 mM stock solutions of $CaCl_2.2H_2O$ was added to 1.5 mL of Fab, LT3015 and NaHEPES buffer solutions to reach the final concentration of 10 mM. The samples were dialyzed against HEPES buffer for >24 hours with 4 exchanges. Samples were sent to California State University at Long beach for ICP-MS.

ICP-MS experiments determine whether the metal selectivity of LT1002 is specific to Ca^{2+} and / or capable of binding other metals. For the selectivity study, we implemented ICP-MS technology because of its superiority to absorbance techniques in both sensitivity (measures down to parts-per-trillion) and minimization of co-absorbance in final abundance measurement. The high temperatures reached with induced-coupled plasma 6,000 K ensure complete ionization the particular measured ion in the matrix, limiting the effects of partial ionization and atomization of all metal ions in the matrix, allowing for significantly greater detection sensitivity. Because mass-spec detects the cations by their mass-to-charge ratio, one can be relatively certain that the measured concentration is due to the metal alone and not from other interferences as often seen in absorbance detection methods due to co-absorbance or ionization suppression effects.

Samples were treated with hot HNO_3 to precipitate protein and release metals into solution. Optionally, samples can be treated by a secondary acid wash procedure including perchloric acid. Samples are cooled and centrifuged at 14,000 x rpm for 10min. Supernatant is collected. Sample is made ready for ICP-MS by dilution 10-Fold with trace metals grade nitric acid and diluted to predetermined volume and mixed before analysis. Samples are analyzed within 1-day of digestion.

Samples are analyzed via Hewlett Packard (Agilent) 4500 Series Inductively Coupled Plasma Mass Spectrometer (ICP-MS) by pumping sample through a concentric nebulizer, producing a fine sample aerosol. An argon gas carrier carries the sample into high temperature radiofrequency argon plasma, which atomizes and ionizes the sample. The ions are extracted from the plasma through differentially pumped vacuum interface and separated on the basis of their mass-to-charge ratio by a quadrupole mass spectrometer. An electron multiplier detector measures the ion concentration of specific mass-to-charge ratio.

2.7 Preparing samples for microscale thermophoresis (MST)

In order to test the metal binding affinities of the antibodies to metals, I used microscale thermophoresis instrument. The MST instrument that I have used was NanoTemper technologies and the model was Monolith NT.115. The protein samples were labeled with fluorescent dye using Monolith NT.115 protein labeling kit red that conjugates to reactive amines. The dye carries a reactive NHS-ester group that modifies primary amines as they are present in amino acids like lysine.

Using the kit manual, different ratio of protein: fluorescence labeled samples were prepared and the concentrations were checked with BioRad Protein Assay. The protein absorbance was checked at 280nm and dye at 650nm. After selecting the best protein to dye ratio (which was the dye concentration 3 times greater than the protein concentration), I ran the protein labeled samples on different capillary types. Among all capillaries, hydrophobic capillaries were the best ones, where the samples did not stick to the surface of the capillaries and the peaks looked great. Also, the tubes were scanned, and the best fluorescence intensity achieved with 10-30% LED power.

The protein and metal samples were diluted in 20mM HEPES buffer. 12 samples were prepared, and the protein labeled samples were titrated with $MgCl_2$, $CaCl_2$ and $ZnCl_2$. The metal samples titrated to protein had concentrations that increased 10 folds starting from 0 to 10^4 μM.

3. Results

LT1009 (sonepcizumab) is a monoclonal antibody that binds to the signaling lipid molecule sphingosine-1-phosphate (S1P). LT1009 is a fully humanized version of the murine LT1002 antibody, and it utilizes light chain CDR loop 1 (CDR-L1) aspartic acid 30, 31, and 32, and also light chain CDR loop 3 (CDR-L3) aspartic acid 92 to form metal binding with its antigen S1P by utilizing two Ca^{2+} cations (J. M. Wojciak et al. 2009). One question we want to discover is whether the anti-S1P metalloantibody is metal binding inherent (i.e., encoded at the germline level) or is it occurring with the affinity maturation process of antibodies in B cells. Using the IgBlast server, we identified three different antibody kappa light chain variable domain genes that contain all of the metal coordinated amino acid residues in the corresponding positions

of the murine mouse anti-S1P antibody. One of these differed only at four amino acid positions from the humanized mouse anti-S1P and so we made the assumption that this gene served as the progenitor. In order to test that this antibody precursor possesses innate potential to bind metal ions, we attempted to express and purify it and test its metal binding potential *in vitro*.

We first attempted expression of the precursor antibody as a Fab fragment in *E.coli*. However, the *E.coli* cells lack an endoplasmic reticulum for proper protein folding and disulfide bond formation of functioning antibodies. Our protein yields were quite low and assessment of the size of our *E.coli* expressed antibodies revealed that they are not correctly assembled. In light of this, we turned our attention to Sf9 cells and baculovirus protein expression system. We were able to express and purify well folded Fab antibody and mutated antibody in Sf9 cells.

3.1 Site directed mutagenesis electropherograms

In order to test the metal binding properties of the antibody, I mutated key residues that are involved with the metal binding. X-ray crystal structure data has showed us promising result of this interaction. By changing aspartic acid 30, 31, 32 and 92 to cysteine and histidine, we were able to express and test the metal binding properties of the mutated Fab antibody to Zn^{2+}, which is more interesting metal than Ca^{2+}. Metalloproteins that bind to zinc can be found in nature and they are involved in many physiological processes. However, finding metalloantibody that interacts with metal is novel. Metal increases the binding affinity of the antibody to antigen. Specifically, zinc antibody discovery is the original novel outcome. This finding could have a potential study area where the binding of the antibody to zinc can selectively increase the conjugation of different molecules such as drugs to antibody. Other aspects could be to be used as catalytic enzymes.

Electropherogram indicates the site directed mutagenesis for the CDR loops on the light chain of the antibody Fab fragment. The electropherograms are as follows:

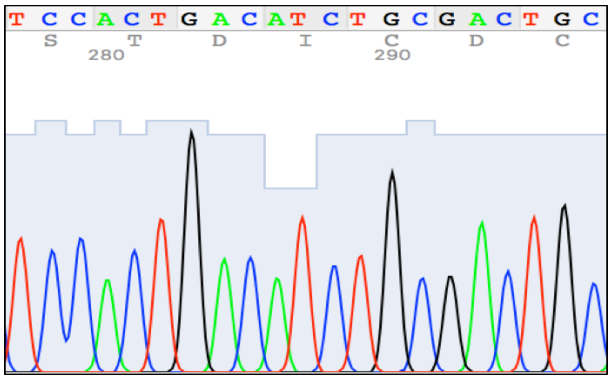

Figure IV.2 Electropherogram for D3032C mutations

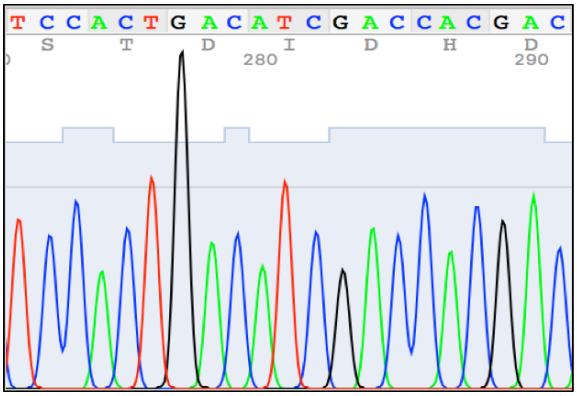

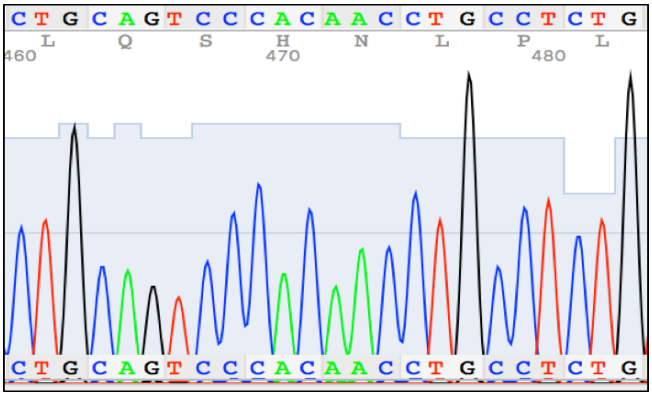

Figure IV.3 Electropherogram for D3192H mutations

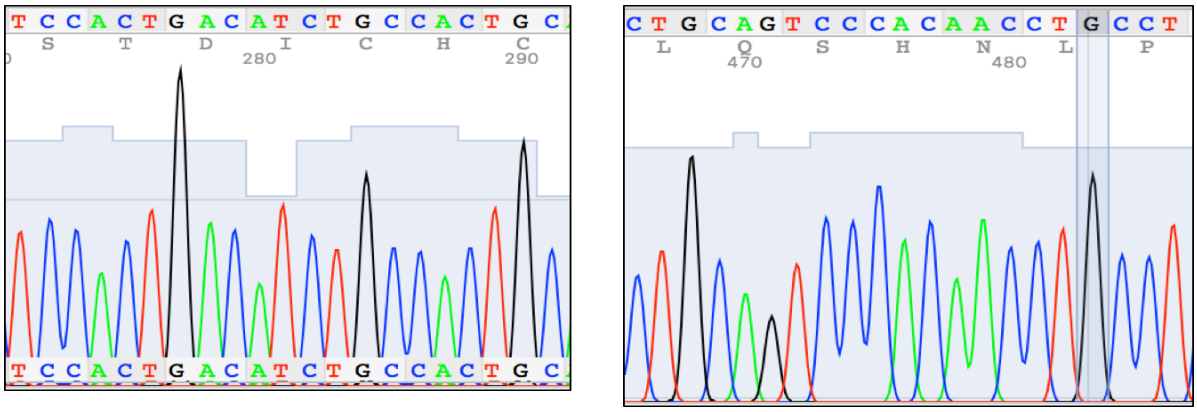

Figure IV.4 Electropherogram for D3032C/D3192H mutations

3.2 Antibody expression and purification

500 mL Sf9 suspension culture has been incubated in a shaker for 72 hours at 27°C. Proteins secrete in supernatant was collected and went through Ni column purification and eluted protein concentrations were determined by Bradford assay and ran on 15% SDS-PAGE gel (Figure IV.6). The most concentrated fractions were combined and filtered. About 2mL of protein sample purified by size exclusion chromatography (SEC). The chromatogram shows one single peak at 280nm, which indicates the purity of Fab antibody (Figure IV.5). The collected fractions were concentrated to 6 mg/mL for 1.5mL, and protein has been frozen and stored at -80°C.

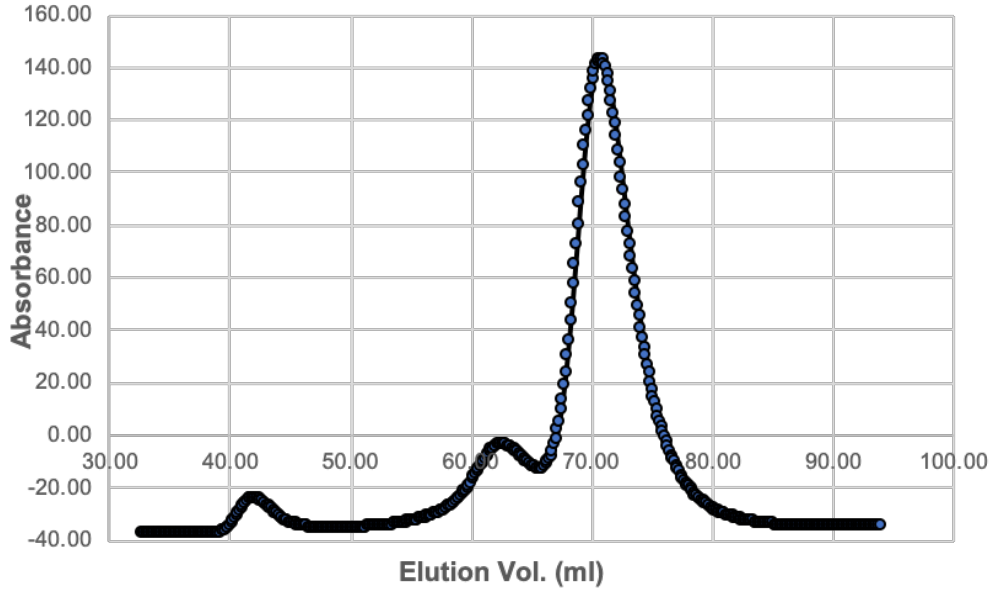

Figure IV.5 Size exclusion chromatography using Superdex 75 16/60 of the His-tagged mutated CHCH Fab antibody.

Purification of the mutated CHCH His-tagged Fab antibody using the Ni affinity column indicates the expression of both heavy and light chains of the antibody. The 15% SDS-PAGE gel is showing the marker lane, lysate, flow through, wash and elution (E1-E6).

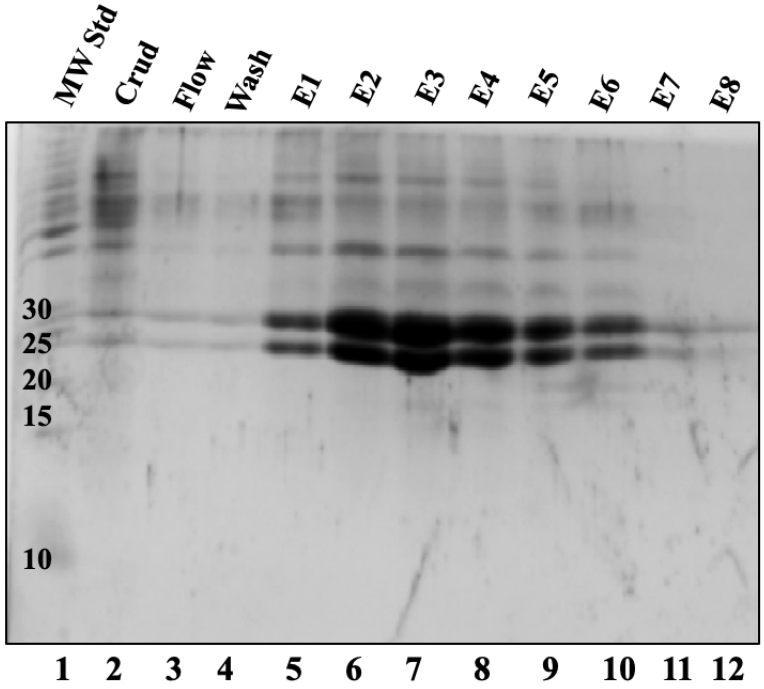

Figure IV.6 Coomassie-stained 15% SDS-PAGE gel for samples from Ni column purification. The size of Fab antibody heavy chain is 26 kDa and the light chain is 24 kDa, and the E2-E4 elutes contain most of the proteins were combined. The double bands show heavy and light chains of the antibody.

3.3 Western blot

In this expression system, recombinant baculovirus has been used to infect suspension culture of Sf9 cells. The viral titer is the main factor for protein yield, and instead of plaque assay, we used chemiluminescence western blotting to determine titer. 2 x 10^6 Sf9 cells with 2mL media per well were seeded in 6-well plates, and after 72 hours incubation the cells were collected, and the concentration of the secreted protein was determined. After finding the best transfection from P1 virus, we did P2 virus from different amounts of P1 virus to get better protein expression. We also did different incubation time (72 and 96 hr) to find the best titer for P2 virus. The best viral titer for P2 virus was P2.10.10 after 72 hour incubation and P2.10.5 after 96 hour incubation (Figure IV.7 and IV.8).

After determining the viral titer for P2 virus, we did expression and purification from $45x10^6$ cells in 25mL suspension culture with 900 µL and 450 µL of titer virus to compare which one is the better titer for suspension culture since the titer we decided above is from adherent cells. Ni column purification was conducted to purify the Fab antibody from the two suspension cultures. From Bradford assay, the calculated protein yield that was infected with 900 µL virus is 0.35 milligrams, and the one infected with half of the viral titer is 0.45 milligrams. These results prove that the viral titer determined by Western blot is only half of the viral volume needed to infect suspension culture for higher protein yield. The amount of virus that have been using for protein expression is essential since the viral stock is not reproducible due to accuracy of cell counting and exact numbers of virus that need to be added to make the same viral stock.

Then we moved on to make P3 virus for large suspension culture protein expression. The best tittered P2 virus has been used to infect Sf9 cells in the 150mm x 15mm tissue culture plates with different amount of virus, after the P3 viruses were made that they have been tested with chemiluminescence western blotting for protein.

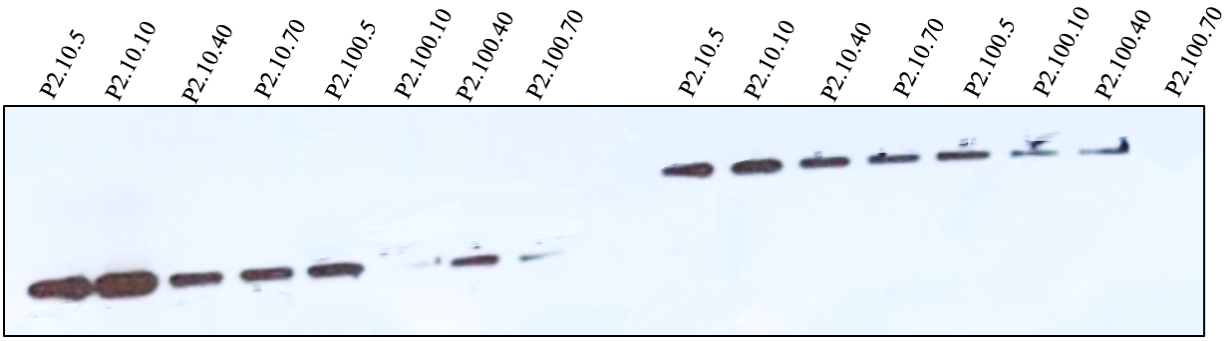

Figure IV.7 Anti-His Western blot data for secreted mutant CHCH Fab antibody. There were 8 different P2 viruses have been made from different amounts of P1 with 72 hour incubation. On the lane 2 of the mutant Fab antibody P2.10.10 after 72 hour incubation shows the thickest band. The first 8 lanes are indicating secreted reduced antibodies and the second 8 lanes are showing non-reduced antibodies.

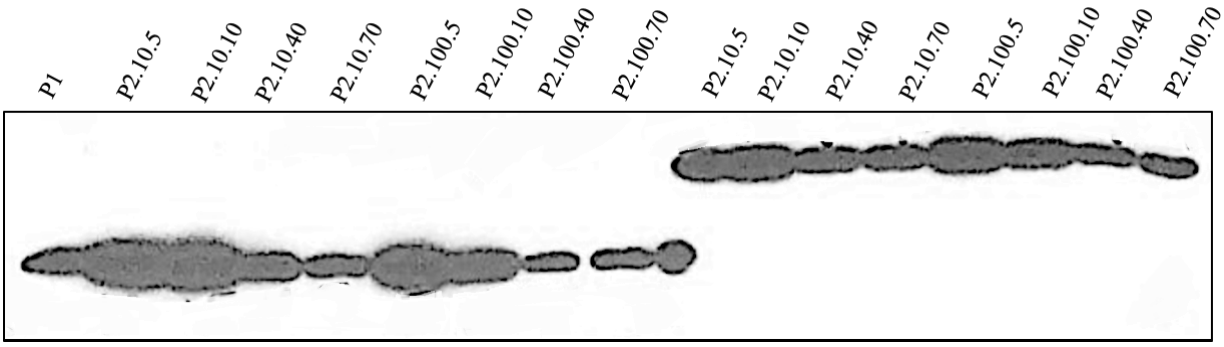

Figure IV.8 Anti-His Western blot data for secreted mutant CHCH Fab antibody. There were 8 different P2 viruses have been made from different amounts of P1 with 96 hour incubation. On the lane 2 of the mutant Fab antibody P2.10.5 after 96 hour incubation shows the thickest band. The first 8 lanes are indicating secreted reduced antibodies and the second 8 lanes are showing non-reduced antibodies.

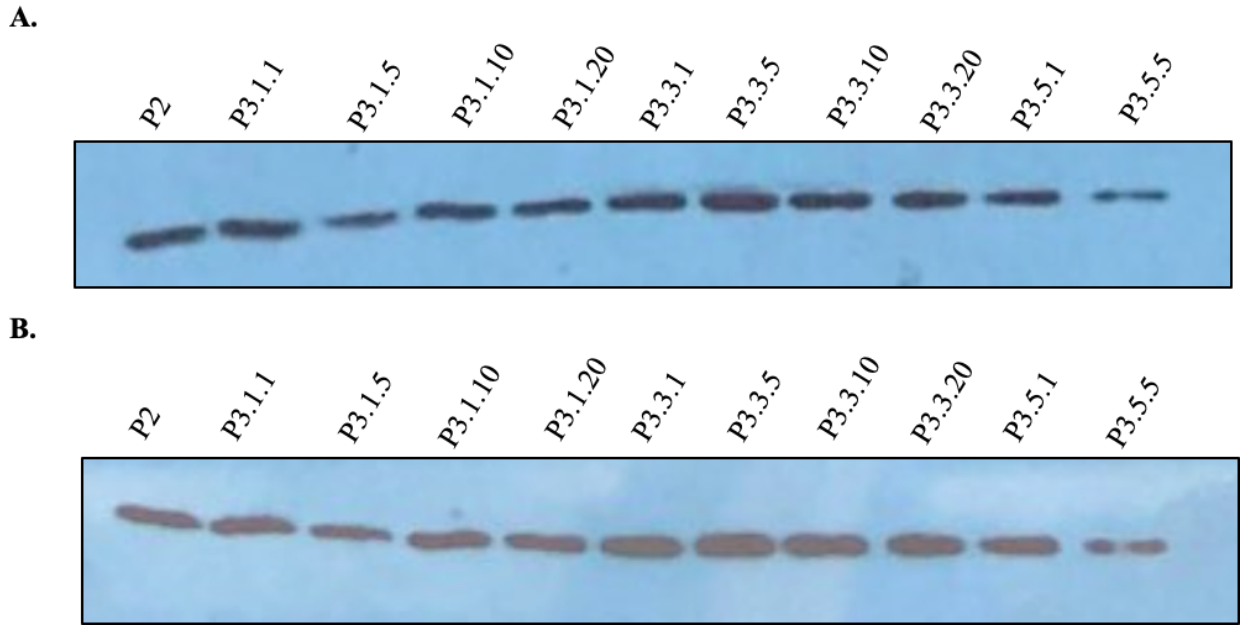

Figure IV.9 Anti-His Western blot data for secreted mutant CHCH Fab antibody P3 virus expression check. P2 virus has been used as control to provide more reliable results. There were 10 different P3 viruses have been made from different amounts of P2 virus. Panel A. is indicating the incubation time after 72 hour and panel B is incubation after 96 hour. Comparing to the control P2 virus from panel A. and B. P3.3.5 is the best among P3 viruses.

After checking the expression of the protein with different viruses, we did a large scale about 500 ml media and purified the secreted proteins through Ni column and ÄKTA. I had used

about 2mg of the protein ICP-MS to test the metal binding properties of the mutant antibody to different metals. Among all of the mutated antibody, D3032C/D3192H antibody was the promising mutant one that binds to zinc. The other mutant antibodies did not show any significant binding to other metals such as Cu^{2+}, Co^{2+}, and Ni^{2+}. In order to test and confirm binding of the mutated CHCH Fab antibody to zinc, I constructed two methods: Microscale thermophoresis and Inductively coupled plasma mass spectrometry.

3.4 Inductively coupled plasma-mass spectrometry (ICP-MS)

Binding of CHCH mutated Fab murine monoclonal antibody to zinc have been analyzed using ICP-MS. Figure IV.10 shows the binding of CHCH Fab fragment antibody to Zn^{2+} and the zinc concentration is greater than the controls. Negative controls are HEPES buffer in the presence of Zn^{2+} and dialyzed overnight which is showing negligible amount of Zn^{2+} and HEPES buffer with Zn^{2+} without dialyzed is showing great amount of Zn^{2+}. From this data we can conclude that Fab monoclonal antibody binds to Zn^{2+}.

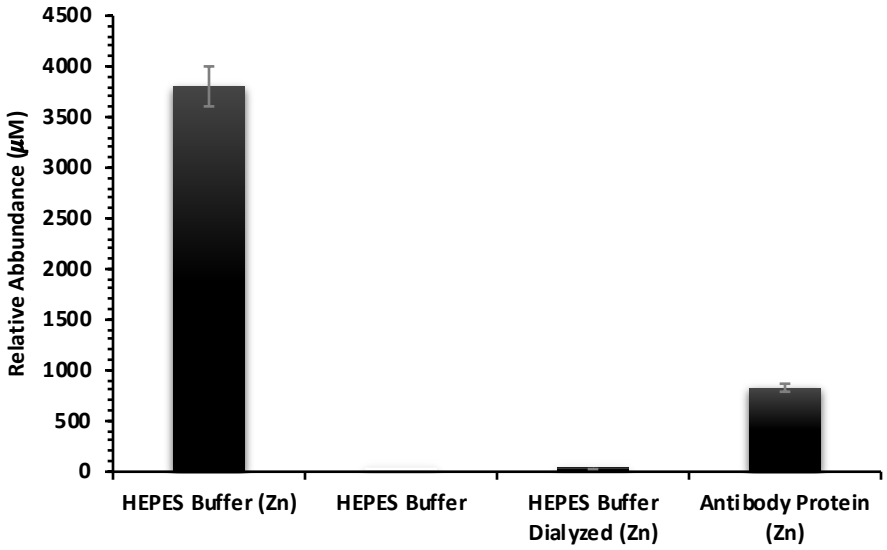

Figure IV.10 ICP-MS data for CHCH mutant Fab antibody. Sample 1 is HEPES buffer without Zn^{2+}. Sample 2 is HEPES buffer with 10mM Zn^{2+} dialyzed. Sample 3 is HEPES buffer with 10mM Zn^{2+} without dialyzing. Sample 4 is mutant CHCH Fab antibody with 10mM Zn^{2+} dialyzed.

3.5 Microscale thermophoresis (MST)

Another method that I used to determine the binding affinity of CHCH mutant Fab antibody to zinc was MST. MST is a technology for the biophysical analysis of interactions between biomolecules. It is based on the principle that molecules move along a temperature gradient in a capillary. MST signal is plotted against the ligand concentration to obtain a dose-response curve, from which the binding affinity can be deduced.

The fluorescence samples were prepared, and I used hydrophobic capillaries. Then, $ZnCl_2$ was titrated to the protein samples. The first titration did not have $ZnCl_2$ but the concentration of Zn^{2+} increased 10-fold up to 10^4 μM. I had a total of 12 samples (Figure IV.11).

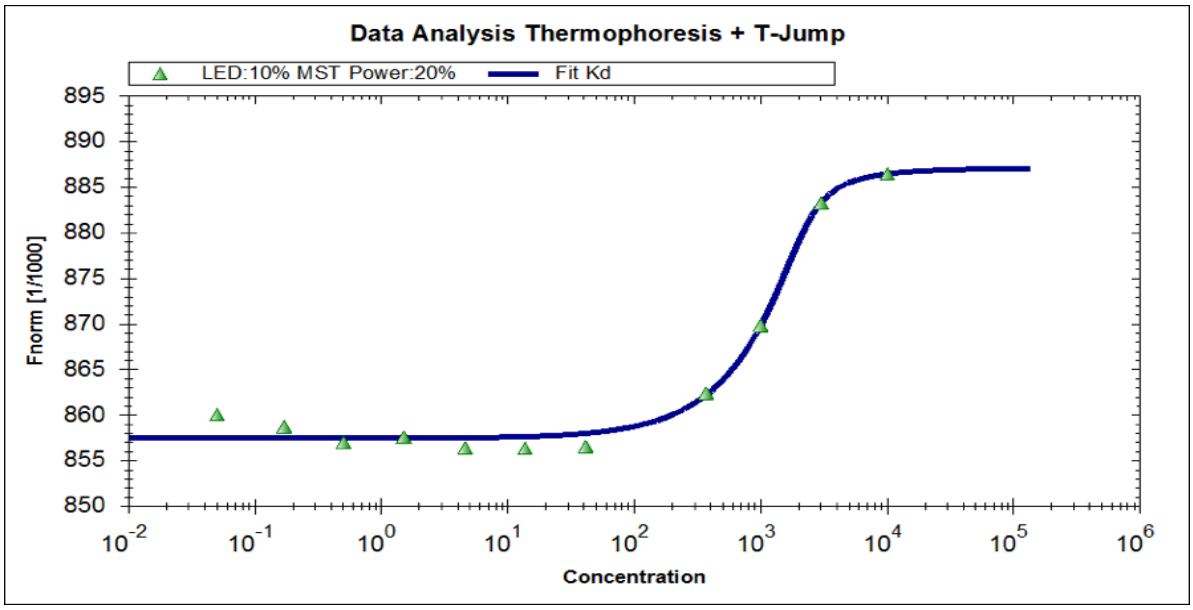

Figure IV.11 MST data for CHCH mutant Fab antibody. Samples were prepared in 20mM HEPES buffer and labeled with the fluorescent dye using Monolith NT.115 protein labeling kit red that conjugates to reactive amines. The first sample was titrated without Zn^{2+} and the rest of the samples were titrated with Zn^{2+} that their concentration increased by 10-fold up to 10^4 μM. The binding affinity (K_D) calculated for this experiment was 168 μM.

3.6 Other metalloantibodies in nature

Other metalloantibodies (e.g. Q425 and 2C10) introduced in Chapter II of this dissertation have the same sequence on their CDRL1-L3 loops as the precursor antibody. This indicates the same binding site on their CDR loops to antigen in the presence of metal ions. Murine 2C10 antibody binds to double stranded DNA (dsDNA) as its antigen.

It was interesting that anti-dsDNA antibodies were found in serum of patients with Systemic Lupus Erythematosus (SLE). SLE is a disease that occurs when the body's immune system attacks healthy connective tissue cells (Y. J. Jang and Stollar 2003). On top of that, Q425 binds to CD4 that protects against HIV infection and requires calcium for recognition of CD4 (T.

Zhou et al. 2005). However, the binding site of Ca^{2+} is different form the binding site of humanized LT1009 antibody with S1P antigen and Fab LT1009 antibody without antigen and in the presence of Ca^{2+}.

We were interested in (i) finding the epitope of CD4 to Q425. We also aimed to explore (ii) if our antibody large scale expression system is able to produce Q425 and 2C10. Furthermore, we were interested in (iii) testing whether 2C10 binds to dsDNA in the presence of metal or not, and (iv) does the metal have any effect in the antibody: antigen binding affinity, since they all have the same homology in their CDR loops of their light chain.

To achieve these goals, I mentored two undergraduate students, Sally Luong and Citlayi Villasenor, in this project in order to perform expression and purification of these antibodies.

The protein expression method used for Q425 and 2C10 were the same as precursor antibody. The Western blot data indicates that both antibodies were expressed but the expression level was lower than the precursor. We were able to use about 2-3 mg of the antibody to do further analyzing such as MST and pull down assays.

3.7 Western blot

The same method was used to express Q425 and 2C10 antibodies. For the best titer, we have used P3 virus and the expression levels were checked with Western blot. The Western blot data indicates both the expression of Q425 and 2C10 antibody after 96 hours. The size of the antibodies for the denaturing (part A) was 25 kDa and for the non-denaturing (part B) was 50

kDa. The best viral titer for P3 virus for Q425 was P3.1.5 and for 2C10 was also P3.1.5 after 96 hours incubation time (Figure IV.12).

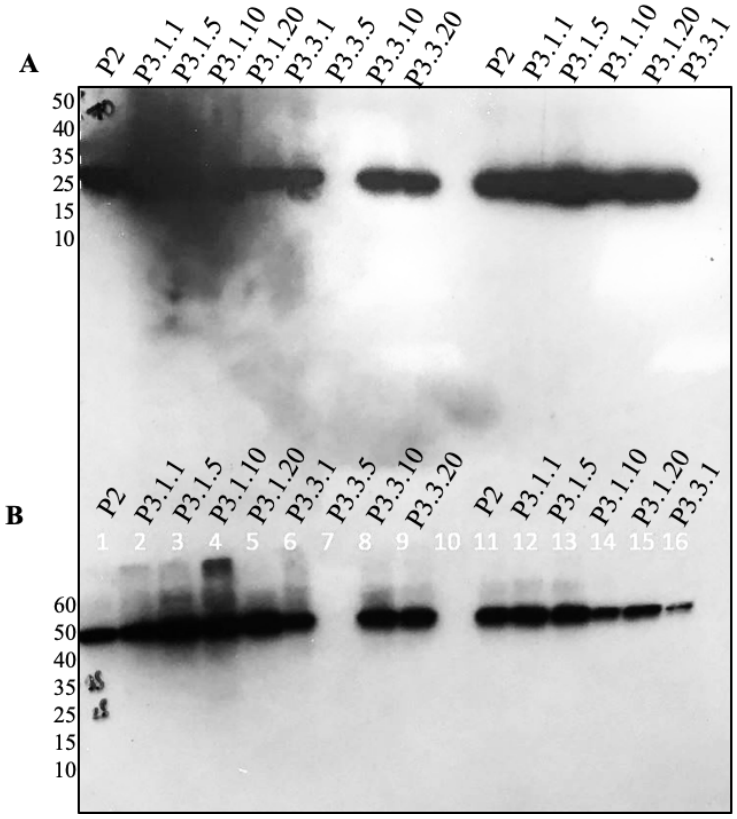

Figure IV.12 Anti-His Western blot data for secreted Q425 and 2C10 antibody. There were 8 different P3 viruses have been made from different amounts of P2 with 96 hour incubation. From lane 1 was the control P2 and from lane 2-9 is Q425 antibody and from 11-16 is 2C10 antibody expression check. Part A is indicating the non-reduced antibody expression level and part B is indicating the reduced expression level.

3.8 Pull down assay

In order to determine if Q425 binds to CD4 with or without Ca^{2+}, Citlayi Villaseñor, did a polyHis-tagged pull down assay and ran murine monoclonal Q425 antibody and CD4 antigen with and without Ca^{2+} on Ni sepharose beads. The His-tagged Q425 binds to the Ni beads and the unbound protein was washed away. By adding CD4 protein to the immobilized Q425 protein

the complex was formed, and the unbound protein was washed away. We have test this in the presence of 10mM Ca^{2+} and without Ca^{2+}. To elute Q425: CD4 complex she used Protein loading dye and SDS solution. The samples were collected at each step and prepared for Western blot. The primary antibody used was anti-CD4 antibody which can detect CD4 and the secondary antibody was goat anti-mouse antibody that can detect mouse Q425.

The Western blot data using anti-CD4 antibody and anti-mouse antibody indicates that Q425 binds to CD4 in the presence of Ca^{2+} in 0.5% Triton-X buffer (Figure IV.13). The molecular weight for the His-tagged heavy chain Q425 antibody is 25 kDa and for CD4 is 55 kDa.

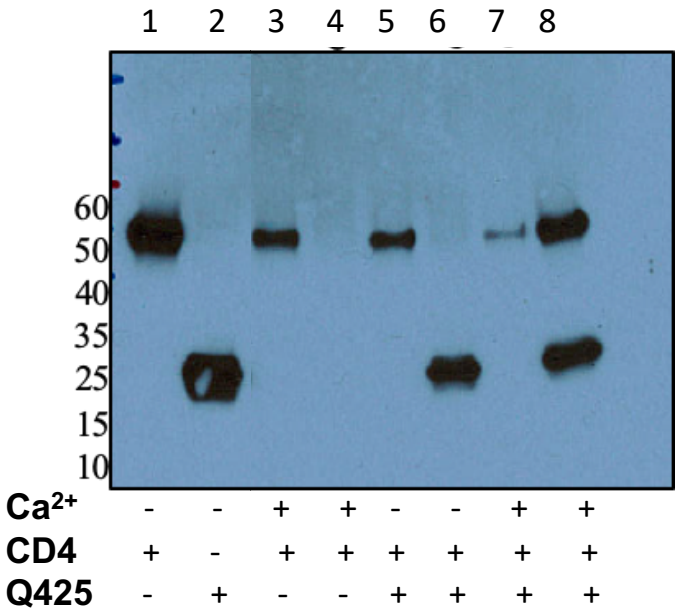

Figure IV.13 Anti-CD4 Western blot data. Lane 1 is CD4, lane 2 is Q425, lane 3 CD4 and Ca^{2+} in wash, lane 4 CD4 with Ca^{2+} in elution, lane 5 Q425 with CD4 in wash, lane 6 Q425 and CD4 in elution, lane 7 Q425 with CD4 and Ca^{2+} wash, lane 8 Q425 with CD4 and Ca^{2+} elution.

3.9 Microscale thermophoresis (MST)

Anti-dsDNAs are used in blood tests in diagnostic laboratories. Analytical technique like immunofluorescence used to detect anti-dsDNA antibodies (Mortensen, Fenton, and Rekvig 2008; Solomon et al. 2002). Anti-dsDNAs are highly diagnostic for SLE disease. To determine if the presence of metal has an effect on binding affinity of 2C10 to dsDNA, I used MST to confirm the binding of 2C10 to dsDNA in the presence of Ca^{2+}, Mg^{2+} and dsDNA. I ran three different MST experiments: First I used 2C10 antibody titrated to dsDNA and Ca^{2+} and measured the binding, second, I titrated 2C10 antibody to dsDNA and Mg^{2+}, and third I titrated 2C10 antibody to dsDNA. The results indicate that metal increases the binding affinity of 2C10 to dsDNA and Mg^{2+} increases the binding affinity slightly (Figure IV.14-16). The protein: fluorescence dye ratio that I used was 1:3 ratio. To each 2C10 antibody samples Gbp3 14-mer dsDNA was titrated that had a concentration about 4,162 ng/μL. For one of the MST experiment, I titrated Ca^{2+} to the samples starting from zero to 10^2 μM and another one I titrated Mg^{2+} to the samples starting from zero to 10^2 μM.

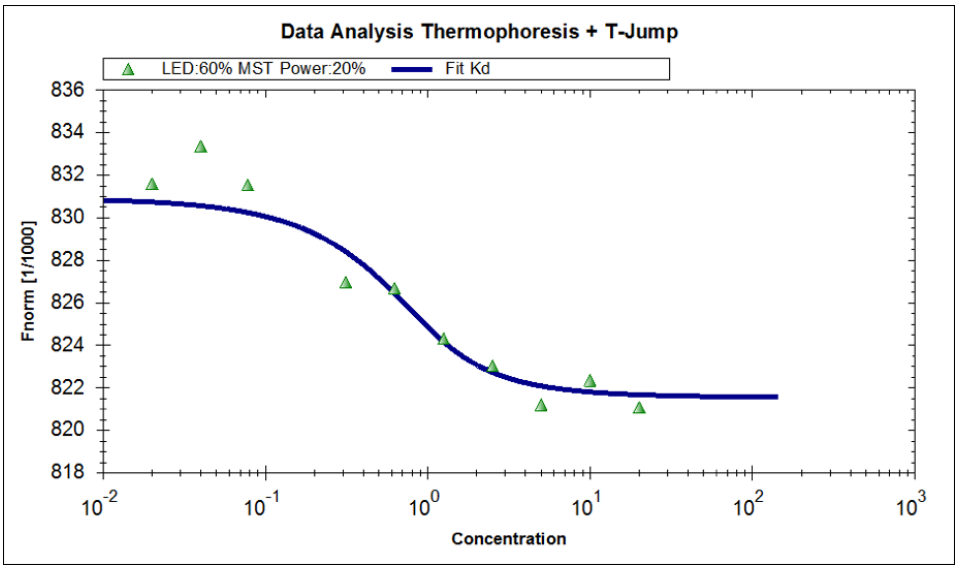

Figure IV.14 MST data for 2C10: dsDNA: Ca^{2+}. Samples were prepared in 20mM HEPES buffer and labeled with the fluorescent dye using Monolith NT.115 protein labeling kit red that conjugates to reactive amines. All sample was titrated with same amount of 2C10 and dsDNA and Ca^{2+} was titrated to the samples and Ca^{2+} concentrations increased by 10 folds in each sample. The binding affinity (K_D) calculated for this experiment was 0.256 µM.

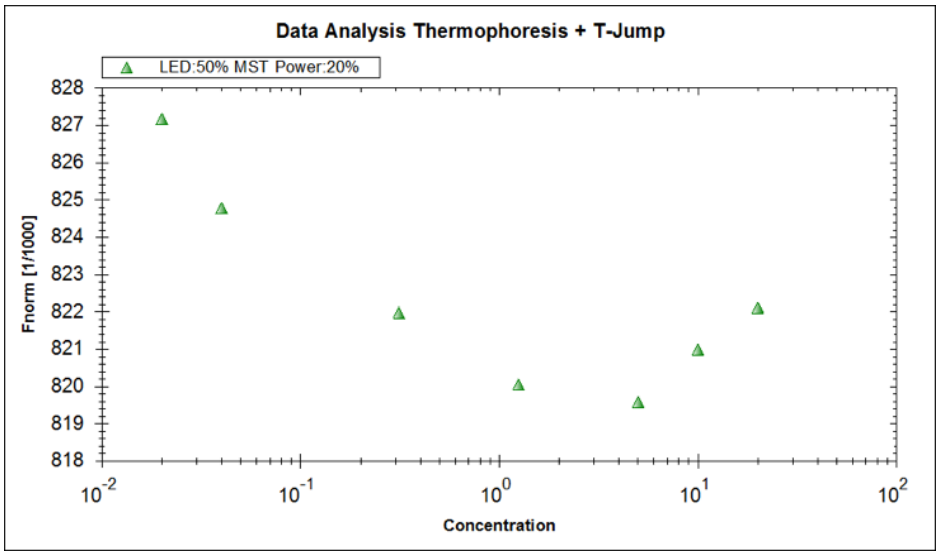

Figure IV.15 MST data for 2C10: dsDNA: Mg^{2+}. Samples were prepared in 20mM HEPES buffer and labeled with the fluorescent dye using Monolith NT.115 protein labeling kit red that conjugates to reactive amines. All sample was titrated with same amount of 2C10 and dsDNA and Mg^{2+} was titrated to the samples and Mg^{2+} concentrations increased by 10 folds in each sample. The binding affinity (K_D) calculated for this experiment was 0.10 µM.

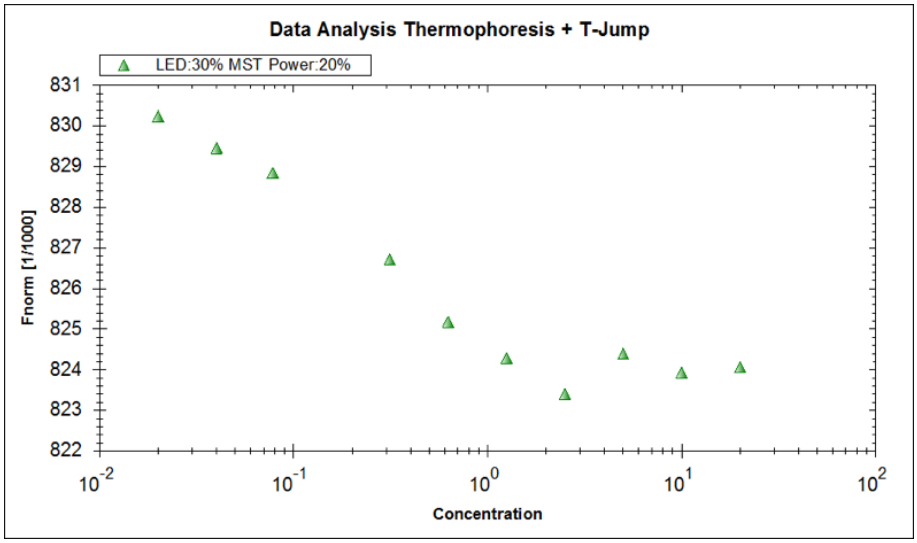

Figure IV.16 MST data for 2C10: dsDNA. Samples were prepared in 20mM HEPES buffer and labeled with the fluorescent dye using Monolith NT.115 protein labeling kit red that conjugates to reactive amines. All sample was titrated with same amount of 2C10 and dsDNA. The binding affinity (K_D) calculated for this experiment was 1.63 μM.

4. Conclusion and future direction

There is a homology between humanized LT1009, Q425, and 2C10 antibody CDR sequence of their light chain. Therefore, we prepared precursor antibody that has the same sequence on their CDRL1-L3 loops. X-ray crystallography data indicates that LT1009 antibody binds to S1P antigen in the presence of metal. The binding affinity gets 10 times greater in the presence of Ca^{2+} (J. M. Wojciak et al. 2009). We were interested to determine if these metalloantibody binds to other metals instead of Ca^{2+}. Therefore, I expressed and purified Fab precursor antibody and with site directed mutagenesis I changed the amino acids that were involved in the binding site. I prepared three different constructs, which where D3032C, D3192H and D3032C/D3192H. The large scale expression and purification of these construct went well

and I was able to get 8-10 mg of the mutant antibodies from 500 mL culture. After that, I tested to see if mutant antibody binds to Cu^{2+}, Zn^{2+}, Co^{2+} and Ni^{2+}. Among all mutant D3032C/D3192H interacted to Zn^{2+}. To confirm this, ICP-MS data indicated that this construct binds to Zn^{2+} compared to negative controls and also MST data showed good binding curve of the labeled mutant antibody to Zn^{2+}. The K_D for this binding was about 168 μM.

We were also able to express both antibodies Q425 and 2C10 large expression using baculovirus and Sf9 insect system. Both heavy and light chains were expressed with our Sf9 tissue culture system. MST data indicated that metal has a small effect on 2C10: dsDNA binding affinity. To further analyze this, Citlayi Villasenor, is going to do gel shift assay to determine the binding of dsDNA to 2C10 antibody with and without metal. The pull down assay data indicates that Q425 binds to CD4 in the presence of Ca^{2+} in the Triton-X buffer. Further analysis is necessary to determine the epitope mapping of CD4 to Q425 antibody.

Chapter V

Conclusion and Discussion

There are many different examples of metalloproteins in nature that were studied before, but what is novel is the fact that metal has an effective role in stabilizing the binding interaction between the antibody and antigen in metalloantibodies.

We were interested in studying this class of antibodies to find answers to the following research questions: (i) Can LT1009 antibody bind to Ca^{2+} independent of antigen? (ii) Can LT1009 antibody bind to any other metal ions? (iii) Are their other examples of antibodies that employ this use of metals as bridging ligands in antigen binding? (iv) Did LT1009 metal binding develop during maturation or is it present in germline variable domain gene sequences? (v) Can we engineer specificity toward metals other than Ca^{2+}?

In order to answer all these questions and be able to do routine mutagenesis and purification of antibodies for binding structural studies, we needed a large scale expression system to express and purify antibodies, but first let's summarize the previous literatures.

Previously, murine LT1002 antibody has been reported as an antibody that binds specifically to sphingosine-1-phosphate as an antigen (O'Brien, Jones, et al. 2009). Later on, in Dr. Huxford's lab we crystallized LT1009 humanized version of LT1002 antibody in the presence of metal and sphingosine-1-phosphate as a lipid antigen. X-ray crystal structure and ICP-MS data indicated that Ca^{2+} has a great effect in stabilizing S1P:LT1009 interaction. The X-ray crystallography has distinguished two Ca^{2+} ions in coordination with CDRL1-L3 loops of LT1009 and S1P (J. M. Wojciak et al. 2009). Furthermore, another group at the national institute of health reported that murine Q425 antibody has interaction with CD4 as an antigen. The X-ray crystal structure has shown that this antibody has the potential to cure HIV. Also, in their crystal

structure, Ca^{2+} and Ba^{2+} has an effective role in stabilizing the interaction between CD4:Q425 (T. Zhou et al. 2005). However, the binding site of Ca^{2+}/Ba^{2+} is different from LT1009 binding site to Ca^{2+}.

In order to find out whether LT1009 antibody binds to Ca^{2+} independent of antigen or not, we have crystallized LT1009 antibody with Ca^{2+} in the absence of S1P. 2.8 Å X-ray crystal structure shows that LT1009 binds to Ca^{2+} without S1P, and metal coordination dimensions at the binding site are slightly greater in comparison with the presence of S1P.

By searching the IgBlast server we found the metal binding coordination site sequence of the CDRL1-L3 loops of LT1009 antibody homology in other species such as rat, human, monkey and mouse antibodies. Using the IgBlast server, we found the variable domain genes that most closely matched to the mouse anti-S1P antibody, and we designed the heavy and light chain precursor plasmid of the Fab antibody.

First, I used *E.coli* (BL21(DE3) and T7 shuffle cells) to express the antibodies but I observed low expression yields, such that the protein concentration was not enough for further analysis assays. The purification of the antibody had some difficulties either. After purifying it from Ni affinity column, I used size exclusion chromatography to do the second step of purification and observed that always the peaks from SEC were two separate peaks that were exactly identical on SDS-PAGE gel (Figure V.1).

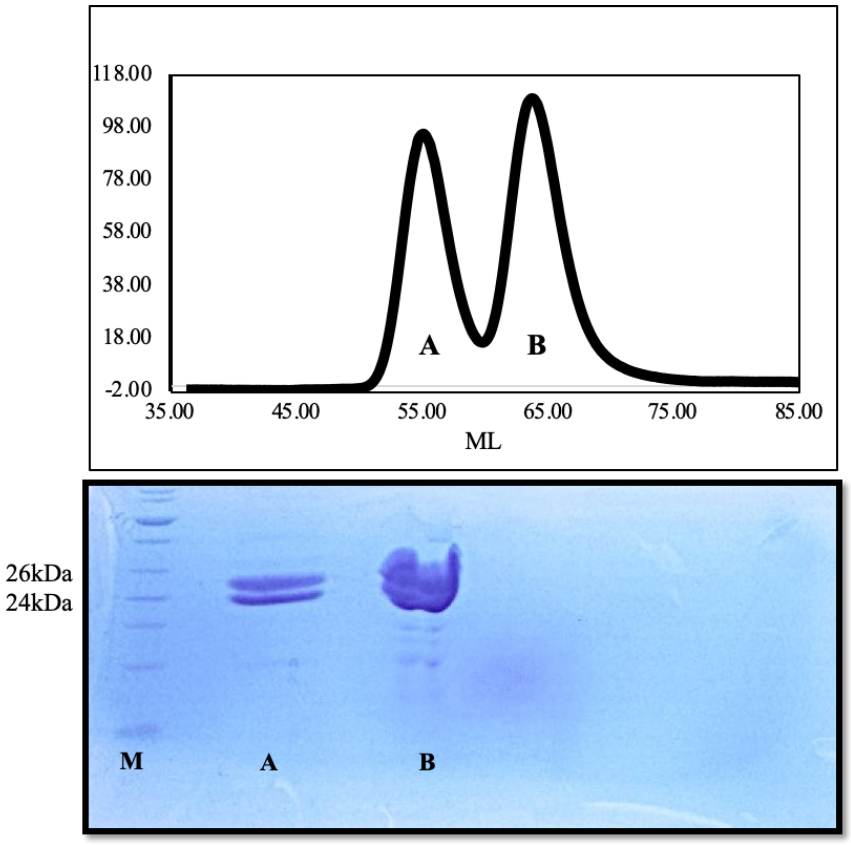

Figure V.1 SEC and SDS-PAGE gel data for the precursor antibody expression in *E.coli.* Size exclusion chromatography shows two peaks at the purification step and 15% SDS-PAGE gel shows that both peaks show at the same place on the gel.

To find out which peak is which, I performed size exclusion chromatography with multi-angle light scattering to identify the molecular weight of the protein in solution independent of its antigen. Therefore, I separately ran the peaks on SEC-MALLS and the results indicated that one of the peaks was 50 kDa and another one was 25 kDa. By running the standard LT1009 antibody that Lpath, LLC has provided us, we found out that LT1009 Fab antibody ran at 25 kDa. One of the precursor peaks molecular weight was double the size of the other peak. This could be because of dimerization of the antibody and not being properly folded.

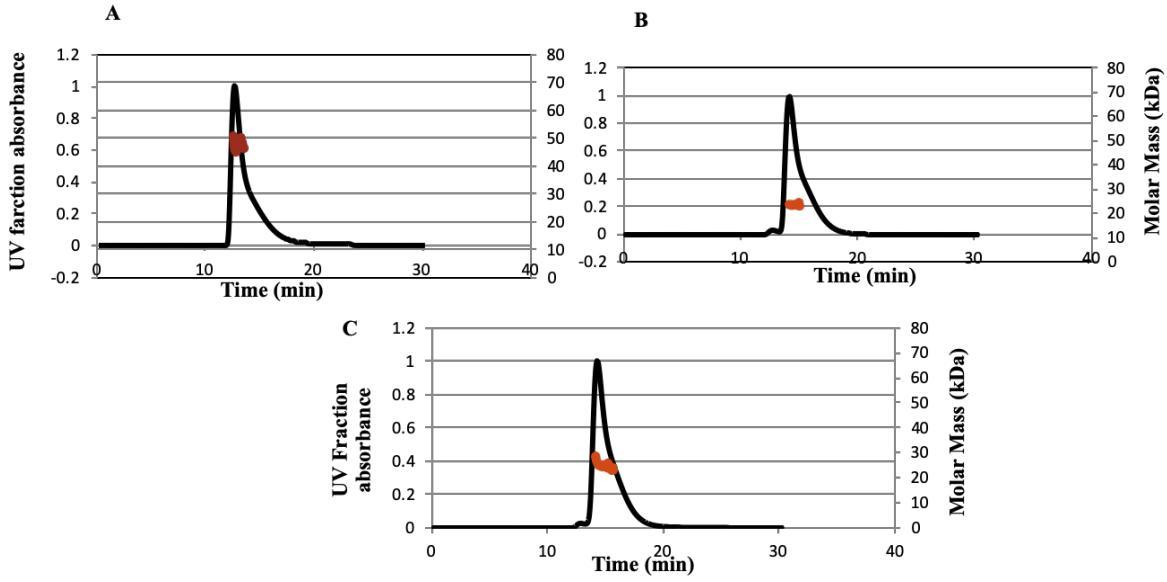

Figure V.2 Size exclusion chromatography with multi-angle light scattering data for the precursor antibody expression in *E.coli.* Chromatogram A shows the first peak molecular weight 50 kDa, chromatogram B shows the second peak molecular weight 25 kDa and chromatogram C shows the molecular weight of Fab LT1009 25 kDa.

After that, we looked at eukaryote cells to express the antibody. We followed the procedure in an article in the literature that suggested to use pFastBac dual plasmid with gp64 as a signal peptide (Furuta et al. 2010). Then, I started to clone pFastBac dual plasmid with the heavy and light chains inserted in the plasmid with the p10 promoter used for the light chain, pH promoter used for the heavy chain and gp64 signal peptide at the beginning of each chain. Next, I used our Sf9 insect system facility to express the antibody. The first Western blot from P1 virus seemed promising. Then, I got P2 and P3 viruses in order to get better yield of antibodies. After protein expression and purification, I was able to get about 8 mg/mL protein from 500 mL of media.

Then, we performed ICP-MS analysis to test the metal binding properties of the precursor antibody to Ca^{2+} in the absence of antigen. The data indicated that the precursor antibody binds to Ca^{2+} much greater than the control LT3015 antibody that does not bind to metal.

I then tried to alter the residues involved in the binding site of the LT1009 antibody in coordination with Ca^{2+} and S1P antigen. I tried to prepare 3 mutants with different mutations on the binding site. The residues on the binding sites of CDR-L1 and CDR-L3 loops were Asp30, Asp31, Asp32 and Asp92. By mutating these residues to D3032C, D3192H and finally D3032C/D3192H, we wanted to test to see if the mutant antibodies bind to any other metals instead of Ca^{2+}. We also wanted to see if the new mutant antibodies can be used as catalytic enzymes. Therefore, I dialyzed the new mutant antibodies with 10 mM of Co^{2+}, Zn^{2+}, Ni^{2+} and Cu^{2+} and sent the results to ICP-MS data at California state, Long Beach. The results indicated that the mutant D3032C/D3192H binds to Zn^{2+}. I further tested the binding of the fluorescence mutant antibody to Zn^{2+} and looked at its binding curve using MST. The binding curve looks good with a K_D value to be 168 μM.

Another antibody found in nature that we were interested in studying is Q425 and 2C10 antibody. Both are murine antibodies that have the same homology in their CDRL1-L3 loops. By using MST, the fluorescence murine 2C10 antibody showed that metal increases the binding affinity of the antigen: antibody interaction. MST data also indicates that Mg^{2+} (K_D=0.10 μM) has greater effects than Ca^{2+} (K_D=0.256 μM) in the binding affinity.

Finally, we concluded that the homology found in metalloantibodies CDR loops in different species from mouse, rat, human and monkey indicates that the metal binding is present

in the germline variable domain gene sequences of the antibodies. Also, the mutant metalloantibody binds to Zn^{2+} by the mutation of the CDR loops to D3032C/D3192H.

In conclusion, the metal binding ion motif can be used as a highly selective site for specific conjugation, which the cysteine reactivity can be protected against O_2 in the presence of metals. This site-specific conjugation strategy can be used for antibody-drug conjugates. This metalloantibodies can stabilize and increase the affinity of the antibody to different antigens. In a different study, the human light chain of A18b antibody was characterized and was capable of enzymatic activities like hydrolyzing vasoactive intestinal polypeptide and nucleophilic properties (V. Sharma et al. 2009). This indicates that the metalloantibody can be used in biotechnology as future engineered catalytic metalloantibodies.

References

Adamkewicz, J. I., Kiialainen, A., & Paz-Priel, I. (2019). Effects and interferences of emicizumab, a humanized bispecific antibody mimicking activated factor VIII cofactor function, on lupus anticoagulant assays. *International Journal of Laboratory Hematology*. https://doi.org/10.1111/ijlh.13114

Adams, P. D., Afonine, P. V., Bunkóczi, G., Chen, V. B., Davis, I. W., Echols, N., Headd, J. J., Hung, L.-W., Kapral, G. J., Grosse-Kunstleve, R. W., McCoy, A. J., Moriarty, N. W., Oeffner, R., Read, R. J., Richardson, D. C., Richardson, J. S., Terwilliger, T. C., & Zwart, P. H. (2010). PHENIX: a comprehensive Python-based system for macromolecular structure solution. *Acta Crystallographica Section D Biological Crystallography* (Vol. 66, Issue 2, pp. 213–221). https://doi.org/10.1107/s0907444909052925

AlDeghaither, D., Smaglo, B. G., & Weiner, L. M. (2015). Beyond peptides and mAbs-current status and future perspectives for biotherapeutics with novel constructs. *The Journal of Clinical Pharmacology* (Vol. 55, Issue S3, pp. S4–S20). https://doi.org/10.1002/jcph.407

Anderson, D. M. (1997). A mRNA Signal for the Type III Secretion of Yop Proteins by Yersinia enterocolitica. *Science* (Vol. 278, Issue 5340, pp. 1140–1143). https://doi.org/10.1126/science.278.5340.1140

Armentrout, E. I., & Rietsch, A. (2016). The Type III Secretion Translocation Pore Senses Host Cell Contact. *PLoS Pathogens*, *12*(3), e1005530.

Audia, J. P., Lindsey, A. S., Housley, N. A., Ochoa, C. R., Zhou, C., Toba, M., Oka, M., Annamdevula, N. S., Fitzgerald, M. S., Frank, D. W., & Alvarez, D. F. (2013). In the absence of effector proteins, the Pseudomonas aeruginosa type three secretion system needle tip complex contributes to lung injury and systemic inflammatory responses. *PloS One*, *8*(11), e81792.

Bajorath, J. (2015). Faculty of 1000 evaluation for Clinical development success rates for investigational drugs. *F1000 - Post-publication peer review of the biomedical literature*. https://doi.org/10.3410/f.718236299.793509111

Blake, D. A., Chakrabarti, P., Khosraviani, M., Hatcher, F. M., Westhoff, C. M., Goebel, P., Wylie, D. E., & Blake, R. C., 2nd. (1996). Metal binding properties of a monoclonal antibody directed toward metal-chelate complexes. *The Journal of Biological Chemistry*, *271*(44), 27677–27685.

Brekke, K. M., & Garrard, W. T. (2004). Assembly and analysis of the mouse immunoglobulin kappa gene sequence. *Immunogenetics*, *56*(7), 490–505.

Brinkmann, U., & Kontermann, R. E. (2017). The making of bispecific antibodies. *mAbs*, *9*(2), 182–212.

Buick, R. (2016, January 15). Why is Antibody Humanization still important in the 21st century? *Fusion Antibodies*. https://www.fusionantibodies.com/news/why-is-antibody-humanization-still-important-in-the-21st-century/

Cassandri, M., Smirnov, A., Novelli, F., Pitolli, C., Agostini, M., Malewicz, M., Melino, G., & Raschellà, G. (2017). Zinc-finger proteins in health and disease. *Cell Death Discovery*, *3*, 17071.

Chen, V. B., Arendall, W. B., 3rd, Headd, J. J., Keedy, D. A., Immormino, R. M., Kapral, G. J., Murray, L. W., Richardson, J. S., & Richardson, D. C. (2010). MolProbity: all-atom structure validation for macromolecular crystallography. *Acta Crystallographica. Section D, Biological Crystallography*, *66*(Pt 1), 12–21.

Chung, H.-S., Lee, S., & Park, S. J. (2016). Oxidation Protection in Metal-Binding Peptide Motif and Its Application to Antibody for Site-Selective Conjugation. *PloS One*, *11*(7), e0159451.

Cook, G. (2000). Immunobiology: The Immune System in Health and Disease (4th edn) by C.A. Janeway, P. Travers, M. Walport and J.D. Capra. *Immunology Today* (Vol. 21, Issue 4, p. 201). https://doi.org/10.1016/s0167-5699(00)01613-3

Coppieters, K., Dreier, T., Silence, K., De Haard, H., Lauwereys, M., Casteels, P., Beirnaert, E., Jonckheere, H., Van De Wiele, C., Staelens, L., Hostens, J., Revets, H., Remaut, E., Elewaut, D., & Rottiers, P. (2006). Formatted anti–tumor necrosis factor α VHH proteins derived from camelids show superior potency and targeting to inflamed joints in a murine model of collagen-induced arthritis. *Arthritis & Rheumatism* (Vol. 54, Issue 6, pp. 1856–1866). https://doi.org/10.1002/art.21827

Davis, I. W., Leaver-Fay, A., Chen, V. B., Block, J. N., Kapral, G. J., Wang, X., Murray, L. W., Arendall, W. B., Snoeyink, J., Richardson, J. S., & Richardson, D. C. (2007). MolProbity: all-atom contacts and structure validation for proteins and nucleic acids. *Nucleic Acids Research* (Vol. 35, Issue Web Server, pp. W375–W383). https://doi.org/10.1093/nar/gkm216

DeLano, W. L. (2002.). The PyMOL Molecular Graphics System. *DeLano Scientific: Palo Alto, CA, USA*.

Deng, W., Marshall, N. C., Rowland, J. L., McCoy, J. M., Worrall, L. J., Santos, A. S., Strynadka, N. C. J., & Finlay, B. B. (2017). Corrigendum: Assembly, structure, function and regulation of type III secretion systems. *Nature Reviews. Microbiology*, *15*(6), 379.

Derewenda, U., Mateja, A., Devedjiev, Y., Routzahn, K. M., Evdokimov, A. G., Derewenda, Z. S., & Waugh, D. S. (2004). The structure of Yersinia pestis V-antigen, an essential virulence factor and mediator of immunity against plague. *Structure*, *12*(2), 301–306.

Drake, P. M., Albers, A. E., Baker, J., Banas, S., Barfield, R. M., Bhat, A. S., de Hart, G. W., Garofalo, A. W., Holder, P., Jones, L. C., Kudirka, R., McFarland, J., Zmolek, W., & Rabuka, D. (2014). Aldehyde Tag Coupled with HIPS Chemistry Enables the Production of ADCs Conjugated Site-Specifically to Different Antibody Regions with Distinct in Vivo Efficacy and

PK Outcomes. *Bioconjugate Chemistry* (Vol. 25, Issue 7, pp. 1331–1341). https://doi.org/10.1021/bc500189z

Dübel, S., & Reichert, J. M. (2014). *Handbook of Therapeutic Antibodies*. John Wiley & Sons.

Ecker, D. M., Jones, S. D., & Levine, H. L. (2015). The therapeutic monoclonal antibody market. *mAbs* (Vol. 7, Issue 1, pp. 9–14). https://doi.org/10.4161/19420862.2015.989042

Edwards, B. M., & He, M. (2012). Evolution of antibodies in vitro by ribosome display. *Antibody Engineering* (pp. 281–292). https://doi.org/10.1007/978-1-61779-974-7_16

Els Conrath, K., Lauwereys, M., Wyns, L., & Muyldermans, S. (2001). Camel single-domain antibodies as modular building units in bispecific and bivalent antibody constructs. *The Journal of Biological Chemistry*, *276*(10), 7346–7350.

Emsley, P., & Cowtan, K. (2004). Coot: model-building tools for molecular graphics. *Acta Crystallographica Section D Biological Crystallography* (Vol. 60, Issue 12, pp. 2126–2132). https://doi.org/10.1107/s0907444904019158

Emsley, P., Lohkamp, B., Scott, W. G., & Cowtan, K. (2010). Features and development of Coot. *Acta Crystallographica. Section D, Biological Crystallography*, *66*(Pt 4), 486–501.

Erasmus, M. F. (2012). Characterization of the metal binding by the anti- sphingosine-1-phosphate antibody LT1002. Master thesis, Department of Chemistry, San Diego State University.

Espiritu, M. J., Collier, A. C., & Bingham, J.-P. (2014). A 21st-century approach to age-old problems: the ascension of biologics in clinical therapeutics. *Drug Discovery Today*, *19*(8), 1109–1113.

Feige, M. J., Gräwert, M. A., Marcinowski, M., Hennig, J., Behnke, J., Ausländer, D., Herold, E. M., Peschek, J., Castro, C. D., Flajnik, M., Hendershot, L. M., Sattler, M., Groll, M., & Buchner, J. (2014). The structural analysis of shark IgNAR antibodies reveals evolutionary principles of immunoglobulins. *Proceedings of the National Academy of Sciences of the United States of America*, *111*(22), 8155–8160.

Filpula, D. (2007). Antibody engineering and modification technologies. *Biomolecular Engineering* (Vol. 24, Issue 2, pp. 201–215). https://doi.org/10.1016/j.bioeng.2007.03.004

Fleming, J. K., Glass, T. R., Lackie, S. J., & Wojciak, J. M. (2016). A novel approach for measuring sphingosine-1-phosphate and lysophosphatidic acid binding to carrier proteins using monoclonal antibodies and the Kinetic Exclusion Assay. *Journal of Lipid Research* (Vol. 57, Issue 9, pp. 1737–1747). https://doi.org/10.1194/jlr.d068866

Fleming, J. K., Wojciak, J. M., -A. Campbell, M., & Huxford, T. (2011). *Crystal structure of the humanized apo LT3015 anti-lysophosphatidic acid antibody Fab fragment*. https://doi.org/10.2210/pdb3qct/pdb

Frenzel, A., Hust, M., & Schirrmann, T. (2013). Expression of recombinant antibodies. *Frontiers in Immunology*, *4*, 217.

Furuta, T., Ogawa, T., Katsuda, T., Fujii, I., & Yamaji, H. (2010). Efficient production of an antibody Fab fragment using the baculovirus–insect cell system. *Journal of Bioscience and Bioengineering* (Vol. 110, Issue 5, pp. 577–581). https://doi.org/10.1016/j.jbiosc.2010.06.001

Gagné, O. C., & Hawthorne, F. C. (2016). Bond-length distributions for ions bonded to oxygen: alkali and alkaline-earth metals. *Acta Crystallographica Section B Structural Science, Crystal Engineering and Materials* (Vol. 72, Issue 4, pp. 602–625). https://doi.org/10.1107/s2052520616008507

Galle, M., Carpentier, I., & Beyaert, R. (2012). Structure and Function of the Type III Secretion System of Pseudomonas aeruginosa. *Current Protein and Peptide Science* (Vol. 13, Issue 8, pp. 831–842). https://doi.org/10.2174/138920312804871210

Gardell, S. E., Dubin, A. E., & Chun, J. (2006). Emerging medicinal roles for lysophospholipid signaling. *Trends in Molecular Medicine* (Vol. 12, Issue 2, pp. 65–75). https://doi.org/10.1016/j.molmed.2005.12.001

Gennaro, D. 'amato, Amedeo, P., Antonello, S., Paolo, N., Maria, D. 'amato, & Gennaro, L. (2007). A Recombinant Humanized Anti-IgE Monoclonal Antibody (Omalizumab) in the Therapy of Moderate-to-Severe Allergic Asthma. *Recent Patents on Inflammation & Allergy Drug Discovery* (Vol. 1, Issue 3, pp. 225–231). https://doi.org/10.2174/187221307782418900

Ghannam, A., Kumari, S., Muyldermans, S., & Abbady, A. Q. (2015). Camelid nanobodies with high affinity for broad bean mottle virus: a possible promising tool to immunomodulate plant resistance against viruses. *Plant Molecular Biology* (Vol. 87, Issues 4-5, pp. 355–369). https://doi.org/10.1007/s11103-015-0282-5

Graham, B. S., & Ambrosino, D. M. (2015). History of passive antibody administration for prevention and treatment of infectious diseases. *Current Opinion in HIV and AIDS*, *10*(3), 129–134.

Grossoehme, N. E., Spuches, A. M., & Wilcox, D. E. (2010). Application of isothermal titration calorimetry in bioinorganic chemistry. *Journal of Biological Inorganic Chemistry* (Vol. 15, Issue 8, pp. 1183–1191). https://doi.org/10.1007/s00775-010-0693-3

Hannun, Y. A., & Obeid, L. M. (2008). Principles of bioactive lipid signalling: lessons from sphingolipids. *Nature Reviews. Molecular Cell Biology*, *9*(2), 139–150.

Harding, M. M. (2002). Metal–ligand geometry relevant to proteins and in proteins: sodium and potassium. *Acta Crystallographica Section D Biological Crystallography* (Vol. 58, Issue 5, pp. 872–874). https://doi.org/10.1107/s0907444902003712

Harmsen, M. M., & De Haard, H. J. (2007). Properties, production, and applications of camelid single-domain antibody fragments. *Applied Microbiology and Biotechnology* (Vol. 77, Issue 1, pp. 13–22). https://doi.org/10.1007/s00253-007-1142-2

Healey, D., Dianda, L., Moore, J. P., McDougal, J. S., Moore, M. J., Estess, P., Buck, D., Kwong, P. D., Beverley, P. C., & Sattentau, Q. J. (1990). Novel anti-CD4 monoclonal antibodies separate human immunodeficiency virus infection and fusion of CD4 cells from virus binding. *The Journal of Experimental Medicine* (Vol. 172, Issue 4, pp. 1233–1242). https://doi.org/10.1084/jem.172.4.1233

Holm, R. H., Kennepohl, P., & Solomon, E. I. (1996). Structural and Functional Aspects of Metal Sites in Biology. *Chemical Reviews* (Vol. 96, Issue 7, pp. 2239–2314). https://doi.org/10.1021/cr9500390

Hu, C., Chan, S. I., Sawyer, E. B., Yu, Y., & Wang, J. (2014). Metalloprotein design using genetic code expansion. *Chemical Society Reviews*, *43*(18), 6498–6510.

Im, S.-R., Im, S.-W., Chung, H.-Y., Pravinsagar, P., & Jang, Y.-J. (2015). Cell- and nuclear-penetrating anti-dsDNA autoantibodies have multiple arginines in CDR3 of VH and increase cellular level of pERK and Bcl-2 in mesangial cells. *Molecular Immunology*, *67*(2 Pt B), 377–387.

Inoue, K., Ishizawa, M., & Kubota, T. (2020). Monoclonal anti-dsDNA antibody 2C10 escorts DNA to intracellular DNA sensors in normal mononuclear cells and stimulates secretion of multiple cytokines implicated in lupus pathogenesis. *Clinical and Experimental Immunology*, *199*(2), 150–162.

Jackson, G. G., & Thomas, H. (2013). *The Pathogenesis of Bacterial Infections*. Springer Science & Business Media.

Jahnichen, S., Blanchetot, C., Maussang, D., Gonzalez-Pajuelo, M., Chow, K. Y., Bosch, L., De Vrieze, S., Serruys, B., Ulrichts, H., Vandevelde, W., Saunders, M., De Haard, H. J., Schols, D., Leurs, R., Vanlandschoot, P., Verrips, T., & Smit, M. J. (2010). CXCR4 nanobodies (VHH-based single variable domains) potently inhibit chemotaxis and HIV-1 replication and mobilize stem cells. *Proceedings of the National Academy of Sciences* (Vol. 107, Issue 47, pp. 20565–20570). https://doi.org/10.1073/pnas.1012865107

Jamieson, A. C., Miller, J. C., & Pabo, C. O. (2003). Drug discovery with engineered zinc-finger proteins. *Nature Reviews Drug Discovery* (Vol. 2, Issue 5, pp. 361–368). https://doi.org/10.1038/nrd1087

Janeway, C., & Travers, P. (1994). *Immunobiology: The Immune System in Health and Disease*. Taylor & Francis.

Jang, E.-J., Nahm, D.-H., & Jang, Y.-J. (2009). Mouse monoclonal autoantibodies penetrate mouse macrophage cells and stimulate NF-κB activation and TNF-α release. *Immunology Letters* (Vol. 124, Issue 2, pp. 70–76). https://doi.org/10.1016/j.imlet.2009.04.005

Jang, Y. J., & Stollar, B. D. (2003). Anti-DNA antibodies: aspects of structure and pathogenicity. *Cellular and Molecular Life Sciences (CMLS)* (Vol. 60, Issue 2, pp. 309–320). https://doi.org/10.1007/s000180300026

Jennings, E., Esposito, D., Rittinger, K., & Thurston, T. L. M. (2018). Structure–function analyses of the bacterial zinc metalloprotease effector protein GtgA uncover key residues required for deactivating NF-κB. *Journal of Biological Chemistry* (Vol. 293, Issue 39, pp. 15316–15329). https://doi.org/10.1074/jbc.ra118.004255

Katz, A. K., Glusker, J. P., Beebe, S. A., & Bock, C. W. (1996). Calcium Ion Coordination: A Comparison with That of Beryllium, Magnesium, and Zinc. *Journal of the American Chemical Society* (Vol. 118, Issue 24, pp. 5752–5763). https://doi.org/10.1021/ja953943i

Kawabata, T., Otsuka, T., Fujita, K., Sakai, G., Kim, W., Matsushima-Nishiwaki, R., Kuroyanagi, G., Kozawa, O., & Tokuda, H. (2018). HSP70 inhibitors reduce the osteoblast migration by epidermal growth factor. *Current Molecular Medicine*, *18*(7), 486–495.

King, A. N., Fleming, J. K., Knapik, S. S., Visentin, B., Wojciak, J. M., & Huxford, T. (2017). High-affinity pan-specific monoclonal antibodies that target cysteinyl leukotrienes and show efficacy in an acute model of colitis. *Journal of Lipid Research* (Vol. 58, Issue 7, pp. 1386–1398). https://doi.org/10.1194/jlr.m075614

Klug, A., & Rhodes, D. (1987). Zinc Fingers: A Novel Protein Fold for Nucleic Acid Recognition. *Cold Spring Harbor Symposia on Quantitative Biology* (Vol. 52, Issue 0, pp. 473–482). https://doi.org/10.1101/sqb.1987.052.01.054

Kobayashi, H., Kobayashi, O., & Kawai, S. (2009). Pathogenesis and clinical manifestations of chronic colonization by Pseudomonas aeruginosa and its biofilms in the airway tract. *Journal of Infection and Chemotherapy* (Vol. 15, Issue 3, pp. 125–142). https://doi.org/10.1007/s10156-008-0691-3

Kretsinger, R. H., Uversky, V. N., & Permyakov, E. A. (2013). *Encyclopedia of Metalloproteins*. Springer.

Kubota, T., Akatsuka, T., & Kanai, Y. (1986). A monoclonal anti-double stranded DNA antibody from an autoimmune MRL/Mp-lpr/lpr mouse: specificity and idiotype in serum immunoglobulins. *Immunology Letters* (Vol. 14, Issue 1, pp. 53–58). https://doi.org/10.1016/0165-2478(86)90020-9

Kubota, T., Watanabe, N., Kanai, Y., & Stollar, B. D. (1996). Enhancement of oxidative cleavage of DNA by the binding sites of two anti-double-stranded DNA antibodies. *The Journal of Biological Chemistry*, *271*(11), 6555–6561.

Landry, R. C., Klimowicz, A. C., Lavictoire, S. J., Borisova, S., Kottachchi, D. T., Lorimer, I. A. J., & Evans, S. V. (2001). Antibody recognition of a conformational epitope in a peptide antigen: Fv-peptide complex of an antibody fragment specific for the mutant EGF receptor, EGFRvIII. *Journal of Molecular Biology* (Vol. 308, Issue 5, pp. 883–893). https://doi.org/10.1006/jmbi.2001.4628

Lee, P.-C., Stopford, C. M., Svenson, A. G., & Rietsch, A. (2010). Control of effector export by thePseudomonas aeruginosatype III secretion proteins PcrG and PcrV. *Molecular Microbiology* (Vol. 75, Issue 4, pp. 924–941). https://doi.org/10.1111/j.1365-2958.2009.07027.x

Litman, G. W., Rast, J. P., Hulst, M. A., Litman, R. T., Shamblott, M. J., Haire, R. N., Hinds-Frey, K. R., Buell, R. D., Margittai, M., Ohta, Y., Zilch, A. C., Good, R. A., & Amemiya, C. T. (1993). Evolutionary Origins of Immunoglobulin Gene Diversity. *Progress in Immunology Vol. VIII* (pp. 107–114). https://doi.org/10.1007/978-3-642-51479-1_14

Li, Z., Woo, C. J., Iglesias-Ussel, M. D., Ronai, D., & Scharff, M. D. (2004). The generation of antibody diversity through somatic hypermutation and class switch recombination. *Genes & Development*, *18*(1), 1–11.

Lu, L., Vollmer, J., Moulon, C., Weltzien, H. U., Marrack, P., & Kappler, J. (2003). Components of the Ligand for a Ni Reactive Human T Cell Clone. *The Journal of Experimental Medicine* (Vol. 197, Issue 5, pp. 567–574). https://doi.org/10.1084/jem.20021762

Madden, T. L., Tatusov, R. L., & Zhang, J. (1996). Applications of network BLAST server. *Methods in Enzymology* (pp. 131–141). https://doi.org/10.1016/s0076-6879(96)66011-x

Marmion, C. J. (2014). A. Sigel, H. Sigel, R. K. O. Sigel (Eds): Interrelations between essential metal ions and human diseases. Vol. 13 of Metal ions in life sciences. *Transition Metal Chemistry* (Vol. 39, Issue 8, pp. 971–972). https://doi.org/10.1007/s11243-014-9883-0

Martinez-Jean, C., Folch, G., & Lefranc, M.-P. (2001). Nomenclature and Overview of the Mouse (*Mus musculus* and *Mus* sp.) Immunoglobulin Kappa (IGK) Genes. *Experimental and Clinical Immunogenetics* (Vol. 18, Issue 4, pp. 255–279). https://doi.org/10.1159/000049204

Maverakis, E., Kim, K., Shimoda, M., Eric Gershwin, M., Forum Patel, Wilken, R., Raychaudhuri, S., Renee Ruhaak, L., & Lebrilla, C. B. (2015). Glycans in the immune system and The Altered Glycan Theory of Autoimmunity: A critical review. *Journal of Autoimmunity* (Vol. 57, pp. 1–13). https://doi.org/10.1016/j.jaut.2014.12.002

McCoy, A. J., Grosse-Kunstleve, R. W., Adams, P. D., Winn, M. D., Storoni, L. C., & Read, R. J. (2007). Phaser crystallographic software. *Journal of Applied Crystallography*, *40*(Pt 4), 658–674.

Milstien, S., & Spiegel, S. (2006). Targeting sphingosine-1-phosphate: A novel avenue for cancer therapeutics. *Cancer Cell* (Vol. 9, Issue 3, pp. 148–150). https://doi.org/10.1016/j.ccr.2006.02.025

Möller, A., Pion, E., Narayan, V., & Ball, K. L. (2010). Intracellular Activation of Interferon Regulatory Factor-1 by Nanobodies to the Multifunctional (Mf1) Domain. *Journal of Biological Chemistry* (Vol. 285, Issue 49, pp. 38348–38361). https://doi.org/10.1074/jbc.m110.149476

Mordasini, T., Curioni, A., & Andreoni, W. (2003). Why do divalent metal ions either promote or inhibit enzymatic reactions? The case of BamHI restriction endonuclease from combined quantum-classical simulations. *The Journal of Biological Chemistry*, *278*(7), 4381–4384.

Morrison, C. (2019). Nanobody approval gives domain antibodies a boost. *Nature Reviews. Drug Discovery*, *18*(7), 485–487.

Morrow, T., & Felcone, L. H. (2004). Defining the difference: What Makes Biologics Unique. *Biotechnology Healthcare*, *1*(4), 24–29.

Mortensen, E. S., Fenton, K. A., & Rekvig, O. P. (2008). Lupus Nephritis. *The American Journal of Pathology* (Vol. 172, Issue 2, pp. 275–283). https://doi.org/10.2353/ajpath.2008.070563

Motzer, R. J., & Bukowski, R. M. (2006). Targeted therapy for metastatic renal cell carcinoma. *Journal of Clinical Oncology* (Vol. 24, Issue 35, pp. 5601–5608). https://doi.org/10.1200/jco.2006.08.5415

Murph, M., & Mills, G. B. (2007). Targeting the lipids LPA and S1P and their signalling pathways to inhibit tumour progression. *Expert Reviews in Molecular Medicine* (Vol. 9, Issue 28, pp. 1–18). https://doi.org/10.1017/s1462399407000476

Murshudov, G. N., Vagin, A. A., & Dodson, E. J. (1997). Refinement of macromolecular structures by the maximum-likelihood method. *Acta Crystallographica Section D Biological Crystallography* (Vol. 53, Issue 3, pp. 240–255). https://doi.org/10.1107/s0907444996012255

Muyldermans, S. (2013). Nanobodies: Natural single-domain antibodies. *Annual Review of Biochemistry* (Vol. 82, Issue 1, pp. 775–797). https://doi.org/10.1146/annurev-biochem-063011-092449

O'Brien, N., Jones, S. T., Williams, D. G., Cunningham, H. B., Moreno, K., Visentin, B., Gentile, A., Vekich, J., Shestowsky, W., Hiraiwa, M., Matteo, R., Cavalli, A., Grotjahn, D., Grant, M., Hansen, G., Campbell, M.-A., & Sabbadini, R. (2009). Production and characterization of monoclonal anti-sphingosine-1-phosphate antibodies. *Journal of Lipid Research*, *50*(11), 2245–2257.

Otwinowski, Z., & Minor, W. (1997). Processing of X-ray diffraction data collected in oscillation mode. *Methods in Enzymology* (pp. 307–326). https://doi.org/10.1016/s0076-6879(97)76066-x

Pabo, C. O., Peisach, E., & Grant, R. A. (2001). Design and Selection of Novel Cys2His2 Zinc Finger Proteins. *Annual Review of Biochemistry* (Vol. 70, Issue 1, pp. 313–340). https://doi.org/10.1146/annurev.biochem.70.1.313

Parakh, S., Parslow, A. C., Gan, H. K., & Scott, A. M. (2016). Antibody-mediated delivery of therapeutics for cancer therapy. *Expert Opinion on Drug Delivery* (Vol. 13, Issue 3, pp. 401–419). https://doi.org/10.1517/17425247.2016.1124854

Patterson, S. D. (2005). Investigating Drug-Induced QT and QTc Prolongation in the Clinic: A Review of Statistical Design and Analysis Considerations: Report from the Pharmaceutical Research and Manufacturers of America QT Statistics Expert Team. *Drug Information Journal* (Vol. 39, Issue 3, pp. 243–265). https://doi.org/10.1177/009286150503900304

Pavletich, N., & Pabo, C. (1991). Zinc finger-DNA recognition: crystal structure of a Zif268-DNA complex at 2.1 A. *Science* (Vol. 252, Issue 5007, pp. 809–817). https://doi.org/10.1126/science.2028256

Quesada-González, D., Jairo, G. A., Blake, R. C., Blake, D. A., & Merkoçi, A. (2018). Uranium (VI) detection in groundwater using a gold nanoparticle/paper-based lateral flow device. *Scientific Reports* (Vol. 8, Issue 1). https://doi.org/10.1038/s41598-018-34610-5

Ràfols, C., Bosch, E., Barbas, R., & Prohens, R. (2016). The Ca2 –EDTA chelation as standard reaction to validate Isothermal Titration Calorimeter measurements (ITC). *Talanta* (Vol. 154, pp. 354–359). https://doi.org/10.1016/j.talanta.2016.03.075

Reth, M., Radbruch, A., Alt, F., Honjo, T., & Neuberger, M. (2004). *Molecular Biology of B Cells*. Elsevier.

Rissiek, B., Koch-Nolte, F., & Magnus, T. (2014). Nanobodies as modulators of inflammation: potential applications for acute brain injury. *Frontiers in Cellular Neuroscience*, *8*, 344.

Robert, R., Streltsov, V. A., Newman, J., Pearce, L. A., Wark, K. L., & Dolezal, O. (2010). Germline humanization of a murine Aβ antibody and crystal structure of the humanized recombinant Fab fragment. *Protein Science* (Vol. 19, Issue 2, pp. 299–308). https://doi.org/10.1002/pro.312

Saeed, A. F. U. H., Wang, R., Ling, S., & Wang, S. (2017). Antibody engineering for pursuing a healthier future. *Frontiers in Microbiology*, 8, 495.

Sato, H., & Frank, D. W. (2011). Multi-Functional Characteristics of the Pseudomonas aeruginosa Type III Needle-Tip Protein, PcrV; Comparison to Orthologs in other Gram-negative Bacteria. *Frontiers in Microbiology*, 2, 142.

Schuermann, J. P., Henzl, M. T., Deutscher, S. L., & Tanner, J. J. (2004). Structure of an anti-DNA fab complexed with a non-DNA ligand provides insights into cross-reactivity and molecular mimicry. *Proteins*, 57(2), 269–278.

Scott, A. M., Wolchok, J. D., & Old, L. J. (2012). Antibody therapy of cancer. *Nature Reviews Cancer* (Vol. 12, Issue 4, pp. 278–287). https://doi.org/10.1038/nrc3236

Sharma, T., & Gupta, S. (2019). Reconstitution of IgG Subclasses following Immunoglobulin Therapy in Adult Primary Hypogammaglobulinemia. *International Archives of Allergy and Immunology*, 1–12.

Sharma, V., Heriot, W., Trisler, K., & Smider, V. (2009). A human germ line antibody light chain with hydrolytic properties associated with multimerization status. *The Journal of Biological Chemistry*, 284(48), 33079–33087.

Shaul, J. D., Farina, A., & Huxford, T. (2008). The human IKKβ subunit kinase domain displays CK2-like phosphorylation specificity. *Biochemical and Biophysical Research Communications* (Vol. 374, Issue 3, pp. 592–597). https://doi.org/10.1016/j.bbrc.2008.07.082

Shehata, L., Maurer, D. P., Wec, A. Z., Lilov, A., Champney, E., Sun, T., Archambault, K., Burnina, I., Lynaugh, H., Zhi, X., Xu, Y., & Walker, L. M. (2019). Affinity Maturation Enhances Antibody Specificity but Compromises Conformational Stability. *Cell Reports*, *28*(13), 3300–3308.e4.

Sigel, R. K. O., & Pyle, A. M. (2007). Alternative roles for metal ions in enzyme catalysis and the implications for ribozyme chemistry. *Chemical Reviews*, 107(1), 97–113.

Silverman, G. J. (2015). Protective natural autoantibodies to apoptotic cells: evidence of convergent selection of recurrent innate-like clones. *Annals of the New York Academy of Sciences*, 1362, 164–175.

Širochmanová, I., Čomor, Ľ., Káňová, E., Jiménez-Munguía, I., Tkáčová, Z., & Bhide, M. (2018). Permeability of the Blood-Brain Barrier and Transport of Nanobodies Across the Blood-Brain Barrier. *Folia Veterinaria* (Vol. 62, Issue 1, pp. 59–66). https://doi.org/10.2478/fv-2018-0009

Skoura, A., Sanchez, T., Claffey, K., Mandala, S. M., Proia, R. L., & Hla, T. (2007). Essential role of sphingosine 1–phosphate receptor 2 in pathological angiogenesis of the mouse retina. *Journal of Clinical Investigation* (Vol. 117, Issue 9, pp. 2506–2516). https://doi.org/10.1172/jci31123

Solomon, D. H., Kavanaugh, A. J., Schur, P. H., & American College of Rheumatology Ad Hoc Committee on Immunologic Testing Guidelines. (2002). Evidence-based guidelines for the use of immunologic tests: Antinuclear antibody testing. *Arthritis & Rheumatism* (Vol. 47, Issue 4, pp. 434–444). https://doi.org/10.1002/art.10561

Stanfield, R. L., Zemla, A., Wilson, I. A., & Rupp, B. (2006). Antibody Elbow Angles are Influenced by their Light Chain Class. *Journal of Molecular Biology* (Vol. 357, Issue 5, pp. 1566–1574). https://doi.org/10.1016/j.jmb.2006.01.023

Sutton, B., Davies, A., Bax, H., & Karagiannis, S. (2019). IgE Antibodies: From Structure to Function and Clinical Translation. *Antibodies* (Vol. 8, Issue 1, p. 19). https://doi.org/10.3390/antib8010019

Swindells, M. B., Porter, C. T., Couch, M., Hurst, J., Abhinandan, K. R., Nielsen, J. H., Macindoe, G., Hetherington, J., & Martin, A. C. R. (2017). abYsis: Integrated Antibody Sequence and Structure-Management, Analysis, and Prediction. *Journal of Molecular Biology*, 429(3), 356–364.

Tavernier, E. D., De Tavernier, E., Detalle, L., Morizzo, E., Roobrouck, A., De Taeye, S., Rieger, M., Verhaeghe, T., Correia, A., Van Hegelsom, R., Figueirido, R., Noens, J., Steffensen, S., Stöhr, T., Van de Velde, W., Depla, E., & Dombrecht, B. (2016). High Throughput Combinatorial Formatting of PcrV Nanobodies for Efficient Potency Improvement. *Journal of Biological Chemistry* (Vol. 291, Issue 29, pp. 15243–15255). https://doi.org/10.1074/jbc.m115.684241

Thomson, A. J., & Gray, H. B. (1998). Bio-inorganic chemistry. *Current Opinion in Chemical Biology* (Vol. 2, Issue 2, pp. 155–158). https://doi.org/10.1016/s1367-5931(98)80056-2

Trautmann, M., Lepper, P. M., & Haller, M. (2005). Ecology of Pseudomonas aeruginosa in the intensive care unit and the evolving role of water outlets as a reservoir of the organism. *American Journal of Infection Control* (Vol. 33, Issue 5, pp. S41–S49). https://doi.org/10.1016/j.ajic.2005.03.006

Tsai, H.-C., & Han, M. H. (2016). Sphingosine-1-Phosphate (S1P) and S1P Signaling Pathway: Therapeutic Targets in Autoimmunity and Inflammation. *Drugs* (Vol. 76, Issue 11, pp. 1067–1079). https://doi.org/10.1007/s40265-016-0603-2

Vincent, K. J., & Zurini, M. (2012). Current strategies in antibody engineering: Fc engineering and pH-dependent antigen binding, bispecific antibodies and antibody drug conjugates. *Biotechnology Journal* (Vol. 7, Issue 12, pp. 1444–1450). https://doi.org/10.1002/biot.201200250

Vollmer, J., Fritz, M., Dormoy, A., Weltzien, H. U., & Moulon, C. (1997). Dominance of the BV17 element in nickel-specific human T cell receptors relates to severity of contact sensitivity. *European Journal of Immunology* (Vol. 27, Issue 8, pp. 1865–1874). https://doi.org/10.1002/eji.1830270808

Waldron, K. J., & Robinson, N. J. (2009). How do bacterial cells ensure that metalloproteins get the correct metal? *Nature Reviews Microbiology* (Vol. 7, Issue 1, pp. 25–35). https://doi.org/10.1038/nrmicro2057

Wilcox, D. E. (2008). Isothermal titration calorimetry of metal ions binding to proteins: An overview of recent studies. *Inorganica Chimica Acta* (Vol. 361, Issue 4, pp. 857–867). https://doi.org/10.1016/j.ica.2007.10.032

Wojciak, J. M., Zhu, N., Schuerenberg, K. T., Moreno, K., Shestowsky, W. S., Hiraiwa, M., Sabbadini, R., & Huxford, T. (2009). The crystal structure of sphingosine-1-phosphate in complex with a Fab fragment reveals metal bridging of an antibody and its antigen. *Proceedings of the National Academy of Sciences of the United States of America*, 106(42), 17717–17722.

Yang, Z., Schmidt, D., Liu, W., Li, S., Shi, L., Sheng, J., Chen, K., Yu, H., Tremblay, J. M., Chen, X., Piepenbrink, K. H., Sundberg, E. J., Kelly, C. P., Bai, G., Shoemaker, C. B., & Feng, H. (2014). A novel multivalent, single-domain antibody targeting TcdA and TcdB prevents fulminant Clostridium difficile infection in mice. *The Journal of Infectious Diseases*, 210(6), 964–972.

Ye, J., Ma, N., Madden, T. L., & Ostell, J. M. (2013). IgBLAST: an immunoglobulin variable domain sequence analysis tool. *Nucleic Acids Research*, 41(Web Server issue), W34–W40.

Yin, L., Crawford, F., Marrack, P., Kappler, J. W., & Dai, S. (2012). T-cell receptor (TCR) interaction with peptides that mimic nickel offers insight into nickel contact allergy. *Proceedings of the National Academy of Sciences of the United States of America*, 109(45), 18517–18522.

Zhou, T., Hamer, D. H., Hendrickson, W. A., Sattentau, Q. J., & Kwong, P. D. (2005). Interfacial metal and antibody recognition. *Proceedings of the National Academy of Sciences of the United States of America*, 102(41), 14575–14580.